

Mixing and Settling Characterization in Low-Quality Bitumen Froth Treatment

by

Colin Saraka

A thesis submitted in partial fulfillment of the requirements for the degree of

Master of Science

in

Chemical Engineering

Department of Chemical and Materials Engineering
University of Alberta

© Colin Saraka, 2017

Abstract

Bitumen froth is an intermediate product of bitumen upgrading which must be treated to remove solids and water. De-mineralization and de-watering occur through a settling operation in which the addition of a diluent and a demulsifier are crucial to its success. This work explores the effect of mixing variables in the addition of demulsifier, a chemical separation aid.

This study probes the use of demulsifier and the effect of mixing on separation in a particularly challenging material: low-quality bitumen froth. Low-quality froth derives from low-quality bitumen ore, and is more challenging to process. Higher water and solids content and other properties, including the nature of the solids, contribute to this challenge. We use many of the same techniques used in previous studies in average-quality bitumen froth and diluted bitumen to analyze the effects of mixing variables in this new and challenging mixture. By some criteria, the mixing variables lead to expected process results: less water and solids are present in the top layer when mixing energy is high and injection concentration is low (in other words, chemical is more pre-diluted). Some unexpected results occurred as well: good mixing led to high induction time, or a long period of time after demulsifier addition before settling was detectable. Good mixing also led to lower water content in the bottom layer.

Focused-beam reflectance measurement (FBRM) is an in-situ technique for particle- and droplet-size detection. It measures and counts chord lengths, which differ from diameter in that they can be read from anywhere on a spherical or non-spherical item. These chord lengths are arranged into a chord length distribution, like a drop size distribution or particle size distribution. By using FBRM, we hope to gain more understanding of the mechanisms that drive the settling process and are in turn affected by the mixing variables. This work marks the first attempt at using the FBRM to characterize mixing and settling in froth treatment.

Acknowledgements

Even though a thesis is ultimately written by one person, it would not be possible without a team of great people. I would like to thank Dr. Suzanne Kresta for believing in me and pushing me to find more signal in the noise of the data. She listened to my crazy ideas about the complexity we were seeing and added some of her own.

I am thankful to Nitin Arora and Anna Xu for their help and teamwork. They both pushed me to think in different ways, and I have only succeeded by building on what came before. Others in the mixing team were invaluable for support and friendship. Marcio Machado, Dustyn Ulrich, Khilesh Jairamdas, Fatemeh Safari, Francesco Maluta, Akshay Bhalerao: sharing ideas and laughs with all of you was part of what made grad school great.

I also want to thank Samson Ng and Sujit Bhattacharya, our project sponsors. Their energy and enthusiasm for the research inspired to push myself for more understanding. I could not have asked for better industrial partners!

Finally my family and friends, and especially my parents, Edward Saraka and Mary Ann Tiga! You nodded politely as I struggled to explain the technical details of my project, then loved and supported me as you always do.

Table of Contents

Abstract.....	ii
Acknowledgements.....	iv
List of Figures	ix
List of Symbols	xiii
Chapter 1 : Oil Sands Processing and Mixing.....	1
1.1 Research Objectives	1
1.2 Oil Sands Processing.....	2
1.2.1 Froth Treatment	3
1.2.2 Water in Crude Oil Emulsions.....	5
1.2.3 Demulsifier in Bitumen Froth	7
1.3 Mixing.....	8
1.3.1 Mixing Characterization.....	8
1.3.2 Mixing in the Oil Sands	11
1.3.3 Mesomixing Phenomena	11
1.3.4 Effects of Mixing on Demulsifier Performance	14
1.4 Experimental Apparatuses and Techniques.....	15
1.4.1 In-Situ Particle Measurements in Liquid-Continuous Systems	15
1.4.2 The Confined Impeller Stirred Tank.....	16
1.5 Settling and Combination Mechanisms	17
1.5.1 Stokes' Law and Hindered Settling.....	19
1.5.2 Binary Coalescence	20
1.5.3 Flocculation and Flocculation-Assisted Coalescence	20

1.5.4 Sweep Flocculation	21
1.5.5 Compaction and Up-Flow	22
1.5.6 Fluid Structure and Consolidation	22
Chapter 2 : Focused-Beam Reflectance Measurement	24
2.1 Overview	24
2.1.1 Size Distributions and Weighting.....	27
2.1.2 Bin Weighting Protocol.....	29
2.2 Challenges	30
2.2.1 Fouling and Sapphire Surface Treatment.....	30
2.2.2 Silanization Surface Treatment	33
2.3 Chord Length Distribution	33
Chapter 3 : Experimental Setup.....	35
3.1 Procedure	36
3.1.1 Pre-Mixing.....	37
3.1.2 Naphtha Blending	38
3.1.3 Demulsifier Dispersion.....	39
3.1.4 Settling	43
3.1.5 Sampling Detail	43
3.2 Apparatus	45
3.2.1 Confined Impeller Stirred Tank (CIST)	45
3.2.2 Heating.....	48
3.3 Material	49
3.4 Dilbit Experiments	50
3.4.1 Experimental Design and Parameters	50

3.4.2 Results and Discussion.....	52
Chapter 4 : Optimizing Chemical Dosage in Low-Quality Froth	57
4.1 Experimental Design	57
4.2 Results and Discussion	58
4.2.1 Induction Time.....	59
4.2.2 Final Water Content	62
4.2.3 Verifying Chosen Condition	65
4.2.4 Other Runs.....	66
4.3 Conclusions.....	67
Chapter 5 : Mixing and Demulsifier Performance in Low-Quality Bitumen Froth Treatment 68	
5.1 Experimental Design	68
5.1.1 Replicated 2-Factor, 2-Level Design	68
5.2 Results & Discussion.....	70
5.2.1 Karl Fischer Results.....	72
5.2.1.1 Select Comparisons of Replicated Data	72
5.2.1.2 Water Content vs. Time Trends	74
5.2.1.3 Final Settling Period	83
5.2.1.4 Comparison of Effects of Mixing Energy and Injection Concentration	85
5.2.1.5 Induction Time	91
5.2.2 Mass Balance	92
5.2.3 FBRM Results	94
5.2.3.1 Data Overview.....	94
5.2.3.2 FBRM Counts During Naphtha Blending.....	95

5.2.3.3 FBRM Counts During Demulsifier Dispersion	97
5.2.3.4 FBRM Counts During 30 minutes of Settling	99
5.2.3.5 Chord Length Distributions of Naphtha Blending.....	101
5.2.3.6 Chord Length Distributions of Demulsifier Dispersion	103
5.2.3.7 Chord Length Distributions of Settling	105
5.3 Dean Stark OWS Data.....	107
5.3.1 Effects Using Dean Stark Data	109
5.4 Selected Microscope Data.....	112
5.4.1 Comparison with Average-Quality Froth.....	114
5.5 Conclusions.....	115
5.6 Future Work	117
5.6.1 Induction Time.....	117
5.6.2 Extend FBRM Data Set	118
5.6.3 PVM for Further Analysis and Interpreting FBRM Data	118
5.6.4 Vessel Redesign	118
5.6.5 Settling Time and Pre-Settling.....	119
References	120
Appendix A : Experimental Data	125
Appendix B : Select Standard Operating Procedures	129
B.1 Bitumen Froth Experiments (Low Quality Froth with FBRM).....	129
B.2 Receiving Test Material from Syncrude.....	132
B.3 Karl Fischer Procedures	133
B.4 Sending End-of-Run Samples to Syncrude.....	134

List of Figures

Figure 1-1: An example of mixing-driven reaction outcomes (Patterson et al., 2004). ...	13
Figure 1-2: Schematic of Proposed Settling and Combination Mechanisms	18
Figure 2-1: Circle showing chord length compared to radial position and diameter.....	25
Figure 2-2: Schematic of operating principle of FBRM (adapted from video by instrument supplier (Mettler Toledo 2016))	26
Figure 2-3: 14mm G400 FBRM Probe (Mettler Toledo, 2013)	26
Figure 2-4: Effect of sapphire repellency treatment on probe fouling	31
Figure 2-5: Fouling index for a full experiment	32
Figure 3-1: Schematic of Experimental Setup and Procedure	36
Figure 3-2: Detailed scale drawing of FBRM probe and feed tube placement in vessel..	40
Figure 3-3: Rendering of CIST showing sampling ports and heating media attachments	46
Figure 3-4: Picture of CIST with heating media attachments, FBRM, and Teflon sampling plugs	48
Figure 3-5: Particle size distribution of solids in froth samples, before separation	49
Figure 3-6: Chord Length Distribution of Dilbit Experiments after 5 min of Settling	52
Figure 3-7: Calculated Drop Size Distribution after 5 min of Settling.....	53
Figure 3-8: Drop size distribution for all experiments at 5 minutes settling time (a) transformed from CLD obtained from FBRM (b) using microscopy and image analysis..	54
Figure 3-9: Chord length counts during demulsifier dispersion in diluted bitumen for good mixing (high J, low IC) cases.....	56
Figure 3-10: Chord length counts during demulsifier dispersion in diluted bitumen for poor mixing (low J, high IC) cases	56
Figure 4-1: Water content over time for all experiments with demulsifier at N:B ratio of 0.7 and good mixing conditions, as determined by Karl Fischer titration.....	59

Figure 4-2: Illustration of settling process with 3 stages including significant induction time low quality (LQ) froth. Average quality (AQ) froth shown for comparison (Arora, 2016).	60
Figure 4-3: Comparison of no-demulsifier runs with a typical run with demulsifier	61
Figure 4-4: Final water content vs. Induction Time	62
Figure 4-5: Final water content over bulk concentration (on naphtha-diluted froth basis). Water content of 1% (dashed line) considered successful.....	63
Figure 4-6: Final water content compared to water content at beginning of settling.....	64
Figure 4-7: Verification experiment at chosen BC (200 ppm) and poor mixing conditions	65
Figure 4-8: Runs at high naphtha-to-bitumen ratio and presumed overdosing condition. All runs under good mixing conditions.	66
Figure 5-1: Comparison of Replicates at Z1 for low J, low IC condition	73
Figure 5-2: Comparison of Replicates at Z3 for low J, high IC condition	74
Figure 5-3: Water Content vs. Time at Z1 (topmost sampling point, 52 mm below surface), as determined by Karl Fischer titration (a) all runs including centre-point (b) data averaged between two replicates	75
Figure 5-4: Water Content vs. Time at Z2 (96 mm below liquid surface) as determined by Karl Fisher titration (a) all runs including centre-point (b) data averaged between two replicates.....	78
Figure 5-5: Water Content vs. Time at Z3 (140 mm below liquid surface) as determined by Karl Fischer titration for (a) all runs including centre-point (b) data averaged between two replicates	79
Figure 5-6: Water Content vs. Time at Z3 as determined by Karl Fischer titration for average-quality froth, produced from data collected by Arora (2016) with permission .	80
Figure 5-7: Water Content vs. Time at Height 4 (lowest sampling point) as determined by Karl Fischer titration for (a) all runs including centre-point (b) data averaged between two replicates	82

Figure 5-8: Comparison of Water Content at Beginning of Settling and After (a) 60 min and (b) 120 min.....	84
Figure 5-9: Coefficients for Water Content at Z1 over Time	86
Figure 5-10: Coefficients for Water Content at Z2 over Time	88
Figure 5-11: Coefficients for Water Content at Z3 over Time	89
Figure 5-12: Coefficients for Water Content at Z4 over Time	90
Figure 5-13: Induction Time compared to Water Content at 60 and 120 min.....	91
Figure 5-14: Water content (wt%) vs. height for FD-2 at 60 minutes. Top and bottom points are assumed.....	92
Figure 5-15: FBRM Counts during Naphtha Blending for FA-2 ($X_J = -1$, $X_{IC} = -1$).....	96
Figure 5-16: FBRM Counts during Naphtha Blending for FD-1 ($X_J = +1$, $X_{IC} = -1$).....	96
Figure 5-17: FBRM Counts during Demulsifier Disp. for Experiment CP-1 ($X_J = 0$, $X_{IC} = 0$). Similar to results from FD-1, FD-2.....	98
Figure 5-18: FBRM Counts during Dem. Disp. for Experiment FA-2 ($X_J = -1$, $X_{IC} = -1$)	98
Figure 5-19: FBRM Counts during 30 minutes of Settling for CP-1 ($X_J = 0$, $X_{IC} = 0$)	100
Figure 5-20: FBRM Counts during 30 minutes of Settling for FA-2 ($X_J = -1$, $X_{IC} = -1$)	100
Figure 5-21: Chord Length Distributions for Naphtha Blending of FA-2 ($X_J = -1$, $X_{IC} = -1$)	102
Figure 5-22: Chord Length Distributions for Naphtha Blending of FD-1 ($X_J = +1$, $X_{IC} = -1$)	102
Figure 5-23: Chord Length Distributions for Demulsifier Disp. of FA-2 ($X_J = -1$, $X_{IC} = -1$)	104
Figure 5-24: Chord Length Distributions for Demulsifier Disp. of FD-1 ($X_J = +1$, $X_{IC} = -1$)	104
Figure 5-25: Chord Length Distributions for Settling of FA-2 ($X_J = -1$, $X_{IC} = -1$).....	106
Figure 5-26: Chord Length Distributions for Settling of FD-1 ($X_J = +1$, $X_{IC} = -1$).....	106
Figure 5-27: Water and solids content at top height ($h/H = 0.1$) for all experiments....	108
Figure 5-28: Water and solids content at middle height ($h/H = 0.5$) for all experiments	109
Figure 5-29: Water and solids content at $z/H = 0.9$ for all experiments	112

Figure 5-30: Micrographs showing difference in fluid before and after induction for experiment FA-2 (at 30 min and 45 min, respectively)	113
Figure 5-31: Micrographs showing difference in fluid before and after induction for experiment FD-1 (at 45 min and 60 min, respectively)	113
Figure 5-32: Microscope image of average-quality froth during laboratory naphthenic froth treatment, showing spherical water aggregate (Arora, 2016).....	115

List of Symbols

BC	bulk concentration (demulsifier dosage)
CIST	confined-impeller stirred tank
CLD	chord-length distribution
CP	centre point run
CPA	Coulter particle analysis
d	particle/droplet diameter
d _{pipe}	feed pipe diameter
D	impeller diameter OR diffusivity
DSD	drop size distribution
FA	factorial run A, both variables low. Number denotes replicate.
FB	factorial run B, both variables high
FBRM	focused-beam reflectance measurement
FC	factorial run C, low J high IC
FD	factorial run D, high J low IC
H	liquid height
IC	injection concentration
J	energy input ($t_{\text{mix}} \times P$)
KF	Karl Fischer water titration

MANOVA	multivariate analysis of variance
N	rotational speed
N:B	naphtha-to-bitumen ratio
N_p	power number of impeller
O/W/O	multiple emulsion of oil in water in oil
OWS	oil, water, and solids as detected by Dean Stark extraction
P	power delivered by impeller(s)
PVM	particle video microscopy
Q_i	injection flowrate
Re	Reynolds number
S	impeller submergence
t_{mix}	mixing time
t	settling time
u_0	Stokes' regime settling velocity
u_z'	fluid velocity, fluctuation z component
U_z	fluid velocity, bulk z component
V_{IMP}	impeller-swept volume
V	tank volume
We	Weber number
W/O	water in oil emulsion

X	coded variable: +1 for high level, -1 for low level, 0 for middle level
z	height coordinate, as measured from liquid surface down
Z	sampling height code. Z1 is top, Z4 is bottom.
β	regression coefficient
ε	energy dissipation
ε_{\max}	maximum energy dissipation
μ	dynamic viscosity
ν	kinematic viscosity
ρ	density
σ	interfacial tension

Chapter 1: Oil Sands Processing and Mixing

1.1 Research Objectives

This research project has three major goals. The first is to expand our understanding of mixing effects in bitumen froth treatment to include low-quality froth. Where average-quality bitumen produces a froth that is approximately 60% bitumen, 30% water, and 10% solids, bitumen froth derived from lower quality bitumen is even more challenging, at approximately 50% bitumen, 37% water, and 13% solids. This has many potential consequences for the separation process: not just the quantity but the nature of the solids may be different, leading to different behaviour in the mixture; the higher water and solids loading undoubtedly has an impact on fluid viscosity and density and thus the mixing process; in an already highly-loaded mixture, additional loading (higher amount of water and solids, in this case) will have a great effect on settling.

The second goal was to isolate and understand the role of mesomixing on the process. It was discovered in previous studies (Chong, 2013; Laplante, 2011) that mesomixing plays a role in the performance of the demulsifier: varying injection concentration, or pre-diluting, leads to improved performance of the demulsifier. This indicates that there is an effect due to the initial blending of demulsifier from the feed plume. However, its mechanisms of interaction may differ due to local concentrations. This concept is discussed in more detail in Section 1.3.3.

It is also becoming increasingly clear that the mechanisms of settling and their interaction with mixing conditions need to be more clearly understood. The third goal of this work will be to use the data to suggest possible mechanisms for the settling process occurring. Because of the complex, multiphase nature of the fluid, the possible

mechanisms involved in the settling process are numerous. Any analysis must consider mechanisms not only from liquid-liquid systems, but also solid-liquid, multiple emulsion, and non-Newtonian fluids.

1.2 Oil Sands Processing

The Canadian Oil Sands represent a large portion of the oil reserves in world and Canada: there are a proven 177 billion barrels (Masliyah et al., 2011), second only to Saudi Arabia.

Bitumen is a very heavy, high-viscosity form of oil found in Canada in the form of oil sands. Oil sands are a mixture of bitumen, water, and solids, mostly sands and clays. In the ground the oil surrounds a solid particle with an interstitial layer of water in between. This property, along with bitumen's high viscosity and high levels of impurities, makes extraction and processing very different from that of lighter, more conventional oil deposits. Oil sands close to the surface are extracted via strip-mining. Massive mining equipment and heavy earthworks projects are required to dig the raw oil sand product out of the ground before processing. Other extraction methods are used for deeper deposits, including various heat-based recovery techniques such as SAGD – steam-assisted gravity drainage – and other techniques like solvent extraction.

Oil sands which have been strip-mined must then be processed to extract the hydrocarbon product and render it suitable for downstream upgrading and refining. Dr. Karl Clark, a researcher on the Alberta Research Council patented a process now called the Clark Hot Water Extraction Process to separate the bitumen from the solid by mixture with both hot water and caustic soda and then bubbling air through the resulting mixture to float most of the bitumen to the top of the process in the form of froth (Gray et al., 2009; Masliyah et al., 2011). Although purer than the raw oil sands, this bitumen froth at average quality still only contains about 60% bitumen after de-aeration, along with approximately 30% water and 10% solids. Froth treatment is the

process of removing these water and solids, making an intermediate product that meets pipeline specifications or is suitable for upgrading.

1.2.1 Froth Treatment

Two major variations of the froth treatment process are in use in the Canadian Oil Sands. The older method is naphthenic froth treatment (NFT). The bitumen froth is mixed with naphtha as a diluent at 0.7 parts naphtha to 1 part bitumen (Masliyah et al., 2011). Naphtha is a mixture of light organics, including both saturated and aromatic hydrocarbons. The naphtha lowers both the viscosity and the density of the hydrocarbon phase of bitumen. Lowering the viscosity by adding naphtha and increasing the temperature to 80°C enables settling on an operable time scale. Decreasing the density of organic phase is also very important because without the naphtha diluent, the organic phase has a very similar density to water, which also slows the settling process. Even with these interventions, much of the water in the bitumen froth remains dispersed in the organic phase and is usually termed emulsified water in industry (Masliyah et al., 2011). To further reduce the amount of water and solids, chemical demulsifiers are necessary. These chemicals come in different types, but their purpose is always the same: to help break the stable or metastable bitumen-water-solid emulsion. Section 1.2.3 details these chemicals further.

Paraffinic froth treatment (PFT) is similar except that in place of naphtha, a diluent consisting mostly of saturated alkanes (called paraffins or aliphatic hydrocarbons) is used. The paraffinic diluent drives a component of the oil called asphaltenes out of solution. Asphaltenes are a solubility class of hydrocarbons: they are defined as those hydrocarbons which will dissolve in an aromatic solvent such as toluene, but precipitate in a paraffinic solvent such as n-heptane (Czarnecki et al., 2012). The precipitated asphaltenes act as a flocculant, facilitating the formation of large, complex flocs of asphaltenes, water, and solids which then settle (Romanova et al., 2004). Increasing the

quantity of naphtha will eventually drive asphaltenes out of solution, but more naphtha is required than paraffin because naphtha is a mixture of aliphatic and aromatic compounds.

Each froth treatment strategy has tradeoffs. The product obtained from either froth treatment process is called diluted bitumen, or 'dilbit.' The dilbit from NFT still contains approximately 1-2 wt% water and 0.5 wt% solids; it does not meet pipeline specifications for water and solids content and is not suitable for refining (CanmetENERGY, 2016). In order to process the product it must first be upgraded by coking (CanmetENERGY, 2016). PFT produces a dilbit that meets pipeline specifications and can be refined. However, a higher solvent-to-bitumen ratio is required, necessitating larger vessels and higher capital costs. Since the asphaltenes which precipitate out in PFT are hydrocarbons, removing them also represents a loss of a potential product. Since the Syncrude process has downstream cokers available it makes sense to maximize the recovery of bitumen (Romanova et al., 2004). As NFT processes have driven towards higher product purities, however, bitumen recovery has degraded toward that of PFT (Shelfantook, 2004).

Several papers in the field are devoted to a general overview of froth treatment and its attendant challenges. Romanova et al. (2004) and Shelfantook (2004) both give overviews of froth treatment, some of its technical challenges, and how these challenges fit into the larger economic and historical context. Rao & Liu (2013) collected the current knowledge of the froth treatment process and suggested some directions for future research.

Research in the mixing group at the University of Alberta (Arora, 2016; Chong, 2013; Laplante, 2011; Leo, 2013) has already uncovered connections between mixing and demulsifier performance in bitumen froth treatment. This work expands the use of the techniques used in those works to low quality froth, as well as adding new techniques, to further probe mixing effects in bitumen froth treatment.

1.2.2 Water in Crude Oil Emulsions

Emulsions of water in crude oil are commonly found in petroleum processes and have a negative impact on many aspects of operations (Boxall et al., 2010). They may cause problems in separation equipment, make the oil off-spec, or create high pressure drops in flowlines (Kokal, 2005). In bitumen froth, emulsified water collects salts which contribute to corrosion issues, while solids cause erosion and catalyst poisoning. In general the size of the droplets will determine the stability of the emulsion and the optimal treatment protocol (Kokal, 2005). Rao & Liu (2013) identify three size categories of emulsified water which are useful for discussion: Type I is less than 10 microns, and is not readily removed without growing or flocculating the droplets. Type II is called dispersed water, and comprises droplets between 10 – 60 microns, which will settle slowly under gravity separation but can be removed faster in a centrifuge. Type III is termed free water and consists of water droplets greater than 60 microns. These droplets settle almost immediately. While useful for general discussion it is important to note that these are guidelines rather than rules. Settling conditions can vary widely by application.

Because larger droplets settle faster, combining droplets of water through flocculation or coalescence is a key step in effecting their separation. The ease of coalescence and flocculation is therefore an important parameter in the removal of water. Water can be held in emulsion by naturally-occurring surfactants in the oil such as naphthenic acids (Rao and Liu, 2013), or by non-surfactant species such as bi-wetting solids or asphaltenes (Chen et al., 1999; Masliyah et al., 2011; Rao and Liu, 2013; Sullivan and Kilpatrick, 2002a). Surfactants increase the thermodynamic stability of the emulsion. Non-surfactant components instead stabilize the emulsion through steric means, collecting at the boundary between the water and oil phases and forming a barrier to coalescence (Gray et al., 2009). Fine solids which act in this manner must be much smaller than the emulsion droplets themselves, and are wetted by both the oil and water phases (Chen et al., 1999; Kokal, 2005). Yeung et al. (2000) developed a technique

using micropipettes to identify these 'skins' that cover the water droplets and study their interfacial properties. They noticed that these skins can present a formidable barrier to coalescence and do not tend toward interdroplet adhesion. Sullivan & Kilpatrick (2002) studied the effects of several factors on the emulsion-stabilizing behaviour of particles, including particle size, pre-adsorbed water, and particle concentration. The maximum emulsification is possible in a water in crude oil emulsion at the aliphatic/aromatic ratio just at the point of precipitation (Eley et al., 1988; Masliyah et al., 2011).

There are many factors affecting the makeup and properties of bitumen emulsions. Vast differences in the treatability of emulsions produced from SAGD (steam-assisted gravity drainage) or CSS (cyclic steam stimulation) compared to oil sands treated with the Clark Hot Water Extraction Process prompted researchers to study the effects of salinity, pH, interfacial tension, and more (Rocha et al., 2016). Some of their many results are interesting to those researching low-quality froth. They found that increased salinity and increased pH were associated with lower water recovery. They found that increased salinity was also associated with a smaller Sauter mean diameter and lower packing density (i.e. a less dense packing of water droplets at the bottom of the vessel).

Even oil sands processed through the Clark Hot Water Extraction Process can vary based on the extraction conditions. Romanova et al. (2006) studied both bitumen extraction and froth treatment together to study the effects of extraction on the outcomes in froth treatment. This variability is of interest in this work as we are working with low-quality bitumen froth, which is known to be more difficult to process. It cannot be expected to behave exactly like the bitumen froth encountered in previous works.

The rheology of emulsions can show significant non-Newtonian behaviour and a higher viscosity than either of the oil or water components (Kokal, 2005). Droplet crowding and structural viscosity contribute: water levels above 30% are when non-Newtonian effects are often observable. Low quality bitumen froth has approximately 37% water. Even

after dilution with naphtha the mixture is approximately 27% water: any successful settling operation will thus have zones of greater than 30% water.

In this work, rheology effects due to high droplet population or inter-particle adhesion forces are suspected as factors in the settling dynamics of low-quality bitumen froth.

1.2.3 Demulsifier in Bitumen Froth

Demulsifiers are chemicals added to an emulsion to break the emulsion and effect separation of the emulsified phase. They are used in bitumen froth to facilitate separation of water and solids. Demulsifiers work by two major mechanisms. Flocculant-type chemicals or flocculating chemical aids promote the flocculation of smaller particles into flocs which settle faster due to their increased density. Flocs formed at higher chemical dosage are thought to be 'fluffier'; droplets come into contact aggregate immediately and maintain their original configuration. They are in a sense rigid, whereas at lower chemical dosage droplets and particles can still move within the structure as it forms and thus tend toward denser structures (Masliyah et al., 2011).

Coalescing-type chemicals promote coalescence of small emulsified droplets into larger droplets which settle faster (Masliyah et al., 2011). The birth rate of droplets which coalesce under shear can be approximated by the following equation (Masliyah et al., 2011):

$$\frac{dn_{tot}}{dt} = -\frac{16}{3}a^3Gn_{tot}^2$$

Where n_{tot} is the number of droplets, a is the colliding distance (equal to the sum of the radii of the colliding droplets), and G is the shear rate. Analyses of coalescence generally focus on collisions between two droplets: the incidence of two-droplet collisions far exceeds that of collisions of three or more. Coalescing chemicals are often surfactants, with both hydrophobic and hydrophilic components that help break the emulsion with optimal dosage and a good balance of hydrophilic and hydrophobic components.

Chemicals with functional groups of hydrophilic ethylene oxide (EO) and hydrophobic propylene oxide (PO) groups have been shown to effectively break W/O emulsions when the groups are present in approximately equal proportions (Xu et al., 2005). In fact, this balance of hydrophilic and hydrophobic is called the “hydrophile-lipophile balance” (HLB) and is one of the most important properties of a surfactant in many applications, although other methods of representing this property have been developed, such as the relative solubility number (RSN) (Rondón et al., 2006; Xu et al., 2005).

In practice, demulsifiers from industrial suppliers are often a mix of both coalescing and flocculating chemicals (Masliyah et al., 2011). The demulsifier used in this work is a proprietary formulation, called X-2105 by its supplier, Champion Technologies.

Injection concentration is the concentration of active ingredient in its carrier fluid. It is not reported in many demulsifier studies (Peña et al., 2005; Xu et al., 2005) even though there are studies which show (Arora, 2016; Chong, 2013; Chong et al., 2016; Laplante et al., 2015) that it has an effect, especially at bulk concentrations much higher or lower than the optimal point.

1.3 Mixing

1.3.1 Mixing Characterization

To a layman, mixing is a simple process; a mixture is either well-mixed or not. Many in industry know that mixing can be a subtle and complex phenomenon that can lead to issues if it is not well-designed. Mixing is at the core of countless process operations and the description of mixing is as varied as these process operations. Nevertheless, most mixing problems can be described with some combination of three dimensions: intensity of segregation, scale of segregation, and mixing time (Kresta et al., 2009, 2015; Kukukova et al., 2009). Intensity of segregation is the degree to which concentration

varies between two zones of interest, often quantified with the concentration variance, expressed with the coefficient of variance (CoV) (Kukukova et al., 2009):

$$CoV = \sqrt{\frac{1}{N_t} \sum_{i=1}^{N_t} \left(\frac{C_i - C_{mean}}{C_{mean}} \right)^2}$$

Where N_t is the total number of sampling points and should be high enough to accurately represent the system. C_i and C_{mean} are the concentration at point i and mean concentration, respectively. By inspecting the equation one can observe that a larger concentration difference will lead to a larger coefficient of variance.

Imagine adding a drop of food coloring first to a clear glass of water, and then to a glass of water which already has some food coloring. In the first case, the intensity of segregation is greater immediately after addition, because the clear water has zero food coloring, while the newly-added drop of food coloring is highly concentrated. In the second example, the concentration of the droplet has not changed, but since there is some coloring already in solution, the intensity of segregation is less. Of course, the intensity of segregation is quickly reduced as the droplet diffuses into the system. Not all mixing problems have an intensity of segregation component: it is impossible to reduce the intensity of segregation of a solid-solid system; one cannot reduce the intensity of segregation of the two liquids in a completely immiscible liquid-liquid system.

The scale of segregation is the size at which the mixture is still separate. Imagine again a droplet of food coloring being added to water. Even as it is diffusing, it will also twist, curl, and stretch through the liquid. The width of these curls or twists is the scale of segregation. In a liquid-gas system it is the size of bubbles or droplets. In a solids system it is the size of the solids. Turbulent mixing quickly reduces the scale of segregation through dissipation of turbulent energy in the form of eddies. Laminar mixing also reduces scale of segregation: laminar static mixers cut and fold the flow, and even

laminar pipe flow stretches the lamellae, increasing surface area while reducing the width of the lamellae.

Mixing time is the third dimension detailed by Kresta et al. (2016). There are several levels of mixing time: the blend time, for example, is the characteristic time for reducing large scale unmixedness in the vessel. Micromixing is mixing at the smallest scales in the vessel. Mixing time is closely related to the driving force for reducing segregation and the rate of change of separation (Kukukova et al., 2009). Both the scale of separation and intensity of separation will affect the mixing time. Reducing the scale of separation increases the area over which mass transfer can take place, while concentration difference is the driving force for diffusive mass transport by Fick's Law, shown here in its 1-dimensional form:

$$J = -D \frac{dc}{dx}$$

Where here J refers to the molar flux (in $\text{mol}\cdot\text{m}^{-2}\cdot\text{s}^{-1}$) of the diffusing species. D is the diffusivity (in $\text{m}^2\cdot\text{s}^{-1}$), and dc/dx is the differential difference in concentration along the dimension of interest. Because the flux is specified on an area basis, increasing the area of exposure increases the total mass transfer. The driving force behind this diffusion is Brownian motion.

In turbulent mixed systems, the diffusivity is replaced with the turbulent diffusivity D_T , which is also a function of the local flow field and can be estimated using knowledge of the local energy dissipation. Essentially this is an empirical method of acknowledging that turbulent eddies multiply the effective area and increase the fluid exchange in a way that is both highly efficacious in promoting mass transfer and very difficult to quantify.

1.3.2 Mixing in the Oil Sands

As in life, mixing is found everywhere in the exploitation of Canadian Oil Sands. The surface-mined oil sands are first mixed when they are exposed to hot water and sodium hydroxide. Mixing phenomena play a part in the flotation cells, where the mix of hot water, sodium hydroxide, and bitumen is contacted with air to liberate the bitumen from the solid particles and small layers of water.

In this study, however, froth treatment – and specifically naphthenic froth treatment – is the process to which our group brings a mixing perspective. It is a challenging process; fine water droplets are stabilized in oil by processes and species which are still being characterized by researchers. Varying ore quality causes a moving target for researchers building their understanding. Demulsifier must be dispersed in this mixture.

1.3.3 Mesomixing Phenomena

Mesomixing refers to all intermediate scales of mesomixing – smaller than the scale of the tank, but larger than the scale of the turbulent eddies and concentration striations – but is usually focused on the feed pipe or jet, where the feed rate is often greater than the local mixing, leading a region of high local concentrations emanating from the feed point, called a plume (Patterson et al., 2004). This region of high local concentration can lead to unintended effects in a mixing system, as will be discussed in a few examples.

The competition between a reaction and mixing is captured in the mixing Damkoehler number (Kresta et al., 2015):

$$Da_M = \frac{\tau_M}{\tau_R}$$

Which is the ratio of the time constant of mixing to the time constant of reaction, or the ratio of reaction rate to mixing rate. The mixing Damkoehler number is important in

determining the rate-limiting process: if $Da_M \ll 1$, then the overall rate is limited by the reaction and mixing is not a concern. If $Da_M \gg 1$ then the reaction rate is faster than the rate of mixing. This is concerning in systems where there may be undesirable side products formed or alternative mechanisms engaged by regions of high local concentration. This in turn can lead to undesirable process results, such as loss of yield or selectivity (Patterson et al., 2004). In a crystallization example detailed by Sarafinas & Teich (2016), a reactive precipitation formed smaller product upon scale-up. Because of mixing conditions, regions of high local concentrations were forming faster than the mixing could dissipate them, and the local supersaturation led to more primary nucleation (i.e. small crystals forming spontaneously) than expected and thus a greater quantity of smaller precipitates.

Figure 1-1 below shows another example of a system wherein inadequate mixing can lead to undesirable or unexpected results. If a reaction producing a side product (S) is much slower than the reaction producing the desired product (R), an engineer may expect to conduct this reaction and produce only a small amount of the side product. However, if mixing does not keep pace with the reaction, then a region of high concentration of R can form at the front between two unmixed regions of A and B. The high local concentration drives the secondary reaction to produce more side product than expected.

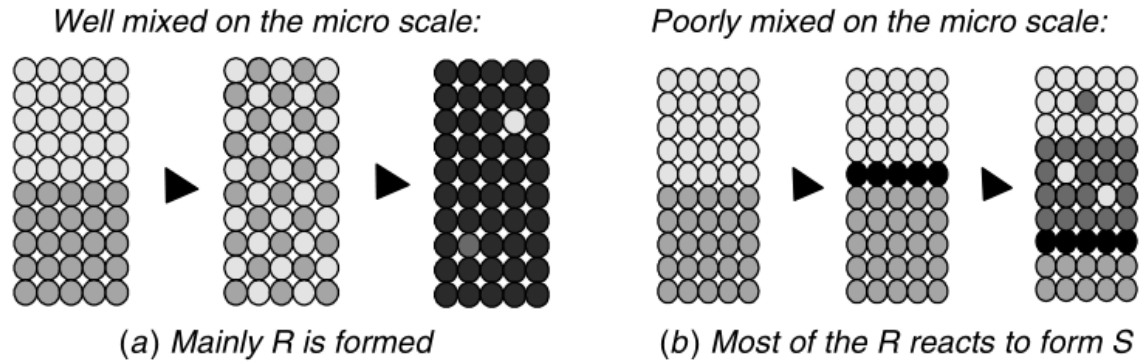


Figure 1-1: An example of mixing-driven reaction outcomes (Patterson et al., 2004).

Though most discussion of mesomixing refer to reaction systems, as in the examples above, it is possible that other mechanisms may be affected by local mixing rates. For example, in aerobic biological systems it is essential for the cells to receive oxygen constantly. If the local area surrounding a cell becomes deficient in oxygen because the rate that the cell is consuming oxygen is greater than the rate at which new oxygen is being delivered by mixing, then the cell will die for lack of oxygen and the process is compromised.

In the system studied in this work, the chemical additive is injected at the top of the vessel, above the first impeller. If the system is said to be mesomixing controlled, then there is a detrimental effect due to a plume of feed forming. The mesomixing time can be estimated as (Patterson et al., 2004):

$$t_{meso} = \frac{Q_i}{UD_T}$$

Which is based on the feed rate of the injected demulsifier Q_i the bulk velocity of the surrounding fluid U , and the local turbulent diffusivity D_T . In order to avoid plume

formation the mesomixing time should be less than 20% of the micromixing time (Anthieren, 2003).

The formation of a plume of high concentration of additive is expected to contribute to unexpected consequences relating to local conditions: for example, the additive may self-associate upon introduction into the larger system, or attach to its intended substrate in greater quantities than desired. Because the chemical used in this work is proprietary, we do not speculate further on the exact mechanism.

Instead, the feed rate is controlled to avoid plume formation. The derivation of a suitable feed rate has been determined for this system (Chong, 2013) and is discussed in more detail in Section 3.1.3.

1.3.4 Effects of Mixing on Demulsifier Performance

Previous studies in the mixing group at the University of Alberta have uncovered the importance of mixing to demulsifier usage in bitumen froth treatment. Laplante (Laplante, 2011; Laplante et al., 2015) designed the test vessel and showed that bulk concentration of demulsifier is the dominant variable but favourable mixing conditions – energy dissipation, mixing time, and injection concentration – allows for optimizing performance in diluted bitumen. This work also showed that solid removal is a function of water removal, and that results from shaker tables did not compare well to the mixing test cell.

The next set of work (Chong, 2013; Chong et al., 2016; Leo, 2013) generalized this finding by proving that the same mixing effects also impacted performance of a different demulsifier in dilbit. Chong's work also extended the experimental protocol to bitumen froth (in this case, froth with high solids content) and found that the same effects were present, and found that better performance was achieved through altering the mixing order. Chong found that good mixing was required to overcome the effects of overdosing. Leo pioneered the use of image analysis to detect circular water droplets

in micrographs of samples taken from dilbit experiments. Arora (Arora, 2016; Arora et al., 2015a) used average quality froth (approximately 60% bitumen, 30% water, and 10% solids) and found that mixing effects were again important. Water droplets in this system were not confined to single spherical droplets but were often larger, non-spherical, and collected into flocs.

1.4 Experimental Apparatuses and Techniques

1.4.1 In-Situ Particle Measurements in Liquid-Continuous Systems

Chen et al. (2015) established the feasibility of using focused-beam reflectance measurement (FBRM) on-line to measure droplet size – in the form of chord lengths – in reconstructed water in oil petroleum emulsions and used it to quantify factors influencing size distribution using an ethyl cellulose demulsifier.

Boxall et al. (2010) utilized both particle-video microscopy (PVM) and FBRM in water-in-crude-oil emulsions. Using the PVM and ImageJ, a free image manipulation program, to perform image analysis, they found that the FBRM vastly undersized the droplets in comparison, even after accounting for the difference between a chord length and a diameter. They suggested a quadratic correlation to give reasonable agreement (to error < 20%). They also found that the shape and magnitude of the measured droplet size distribution were independent of dispersed phase fraction between 10-20 vol%. This was true for size distributions from both the PVM and FBRM.

The FBRM and its working principles are discussed in more detail in Chapter 2.

1.4.2 The Confined Impeller Stirred Tank

The confined impeller stirred tank, or CIST, was first developed in diluted bitumen settling experiments and termed a shear and sedimentation test cell (Laplante, 2011). It is a mixing tank with a high height-to-diameter ratio of 3 and multiple impellers (5-6). The goal of its design was to provide a small-scale vessel with more volume in active circulation and a more uniform turbulence dissipation (Machado and Kresta, 2013) while maintaining enough height relative to volume to resolve settling trends (Laplante, 2011). In a conventional stirred tank, the energy dissipation can vary at different locations by a factor of up to 100 (Zhou and Kresta, 1996), and up to one third of the tank volume is not in active circulation (Bittorf and Kresta, 2000). When scaling down for lab tests of industrial operations, this is potentially a significant problem. The Reynolds number for the flow generated by an impeller is calculated as follows:

$$Re_{imp} = \frac{\rho ND^2}{\mu}$$

Wherein ρ , N , D , and μ are, respectively, the fluid density, impeller speed, impeller diameter, and fluid viscosity. At the large scale, Reynolds numbers are several orders of magnitude higher so even far away from the impeller there is turbulent flow. Scaling down with geometric similarity, the Reynolds number falls with the square of diameter, leading to a lower Reynolds number at the impeller and transitional or laminar flow away from the active zone. The CIST allows for turbulence throughout the tank at a Reynolds number 10x less than a conventional stirred tank (Machado and Kresta, 2013). At the lab scale, an impeller Reynolds number of more than 300 000 was required for fully turbulent flow in the top third of the conventional stirred tank (Machado et al., 2013). Active circulation is important especially at the surface, where chemical is often added. If this region is not in active circulation, then chemical added at the surface can linger in a plume of high local concentration rather than mix into the bulk volume.

The flow field in the CIST was characterised using laser Doppler anemometry for three different impeller geometries – Lightnin A310 and Rushton turbines, and Ekato Internig turbines (Machado and Kresta, 2013). The middle impellers showed identical behaviour with similar impeller properties such as the power number (N_p), momentum number (Mo), and volumetric flow number (N_Q), suggesting there is scope to reduce the height of the CIST even further while maintaining the properties that make it useful for study in scale-down.

1.5 Settling and Combination Mechanisms

Settling is the mechanism whereby water and solids are ultimately removed from bitumen froth. Because larger droplets and flocs settle faster, bringing species together through combination is key to finding success in settling operations.

Long et al. (2002) studied the settling rates in both NFT-type and PFT-type systems by monitoring the phase interfaces and fitted their findings to the Richardson and Zaki settling correlation. Kirpalani & Matsuoka (2008) modelled the settling process in bitumen froth, considering hindered settling due to high dispersed phase loading. Long et al. (2004) later studied the effect of mixing temperature on aggregate structure and settling rate in a system with precipitated asphaltenes.

Due to unexpected and difficult-to-characterize settling behaviour in low-quality bitumen froth that was observed during the course of this work, a full assessment of the various settling and combination methods which were deemed likely to be present in this system is carried out below. Figure 1-2 summarizes these mechanisms visually before they are explored in this section:

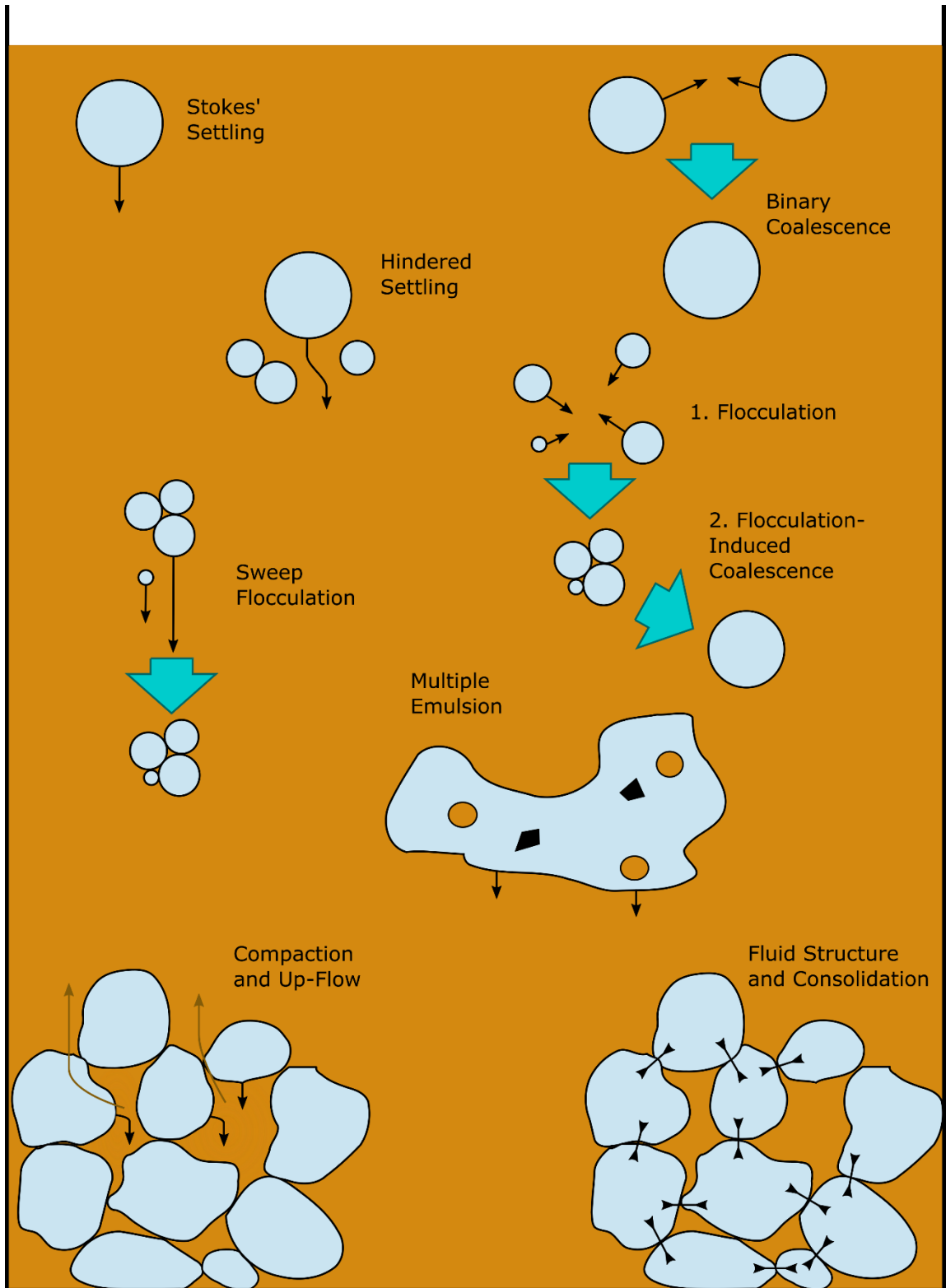


Figure 1-2: Schematic of Proposed Settling and Combination Mechanisms

1.5.1 Stokes' Law and Hindered Settling

The beginning of any discussion of settling is Stokes law (Stokes, 1850), which describes forces on a particle settling in the laminar regime in an infinitely dilute fluid:

$$F_D = 3\pi\mu d_p u$$

μ is the fluid viscosity, d_p is the diameter of the particle of interest, and u is its settling velocity. By considering the forces of gravity and buoyancy, the terminal settling velocity of a single hard sphere in an infinite fluid becomes:

$$u_0 = \frac{\rho_p - \rho_f}{18\mu} g d_p^2$$

Wherein ρ_p and ρ_f are the densities of the particle and the fluid, respectively, and g is the gravity constant. The key assumption implicit in Stokes law is that the particle in question is settling in an infinitely dilute fluid and thus is not influenced by nearby particles. Models which take into account the increased resistance to settling that is caused by nearby particles are usually termed hindered settling. As more particles are added to the system, the displacement of continuous fluid caused by settling increases the relative velocity experienced by the settling particle of interest. Many empirical correlations have been derived to accommodate for the increased resistance to flow. One is the Richardson and Zaki equation (Johnson et al., 2016; Seville and Wu, 2016):

$$u = k u_0 \phi^n$$

Where the hindered settling velocity is a function of the Stokes' settling velocity, a dimensionless multiplier k , the void fraction ϕ , equal to $1 - C_v$ (the volumetric concentration of particles), and the exponent n which is a function of the single-particle Reynolds number. A notable feature of this correlation is that the effect of solids concentration is high at low Reynolds number (Seville and Wu, 2016). Another alternative is the exponential empirical Vesilind equation:

$$u = k u_0 e^{-n\phi}$$

Spherical particles are often assumed for all the above correlations. However, the non-spherical nature of settling aggregates can be captured empirically by using modified exponents for the Richardson-Zaki equation (Kirpalani and Matsuoka, 2008; Long et al., 2002).

1.5.2 Binary Coalescence

Coalescence in a liquid-liquid system is the combination of two or more droplets combining to form a larger droplet. This larger droplet will settle faster than the small droplets. Coalescence occurs due to droplet collision, when droplets collide in a moving carrier fluid. In practice, if droplet collision leading to fast coalescence is the only mechanism of particle interaction, then the probability of more than two droplets colliding is vanishingly small, and binary coalescence dominates. Binary coalescence can occur as a result of bulk flow, as in a flowing pipe or a mixed tank, or when droplets rise in creaming or settle due to gravity (Leng and Calabrese, 2004). Analysis of binary coalescence is usually divided into two terms: the *collision frequency*, or how often droplets come into contact, and the *coalescence efficiency*, which is the probability that a collision leads to a coalescence event (Leng and Calabrese, 2004). The collision frequency is a function of the concentration of the dispersed phase and the flow field. Coalescence efficiency can depend on many factors, including on the force of collision, the cleanliness of the interface, and the angle of collision (Leng and Calabrese, 2004).

1.5.3 Flocculation and Flocculation-Assisted Coalescence

Flocculation is the aggregation of particles into closely associated groups which are easier to remove (Crittenden et al., 2012). Instead of combining to form one large droplet, as in coalescence, droplets or particles come together to form a floc, a collection of species that binds together without combining into one larger droplet. Flocs

may also settle faster than their constituent droplets and particles due to their larger size. Flocculation is enhanced by flocculant aids, usually organic polymers that encourage flocculation and favour properties that improve settling or creaming and filtration (Crittenden et al., 2012; Masliyah et al., 2011). Crittenden et al. (2012) distinguish between two types of flocculation: (1) *microflocculation*, or *perikinetic flocculation*, in which Brownian (random, thermal) motion of particles flocculates particles, and (2) *macroflocculation*, or *orthokinetic flocculation*, in which flocculation is effected by local velocity gradients (i.e. a flow field). Differential settling of particles or flocs can also bring particles, droplets, or flocs together to flocculate further (Crittenden et al., 2012).

Coalescence following flocculation or flocculation-assisted coalescence is described or tacit in numerous studies, including in froth treatment (Chen et al., 2015; Kokal, 2005). Prolonged contact between droplets obviates the need for a “successful” collision – i.e. a collision leading to fast coalescence – to bring about the coalescence of two droplets. Instead, two or more droplets which are already flocculated can slowly come together to eventually form one larger droplet. Since this is a slow process and perhaps due to the mechanical properties of the protective skins it is possible to observe intermediate states: Arora (2016) captured several partially-coalesced droplets in average-quality bitumen froth.

1.5.4 Sweep Flocculation

Also called enmeshment, sweep flocculation is the capture of particles by larger amorphous precipitates (Crittenden et al., 2012). The sweeping action can be effected by differential velocities in the flow field or faster settling of a large floc compared to a smaller particle or droplet. Colloidal droplets or particles – droplets or particles that would normally remain in suspension due to their small size – can be swept up in this

fashion and become a part of the capturing floc. Thus droplets or solids that would normally remain in suspension can be removed by sweep flocculation.

1.5.5 Compaction and Up-Flow

A tightly-packed collection of particles, droplets, or flocs with continuous phase in between will continue to settle due to their weight. This is obviously quite different from a freely settling particle in the Stokes regime or even a particle under hindered settling. The particles are already sitting on top of and amongst other particles. They will shift around and gradually move toward a tighter packed configuration and the interstitial fluid displaced by this shuffling will flow upward in settling operations (Crittenden et al., 2012). The effect due to this “compaction zone” is often neglected in models (Kirpalani and Matsuoka, 2008) but becomes increasingly important as the fraction of water and solids increases. When there is large effect due to compression or compaction, the flow field will change due to the up-flow caused by displacing particles and this must be considered in the analysis.

Kirpalani & Matsuoka (2008) further detail the packing process. Important parameters in a porous bed are the porosity and permeability of fluid, which in turn depend on the initial settling which produced the bed and the weight of solids above. Compaction was not identified in previous studies with average-quality bitumen froth (Arora, 2016; Chong, 2013). However, due to the higher water and solids content and some unexpected behaviour encountered in low-quality froth, it is important to consider this compaction as possibly an important mechanism.

1.5.6 Fluid Structure and Consolidation

In the processing of oil sands tailings, researchers study the presence of a structure to the fluid arising from inter-particulate interactions; this may also be called consolidation

in a settling context (Kasperski, 1992). Though fluid structure and consolidation phenomena are not typically discussed with reference to bitumen froth, it may become more necessary with lower-grade ores being processed.

Muñoz et al. (2003) studied the morphological properties of bitumen which reported to tailings; no matter the source, they were distinguished by complex structures that also included water and solids and morphologies which tended to trap other components. They also introduced the concept of *degraded bitumen* to cover changes in bitumen chemistry which contribute to difficulty in processing. This includes problem oil-sands ores, which are the source of the low-quality bitumen froth studies in this work.

Chapter 2: Focused-Beam Reflectance Measurement

2.1 Overview

Focused beam reflectance measurement, or FBRM, is the name for a series of probes which operate on the same principle. The probe directs a laser into the fluid and then the laser rotates so that the scan path is a small circle in the fluid. The probe measures the amount of light that is backscattered by the fluid and particles therein. When the laser moving along the scan path crosses a particle or droplet the amount of backscatter changes, and this is interpreted as a “chord length.” A chord length is distinct from a diameter because even on a circular droplet or particle the laser path is not likely to cross at exactly the location of the diameter. Instead, the chord length is measured wherever the laser crosses. Its maximum size on a spherical particle is the diameter. While there is theoretically no lower limit to the chord length, chord lengths much smaller than the diameter are much less likely to be detected on a spherical particle. This is because the chord length drops off quickly with the radius at which the chord is detected. Even at a radial position of 0.9 of the radius of the circle the chord length is more than 40% of the diameter, as can be visualized in Figure 2-1 below. If it is equally likely to read a chord from anywhere along a given radial line segment of the circle, then the chances of reading a chord less than or equal to some fraction of the diameter can be calculated and is given in Table 2-1:

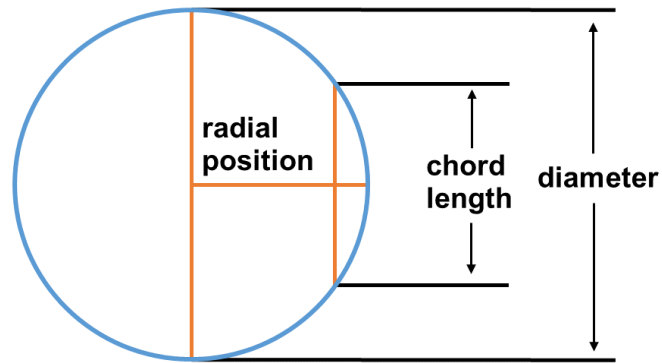


Figure 2-1: Circle showing chord length compared to radial position and diameter

Table 2-1: Probability distribution of chords according to radial position

Chord Length	Probability that Chord Length is Greater Than	Probability of Reading Chord Length is Less Than
0.9r	43.6%	56.4%
0.75r	66.1%	33.9%
0.5r	86.6%	13.4%
0.25r	96.8%	3.2%
0.10r	99.5%	0.5%

The laser moves along its circular path moves fast (2 m/s) compared to other velocities in the tank and the length of the scan path is very large compared to the size of the particles, so the software reads many chord lengths, groups them into various size bins, and reports them as a histogram. The curvature of the scan path is also negligible over the diameter of the particles. The chord lengths are collected and reported every 10 seconds, so each chord length distribution represented the laser rotating and collecting particle data for 10 seconds.

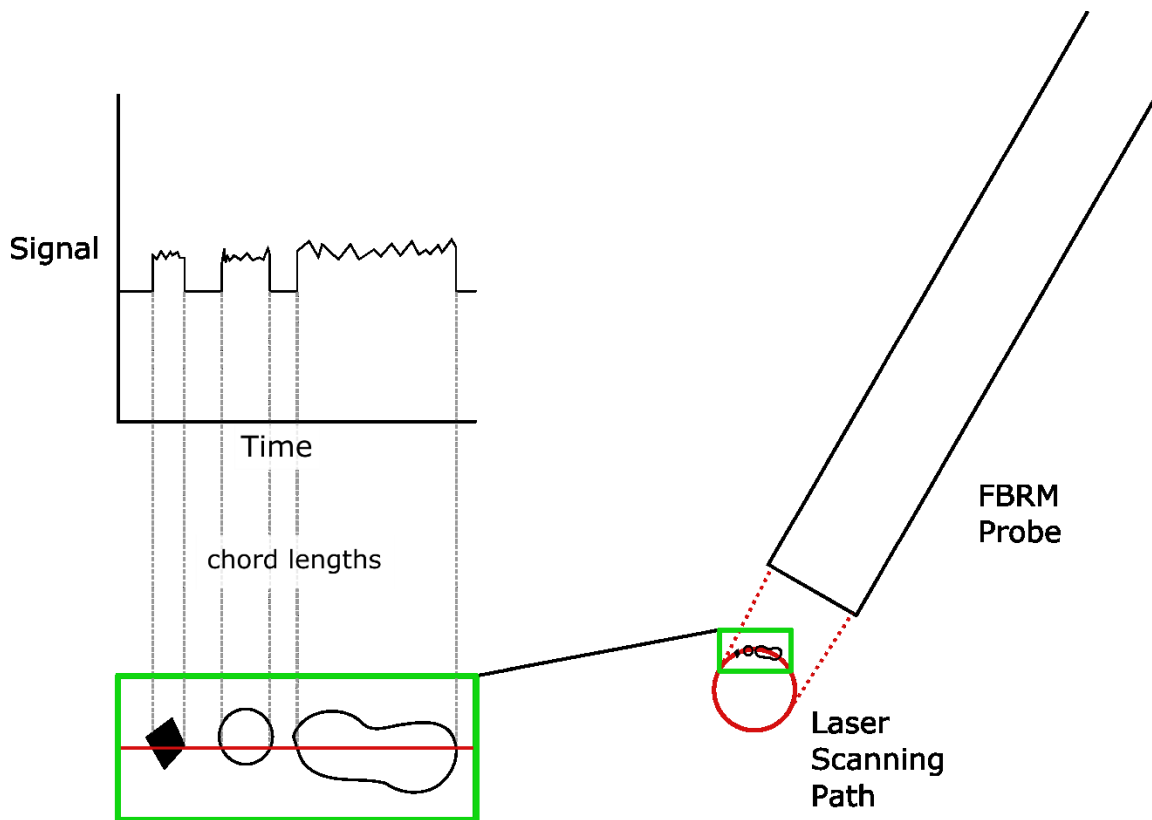


Figure 2-2: Schematic of operating principle of FBRM (adapted from video by instrument supplier (Mettler Toledo 2016))

The probe used for these experiments was the 14 mm G400 probe.

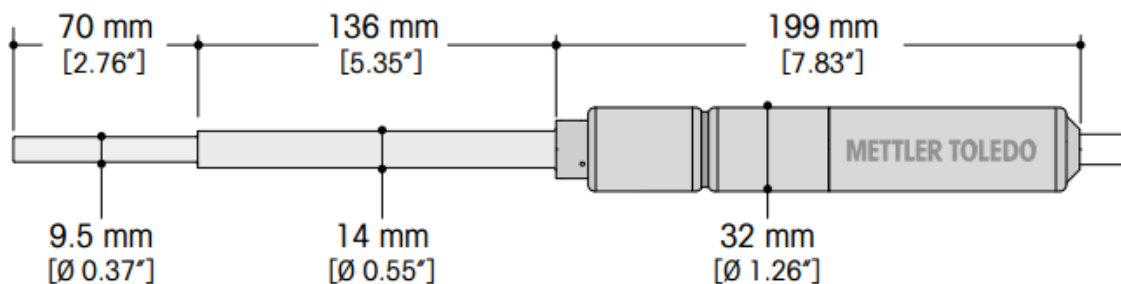


Figure 2-3: 14mm G400 FBRM Probe (Mettler Toledo, 2013)

The wetted length is the length to which the probe can be inserted into a liquid before there is significant risk of liquid ingress that may damage the probe. The wetted length on the G400 probe is 206 mm, corresponding to the two leftmost sections of the probe,

seen on Figure 2-3. The probe is made of Hastelloy C22, which is very resistant to corrosion.

Crucially, the FBRM does not provide an absolute picture of the chord length distribution in the whole vessel, but rather a snapshot over the small space covered by the circular path of the laser during the ten seconds that it collects data. The data it collects is thus sensitive to the distribution of particles in the vessel. Mettler Toledo recommends placing the FBRM probe in a flow field, facing the main direction of flow but angled at 30-60°. This keeps the particles moving past the window so that the effect of stuck or stagnant particles does not bias the results considerably.

The FBRM software has two different modes for processing the signal obtained from the laser. In Primary mode, the signal is more likely to be interpreted as a greater number of small particles, since small dips in the signal will be interpreted as the boundary between two particles or droplets. In Macro mode, a small dip in the signal is instead passed over, thus reading one larger droplet rather than two or more smaller ones. Macro may be chosen if there are surface imperfections which could lead to false divisions or if the refractory index of the two fluids is similar. For this analysis, Primary mode was chosen because it was thought that due to the highly-loaded system (13% solids, 37% water) the Macro signal processing may lead to a high number of coincidental associations between particles being read as single particles.

2.1.1 Size Distributions and Weighting

It is common in particle or droplet systems to give a particle size distribution (PSD, usually in solid-liquid systems), crystal size distribution (CSD, in precipitation systems) or droplet size distribution (DSD, usually in liquid-liquid systems). In the case of data from the FBRM, it is not the diameter of a component that is measured, but the length of the path where the laser crosses the particle. This is called a chord length, and so the FBRM instead gives a chord length distribution (CLD), which could include the chord length of

primary droplets, primary particles, or aggregates, depending on the nature of the signal captured by the FBRM and the signal processing chosen.

Since a median or mean is often inadequate to describe or predict the behavior of a system, instead particles or droplets are grouped into some number of bins by size and counted. These bins can be graphed to form a histogram in cases where there are few bins. When there are more bins, often the size distribution is instead shown as a continuous function and normalized, so that the total area under the plot is 1, and the chance of a randomly selected particle being between two sizes is the area under the function between those two sizes.

Instead of a size distribution or as complement to it, there are alternative means that capture the effect of larger particles. Other techniques are necessary because often small droplets or particles, called fines, are present in systems in numbers that dominate the arithmetic mean, median, or mode. The Sauter mean diameter is a commonly used mean measure, and is defined as the diameter of a sphere which has the same volume to surface area ratio as the whole range of particles or droplets. It also called the d_{32} , and is calculated by:

$$d_{32} = \frac{\sum d_i^3}{\sum d_i^2}$$

Where d_i is the diameter of the i th particle and the summation is done over all particles. Often the collection of lengths is discretized, in which case the equation takes the form:

$$d_{32} = \frac{\sum n_i d_i^3}{\sum n_i d_i^2}$$

Wherein n_i is the number of particles in the i th bin and d_i is the approximate length every particle in that bin. The Sauter mean diameter is useful in many chemical engineering applications because it characterizes the ratio of volume to surface area of a distribution: volume is the amount of a chemical, while the surface area dictates the exposure to dispersed fluid and thus the mass transfer rate.

The whole distribution can be weighted as well. Just as the arithmetic mean can be dominated by fine particles, so too can the size distribution. To reemphasize the role of larger particles, the size distribution can be weighted by the protocol detailed in Section 2.1.1, found in the FBRM help file and utilized by the FBRM software, iC FBRM:

2.1.2 Bin Weighting Protocol

A bin (or channel) is defined by a size range (1.62 – 1.74 μm , for example) and the quantity (also called the “count”) of measurements that are between those two sizes. A weighted bin has the quantity rescaled with some weighting factor w_i :

$$y_i = w_i n_i$$

Where y_i is the weighted count of bin i , while n_i is the original, unweighted count. In the FBRM software provided by Mettler Toledo and in the chord length distributions presented in this thesis, the weighting factor is obtained using the midpoint M_i of the channel:

$$w_i = \frac{M_i^\gamma}{\sum_{j=1}^N M_j^\gamma} N$$

Where γ is the desired weighting factor and N is the total number of bins. M_i is the midpoint size of the bin: for example, if the bin contains all chord lengths from 1.62 μm – 1.74 μm , then the midpoint is 1.68 μm , and the chord lengths in this bin are all approximately equal to the midpoint. A weighting factor of 2 is used for this thesis, and can be considered somewhat analogous to an area weighting. However, since the system is not made up of spheres, and chord lengths are not equivalent to diameter, calling this weighting “area-weighted” is not strictly correct and so the term “square-weighted” is preferred. The result is a distribution that shows more focus on larger particles and droplets.

2.2 Challenges

The FBRM presented several challenges to its use in collecting data. Many of these challenges stemmed from the fluid itself: unsurprisingly, some components of the complex fluid mixture tend to adhere to the probe window and change the results. This necessitated a treatment, and two different treatments were tried and are described below.

2.2.1 Fouling and Sapphire Surface Treatment

The optical window of the probe is optical sapphire. Like glass, the sapphire mineral structure presents a hydrophilic surface to which water droplets can adhere. If water droplets or solid particles adhere to the sapphire window of the probe, they can skew the results by being counted multiple times by the passing laser and artificially inflating the counts in the size bin to which the stuck particle belongs.

The Mettler Toledo software includes a metric of this effect that can be monitored: the so-called fouling index. The fouling index compares the signals from two consecutive passes of the scanning laser to determine how much of that signal is the same from one reading to the next. A signal that is the same from one reading to the next would indicate that there are stuck particles. With no treatment, the fouling index can quickly escalate, as seen in Figure 2-4 below. 5 minutes into the experiment, the fouling index is over 80%, meaning that the window is approximately 80% covered in stuck particles or droplets. Shortly after, it is over 95%. This is despite the impellers running for much of this experiment. Obviously, this will not give useful data for analysis.

Luckily, treatments are available to reduce the tendency of both water- and oil-wetting components to adhere to the probe window. One such treatment was provided by Aculon. After applying this treatment to the probe window, the fouling index dropped considerably, from readings over 80% to readings in the range of 20-40%, as demonstrated below. This is still much higher than the fouling index seen in other

systems such as simple solid-liquid or liquid-liquid systems, but the surface treatment makes it feasible to collect useful data during mixing and sedimentation. As the group gathers knowledge on best practices for the application of this treatment, the effective fouling index may be reduced further.

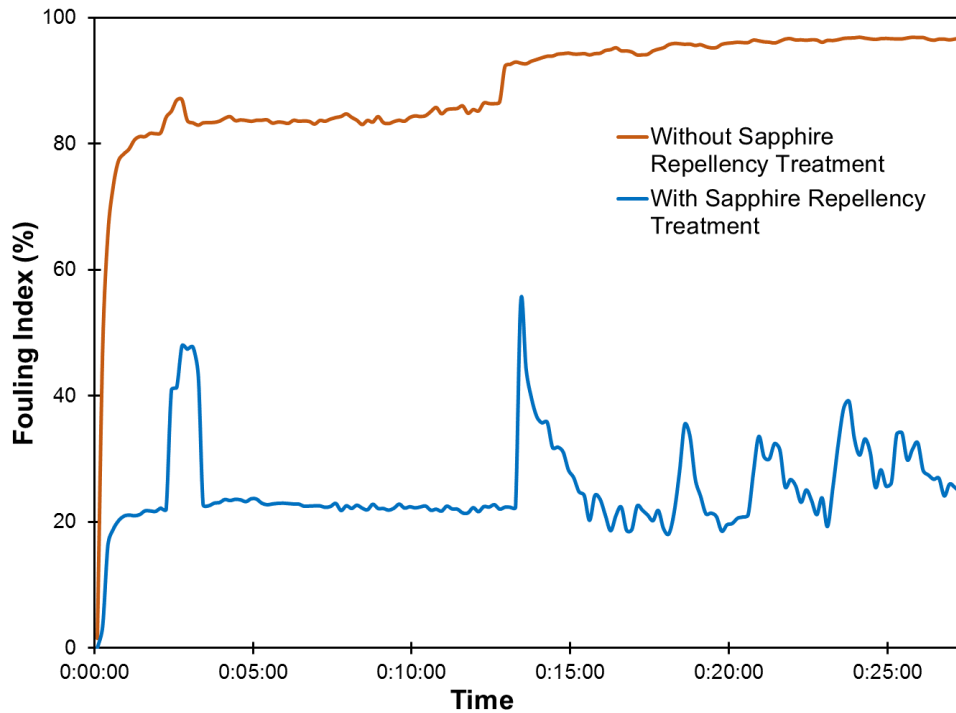


Figure 2-4: Effect of sapphire repellency treatment on probe fouling

In addition, the software includes an option for stuck particle correction. Up to a fouling index of about 10%, stuck particle correction will simply not count signals that are equal from one reading to the next. This way one can continue collecting data knowing that stuck particles are accounted for. This can still introduce some bias into the experiment, for example by reducing the total number of counts (since some of the signal is not being used), which is the reason it is capped at 10%.

Even with treatment, the fouling index can rise to very high levels, as can be seen in the Figure 2-5 below. The peak in fouling index corresponds to the time when the impellers stop at the end of the demulsifier dispersion and the beginning of the settling stage. Both the counts of fines and the fouling index then trend generally downward before

reaching a minimum and then climbing back up. Note that during settling there is very minimal flow past the FBRM probe window. There is no impeller-induced flow, only the flow created by the various settling dynamics in the vessel. It is not surprising to see a rise in fouling index, and a corresponding rise in the counts of fines.

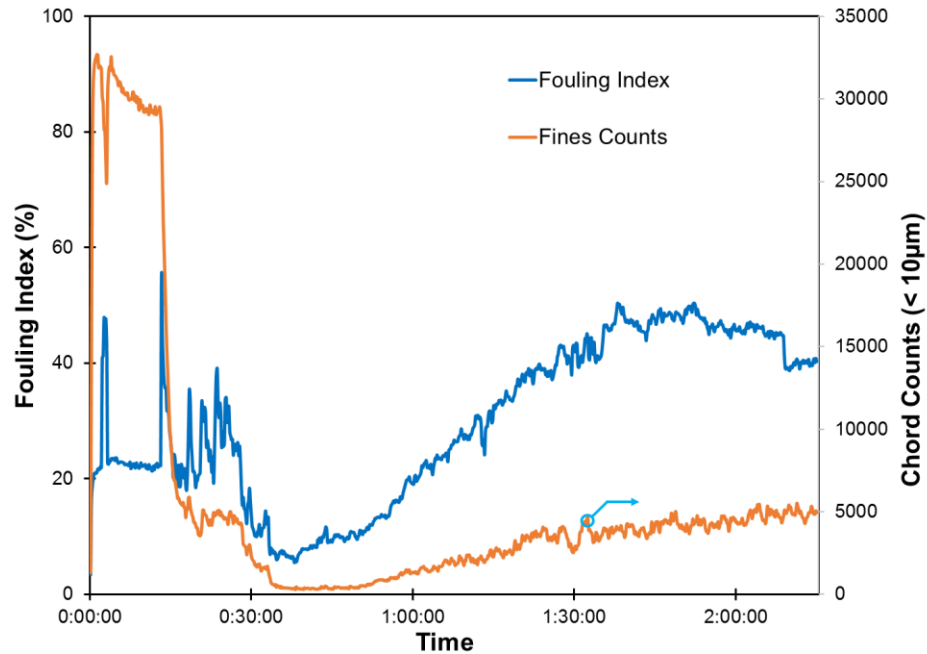


Figure 2-5: Fouling index for a full experiment

It is difficult to imagine a sudden reversal in the general downward trend of fines count is for any reason except the gradual accretion of fines on the probe window or the stagnation of fines in the fluid in front of the window. The flow is inadequate to keep fluid moving past the window and not allowing many particles to get stuck. For this analysis, the data is truncated after 30 minutes of settling to avoid making false conclusions based on this artefact.

From experience gained in the first experimental campaign, we recommend reapplying the sapphire repellency treatment after 2 experiments or anytime the probe has been used in a different fluid. If the sapphire treatment is applied and the fouling index is very high (above 1000 or so), we recommend polishing it off and reapplying.

2.2.2 Silanization Surface Treatment

Before using the sapphire repellency treatment provided by Aculon, another treatment was tried. This treatment was the application of the same chemical used for treating microscope slides and sample needles, as described in Chapter 3.

Dichlorodimethylsilane is comprised of a silicon atom centre, with a tetrahedral arrangement of single bonds: two hydrophobic methyl (-CH₃) and two highly-reactive chloride (-Cl) groups. Applied to glass, it attacks the silicon oxide layer and replaces it with a hydrophobic layer which repels water droplets.

Applying this treatment to the FBRM probe is not recommended. Due to the strength of its bond – the chemical covalently bonds to the mineral structure in the case of glass – it can be difficult to remove. The application of a piranha solution cleaning procedure to remove it was thought to damage the passivating layer on the Hastelloy C22, leading to corrosion of the probe during later use. It is possible that other procedures to remove the hydrophobic layer would not cause this problem, such as simple polishing or ultraviolet treatment, but these were not tried due to the convenience of the Aculon treatment.

2.3 Chord Length Distribution

A chord-length distribution is related but not identical to more well-known distributions such as the droplet-size distribution (DSD), particle-size distribution (PSD), or crystal-size distribution (CSD). According to Bloemen & De Kroon (2005) this different distribution can be managed in one of two ways:

- a) If the connection between the particle size is not well understood, the process outcome of interest can be related empirically to some component of the chord-length distribution.

- b) If there is already a connection between the particle size and the system property or properties of interest one can transform the chord length distribution into a better-understood distribution.

The authors then go on to propose one such transformation using a least squares method.

As this work represents the first exploration into using the FBRM to probe the dynamics of bitumen froth settling, there was no attempt take an approach of type b for bitumen froth. The chord length distribution is taken as is. By observing patterns in the data, hypotheses can be made about the dynamics. These hypotheses can be tested later when there are more data collected with the FBRM.

Chapter 3: Experimental Setup

The experimental setup and protocol used for the campaigns in 3.4 and Chapter 5 have evolved over the course of several generations of research into the form they have reached for this thesis. The Confined Impeller Stirred Tank began as the Shear and Sedimentation Test Cell and was used to test the effects of mixing on demulsifier usage in diluted bitumen (Laplante, 2011). Chong (2013) tested a different demulsifier to generalize the findings of the previous study, and began to test bitumen froth, a more complex fluid. Leo (2013) developed an image analysis protocol based on the spherical droplets of water in diluted bitumen. Arora (2016) started with this protocol but expanded it to account for non-spherical water droplets, solid particles, and aggregates. This new analysis protocol, called a Clustering Algorithm, was used to analyze settling in average-quality bitumen froth. A major redesign of the vessel was undertaken to enable side sampling, reducing error and making the experimental protocol easier (Arora, 2016; Arora et al., 2015b). More improvements to this procedure were made over the course of this research, including:

- Instead of pre-weighing bitumen froth, an excess is prepared. The weight of bitumen froth and therefore the naphtha to bitumen ratio was instead controlled using the weight of the naphtha. The naphtha is poured into the CIST, then the bitumen froth is poured in until the vessel is full. Pre-weighing the bitumen froth can lead to very high N:B ratios, since bitumen froth tends to adhere to the sides of its storage vessel, leading to lower-than-expected amount of froth being added, high N:B ratio, and an underfilled vessel, which are all sources of variation to be avoided if possible.
- Plastic disposable syringes are used for making microscope slides. Previous studies used glass syringes that were treated with dichlorodimethylsilane to render them hydrophobic. The concern was that water droplets would adhere to

the hydrophilic glass surface in the glass syringe. By using a plastic syringe the same result is achieved with less experimental preparation.

- The lid assembly was changed to accommodate the use of the FBRM (focused beam reflectance measurement) probe.

3.1 Procedure

The general procedure for the experiments in 3.4 and Chapter 5 is outlined below:

Step 1: Pre-Mixing

- Naphtha and bitumen froth heated in bath
- Bitumen froth mixed to resuspend solids and water

Step 2: Naphtha Blending

- Naphtha then bitumen froth poured into CIST
- Fluids blended with same energy every trial

Step 3: Demulsifier Dispersion

- Impellers started then demulsifier injected
- Demulsifier blended into mixture
- Mixing energy, injection concentration (pre-dilution), and bulk concentration (dosage) varied

Step 4: Settling

- Impellers turned off and water and solids allowed to settle
- Samples taken

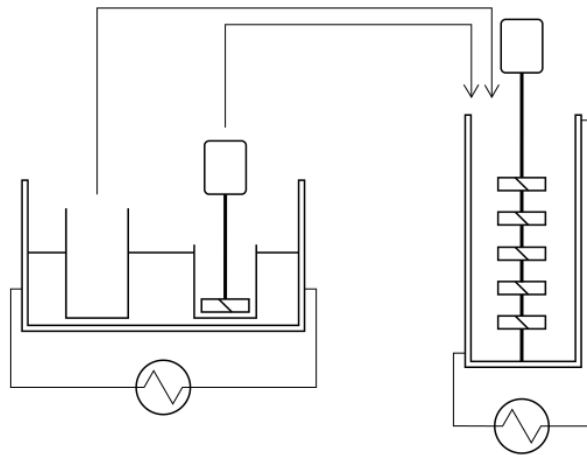


Figure 3-1: Schematic of Experimental Setup and Procedure

Low-quality bitumen froth from the froth treatment process at Syncrude Research was used. Unlike average-quality froth, which is approximately 60% bitumen, 30% water, and 10% solids, low-quality froth is approximately 50% bitumen, 37% water, and 13% solids. The demulsifier used was provided by Syncrude Research and comes from Champion Technologies at a concentration of 35 wt% active ingredient. It is diluted to the level required for each experiment.

Table 3-1: Properties of low-quality bitumen froth

Bitumen Content (wt%)	48.8 - 50.3
Water (wt%)	36.0 - 39.2
Solids (wt%)	11.4 - 13.6
Viscosity (cP)*	5900 - 1100
Density (kg/m ³)**	1138.1

* At 60°C and 80°C, respectively. Estimated using Eq. 6.1 in Khan (2011)

** (Chong, 2013)

The experiment is separated into 4 distinct stages:

3.1.1 Pre-Mixing

Before the experiment day, cans are filled with bitumen froth to a high level and stored upside down so that solids and water can move to the top of the can where they can be more easily re-dispersed.

This 1L paint can is heated to 80°C and mixed using a pitched-blade turbine impeller and a custom lid fitted with 2 baffles set at 90° to each other. The purpose is to re-suspend any settled water or solids to provide consistency between runs, and to provide a worst-case scenario of maximum homogeneity and no bulk phase separation. During premixing, naphtha is heated without mixing in the same glycol bath. A pre-mixed sample of froth is collected with a small spoon for dilution and Karl Fisher titration. No bitumen froth is collected for microscopy, since bitumen froth before dilution is too opaque.

Table 3-2: Premixing mixing geometry and parameters

Impeller	45° Pitched Blade (down-pumping)
Tank Diameter (m)	0.1
Impeller Diameter (m)	0.06
Off Bottom Clearance (m)	0.02
Impeller Speed (rpm)	1000
Reynolds Number	11 - 61
Mixing Time (min)	15

3.1.2 Naphtha Blending

Naphtha in the amount required to attain a naphtha-to-bitumen ratio of 0.7 is poured into the test vessel for naphtha blending. The bitumen froth is poured by hand with thermal protective gloves into the test vessel until full.

The FBRM is set up and inserted before the beginning of naphtha blending. The experimenter begins recording data on the software just before starting the impellers.

The two fluids are blended under the mixing conditions detailed in Table 3-3. The mixing conditions in this stage are designed to be as similar as possible between runs. However, different impellers necessitate varying motor speed to keep energy input constant. Mixing time is also held constant. One sample is collected at the end of naphtha blending for Karl Fisher titration and microscope analysis.

Table 3-3: Naphtha blending mixing geometry and parameters

Impeller	Intermig	Rushton
Number of Impellers	6	5
Impeller Diameter (m)	0.05	0.038
Impeller Speed (rpm)	1060	600
Liquid height (m)	0.225	0.225
Off-Bottom Clearance (m)	0.017	0.013
Submergence (m)	0.05	0.038
Tank Volume (L)	0.994	0.994
Tank Diameter (m)	0.0762	0.0762
Impeller Swept Volume (L)	0.168	0.0431
Power Number per Impeller*	0.63	4.2
Power per Mass (W/kg)	6.55	1.67
$P/\rho V_{IMP}$ (W/kg)**	38.77	38.61
Reynolds Number	7240	2367
Mixing Time (min)	2	2
Mixing Energy (J/kg)	4652	4633

* extrapolated from data in Machado and Kresta (2013)

** power per mass in the impeller swept volume

3.1.3 Demulsifier Dispersion

Figure 3-2 depicts the relative positions of the FBRM probe, feed tube, liquid level, and impeller submergence. The impeller submergence shown is that of the 5 Rushton impellers. Despite the extra impeller, the submergence with 6 Intermig impellers is more, due to the decreased distance between impellers (see Table 3-6 below).

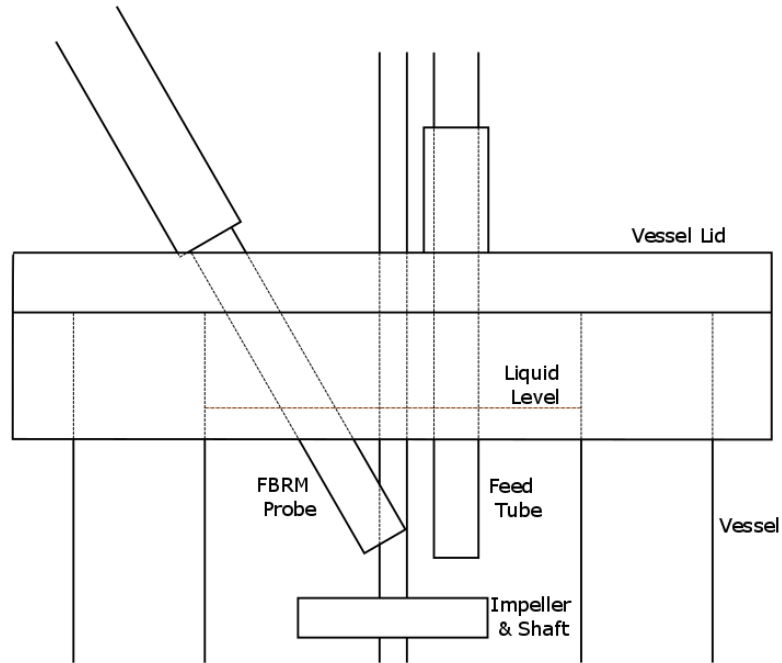


Figure 3-2: Detailed scale drawing of FBRM probe and feed tube placement in vessel

The demulsifier is provided by Champion and called X-2105; it is the same used in previous studies by Chong (2013; 2016) and Arora (2016). The demulsifier was provided at 35 wt% active ingredient and diluted with pure xylene to the desired injection concentration (12 wt%, 16.5 wt%, or 21 wt%), or IC.

Demulsifier is injected with a syringe pump and tubing and mixed into the fluid. The injection location was kept constant: 30 mm below the liquid surface and radially halfway between the centre of the vessel and the wall ($r/R = 0.5$). The injection rate of demulsifier is determined by its dilution and the local turbulence field at the point of injection. Chong (2013) derived the following equation to estimate the volumetric injection rate required to minimize meso-mixing effects:

$$Q_I = 0.54 \frac{\nu^{0.5} U_z d_{pipe}^{1.5}}{u'_z{}^{0.5}}$$

Where Q_I is the volumetric flowrate, ν is the kinematic viscosity of the surrounding fluid, and d_{pipe} is the inner diameter of the feed pipe. U_z and u'_z are the local mean and root

mean square velocities in the z-direction: the values used were determined by using laser Doppler anemometry (Komrakova et al., 2017). Some of the resulting feed rates for the first campaign (3.4) are detailed in Table 3-4, as well as injection volumes, which are determined by the bulk concentration (dosage) and injection concentration (pre-dilution). The syringe pump is only capable of controlling injection volume to the closest tenth of a millimetre.

Table 3-4: Selected demulsifier injection rates under varying mixing conditions (1st Campaign, Chapter 4)

BC (ppm)	Mixing Quality	Mixing Conditions	IC (%)	Injection Volume (mL)	Injection Rate (mL/hr)
204	Good	Rushton, 1000 rpm	12	1.7	634.7
171	Good	Rushton, 1000 rpm	12	0.9	634.7
193	Poor	Intermig, 400 rpm	21	0.9	125.1

For Chapter 5, the demulsifier injection rates and other mixing variables are detailed in Table 3-5. All experiments were done at 200 ppm, as determined in the first campaign (3.4).

Table 3-5: Demulsifier dispersion mixing conditions (2nd Campaign, Chapter 5)

Runs	Impeller	Mixing Speed (rpm)	Mixing Time (min)	Injection Rate (mL/hr)	Injection Volume (mL)
FA	Intermig	400	2	125.1	1.7
FB	Rushton	600	10	634.7	0.9
FC	Intermig	400	2	125.1	0.9
FD	Rushton	600	10	634.7	1.7
CP	Rushton	600	5.25	634.7	1.2

It is during demulsifier dispersion stage that the input variables are changed to determine their effects on the settling process. In 3.4, bulk concentration (or chemical dosage) is varied at good mixing conditions (high energy input, low injection concentration) to determine a reasonable bulk concentration for this froth sample. In

Chapter 5, bulk concentration (dosage) is held constant at 200 ppm while varying mixing variables (energy input J and injection concentration IC). One sample is collected 30s before the end of demulsifier dispersion for Karl Fisher titration (and microscope analysis in Chapter 5), and for analysis, this sample is considered $t = 0$ min of settling. Table 3-6 details the mixing geometry and conditions during demulsifier dispersion. “Poor Mixing” and “Good Mixing” refer to the two mixing conditions used in 3.4, while the two-letter codes refer to the treatments in Chapter 5.

Table 3-6: Demulsifier dispersion mixing geometry and parameters

Run Codes:	FA/FC/“Poor Mixing”	Centre Point (CP)	FB/FD/“Good Mixing”
Impeller	Intermig	Rushton	Rushton
Number of Impellers	6	5	5
Impeller Diameter (m)	0.05	0.038	0.038
Impeller Speed (rpm)	400	600	600
Liquid height (m)	0.225	0.225	0.225
Off-Bottom Clearance (m)	0.017	0.013	0.013
Submergence (m)	0.05	0.038	0.038
Tank Volume (L)	0.994	0.994	0.994
Impeller Swept Volume (L)	0.168	0.0431	0.0431
Power Number per Impeller*	1.5	4.2	4.2
Power per Mass (W/kg)	0.84	1.67	1.67
Power per Mass in Swept V	4.96	38.61	38.61
Reynolds Number	2732	2367	2367
Mixing Time	2	5.25	10
Mixing Energy (J/kg)	595	12161	23164

* extracted from data in Machado and Kresta (2013)

3.1.4 Settling

The impellers are turned off and the water and solids allowed to settle. Small samples (approximately 0.8 mL) are collected throughout the experiment and analyzed with Karl Fisher water titration to get a profile of water content vs. time. In 3.4, only one height was analyzed, while in Chapter 5, all 4 heights are sampled to create a vertical profile of water content over the settling time. The samples are also used for microscope analysis in Chapter 5.

3.1.5 Sampling Detail

Small samples are taken with the use of a metal sample needle, attached to a pipette tip with duct tape. A septum is seated on the inside of each sampling port, and allows the collection of samples through the side of the vessel without significant fluid leakage. The metal sample needles are required to pierce the septa, which reform around the hole when the needles are withdrawn. To prevent damage to the auto-pipette, the pipette tips have filters that prevent the bitumen from flowing back and contacting the auto-pipette.

The small samples are deposited in 20 mL glass vials. 3 mL plastic disposable syringes are used to collect a few droplets of sample for microscopy. Each microscope slide is treated with a 5 wt% solution of dichlorodimethylsilane in heptane which replaces the usual layer of oxide on the glass surface with a hydrophobic layer of methyl groups. This treatment is to minimize the effect of the hydrophilic glass, which may attract water groups, possibly leading to extra coalescence or flocculation events which are not representative of the dynamics in the system. Samples are withdrawn no more than 48 hours after collection then placed on treated microscope slides and covered with a regular glass cover slip.

At the end of each run, 100 mL samples are collected with a 100 mL glass syringe attached to plastic tubing that is marked with the desired depth and inserted through the top of the vessel. These samples are collected in 100 mL glass vials and stored in the refrigerator. At the end of the campaign all samples were sent to Syncrude Research for Dean Stark extraction (also referred to as OWS – oil, water, and solids) and Coulter particle analysis (CPA).

Table 3-7 and Table 3-8 below summarize all samples and other data collected for each experiment. All data is labelled with the run code and the data label. The times at which samples were taken were changed over the course of the first campaign. A complete list of these samples can be found in Table A-1 and Table A-2. Sample B is taken 30 seconds before the end of demulsifier dispersion, but it is assumed for the purposes of further analysis that this sample is the same as at the beginning of the settling step.

Table 3-7: Summary of Data Collection and Analysis, 3.4 Experiments

Data Label	Description	Collection Method	Location	Analysis	Number of Samples
P	End of Premixing	Small spoon	Just below the liquid surface	Karl Fisher titration	1
A	End of Naphtha Blending	Needle tip and pipette	Z1	Karl Fisher titration	1
B	End of demulsifier dispersion	Needle tip and pipette	Z1	Karl Fisher titration	1
Labelled with time (varies)	During settling	Needle tip and pipette	Z1	Karl Fisher titration	varies

The experimental campaign in Chapter 5 is more comprehensive in its sampling and analysis:

Table 3-8: Summary of Data Collection and Analysis, Chapter 5 Experiments

Data Label	Description	Collection Method	Location	Analysis Techniques	Number of Samples
P	End of Premixing	Small spoon	Just below	KF	1
A	End of Naphtha Blending	Needle tip and pipette	Z1	KF, Microscope	1
B (0 minutes)	End of demulsifier	Needle tip and pipette	Z1	KF, Microscope	1
5, 10, 15, 20, 25, 30, 45,	During settling	Needle tip and pipette	Z1, Z2, Z3 (up to	KF (all heights), Microscope (Z1-Z3)	36
DS-1, DS-5, DS-9	End of settling	100 mL syringe and plastic tubing	At z/H = 0.1, 0.5, 0.9	Dean Stark, Coulter Particle Analysis	3
FBRM	From naphtha blending to end	Probe	Below feed		1

3.2 Apparatus

3.2.1 Confined Impeller Stirred Tank (CIST)

The CIST was chosen for its well-characterized mixing and large height to diameter ratio. It is ideal for mixing characterization; the vessel has a much more uniform flow field than a conventional stirred tank or a beaker with a stir bar (Machado and Kresta, 2013). The height is three times the diameter; this tall format is ideal for settling experiments in which observing settling trends over multiple heights is required. The version of CIST used for this experiment also has a heating jacket through which ethylene glycol at 80°C is pumped, and 4 ports on the side for sampling. A Teflon spacer is inserted on the

bottom to secure the shaft. A baffle assembly with four baffles converts rotational flow into axial flow. The figure below depicts a rendering of the CIST showing the sampling ports and the heating jacket:



Figure 3-3: Rendering of CIST showing sampling ports and heating media attachments

Table 3-9: Heights of Sampling Points

Sampling Point	Height below Surface (mm)	z/H	Height above Bottom (mm)
Z1	52	0.231	172
Z2	96	0.427	128
Z3	140	0.622	84
Z4	184	0.818	40

Figure 3-4 shows a picture of the FBRM. The hose attached to the bottom left and top right of the vessel carries the ethylene glycol heating media. It flows in the outer chamber of the vessel. The sampling ports on the front of the vessel go through the outer chamber and into the vessel. The shaft goes through the top of the vessel, and just behind it to the left is the feed port – the steel fitting is a relic of an earlier experimental protocol. The FBRM is on the right: it is held in place with a lab stand. It enters the vessel through an angled port in the lid, and its placement is controlled with the use of a hose clamp and a Teflon spacer.

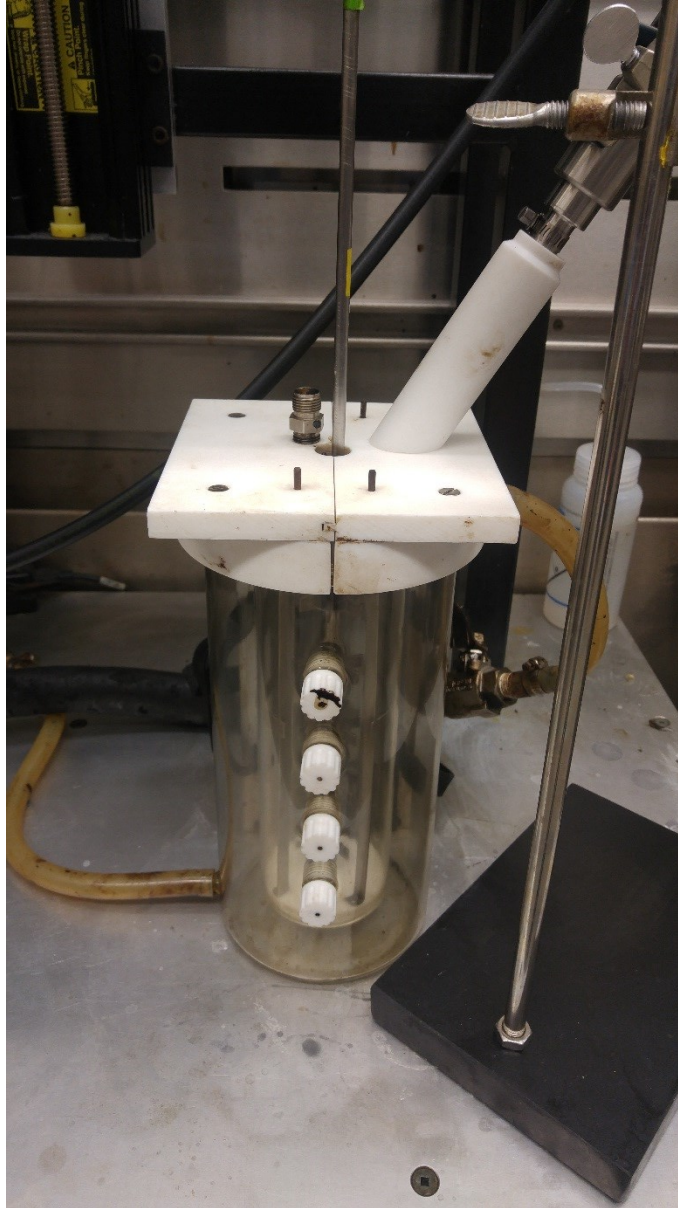


Figure 3-4: Picture of CIST with heating media attachments, FBRM, and Teflon sampling plugs

3.2.2 Heating

Both naphtha and bitumen froth are pre-heated before the beginning of the experiment in a bath of glycol at approximately 82°C. While the naphtha heats up to 80°C in less than half an hour, the low-quality bitumen froth must be heated for at least 2 hours

before reaching its target temperature of 70°C. During the course of the 15-minute premixing step, the bitumen froth heats quickly to 80°C.

Heating during the experiment is provided by circulating ethylene glycol at 80°C through the heating jacket of the CIST. The heat transfer provided by this jacket is not sufficient to heat the fluid but is a good solution to maintain the temperature. The heating jacket is depicted in Figure 3-4 above: it is the outer chamber of the glass vessel pictured.

3.3 Material

Low-quality bitumen froth is used in this campaign. In previous experimental campaigns, so-called average-quality bitumen froth was used. In addition to having a higher amount of water and solids, the nature of the solids is different. Figure 3-5 shows the particle size distribution (PSD) of solids in low quality froth, as used this campaign, and the PSD of the solids in average quality froth, as used by Arora (2016):

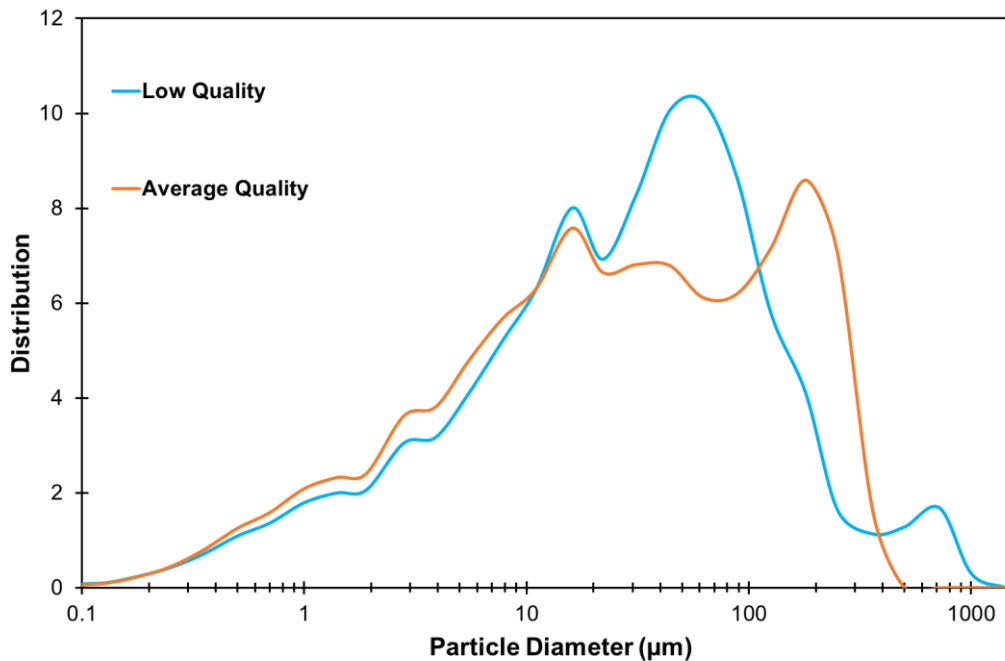


Figure 3-5: Particle size distribution of solids in froth samples, before separation

3.4 Dilbit Experiments

As will be discussed in Chapter 5, the FBRM was used in bitumen froth experiments to obtain the chord length distribution. Due to the challenging nature of the fluid, however, some orienting and validating experiments were conducted in diluted bitumen, the downstream product of bitumen froth treatment, and a much less loaded system. The purpose of these experiments is to determine if FBRM data can be validated with existing data, and see if interesting patterns emerge from a limited study of diluted bitumen.

The composition of diluted bitumen can vary considerably based on operating conditions and the bitumen ore being processed. The composition of the diluted bitumen used for these experiments is shown in Table 3-10:

Table 3-10: Properties of diluted bitumen

Bitumen Content (wt%)	56.6 – 58.0
Water (wt%)	0.62 – 1.66
Solids (wt%)	0.09 – 0.41
Naphtha (wt% by balance)	40.8 – 41.4
Viscosity (cP)*	5900 – 1100
Density (kg/m ³)**	1138.1

* At 60°C and 80°C, respectively. Estimated using Eq. 6.1 in Khan (2011)

** (Chong, 2013)

3.4.1 Experimental Design and Parameters

A simple design of 1 factor and 2 replicates was done to assess the agreement between the drop size distribution obtained from micrographs analyzed using image analysis developed by Leo (2013) and transformed from the chord-length distribution. The

variable used for the design can be considered qualitative for this section. Experiments were done at “good mixing” and “poor mixing” conditions.

Table 3-11: Summary of experimental conditions

Experiment Code	Mixing Quality	Replicate
DA-1	Good	1
DA-2	Good	2
DB-1	Poor	1
DB-2	Poor	2

The mixing conditions corresponding to good and poor mixing are detailed in Table 3-12:

Table 3-12: Mixing conditions for diluted bitumen FBRM experiments

Mixing Quality	Mixing Detail	Injection Concentration (%)	Additive Injection Volume (mL)
Good	Rushton, 600 rpm, 10 min	12	1.7
Poor	Intermig, 400 rpm, 2 min	21	0.9

A previous study in the research group investigated the drop size distribution of diluted bitumen using image analysis (Leo, 2013). For this reason, the same algorithm was applied to micrographs obtained from this diluted bitumen to compare the results from the FBRM. Because the FBRM detects a chord length distribution rather than a drop size distribution, a transformation of the chord length distribution to drop size distribution was performed, using an algorithm developed in the group (Safari Alamuti, 2016).

3.4.2 Results and Discussion

The chord length distribution for the four experiments is plotted below in Figure 3-6 for five minutes after settling has begun. The same data is plotted in Figure 3-7 after transformation to a drop size distribution. As expected, the transformation shifts the distribution toward larger sizes, since the largest chord length that can be read from a spherical particle is the diameter. The peak of the chord length distribution is approximately 4 μm , and the peak of the drop size distribution is very close, also approximately 4 μm .

There is a noticeable difference between conditions A (good mixing) and B (poor mixing) on either Figure 3-6 or Figure 3-7, namely that the counts of fines are higher in the early stages of settling. This is even though a simple linear regression on Karl Fischer water content reveals that good mixing leads to lower water content at the end of settling. This strongly suggests that the demulsifier was better dispersed, as the only available mechanism left to remove these fines is flocculation during settling, which depends on the demulsifier to effect attachment.

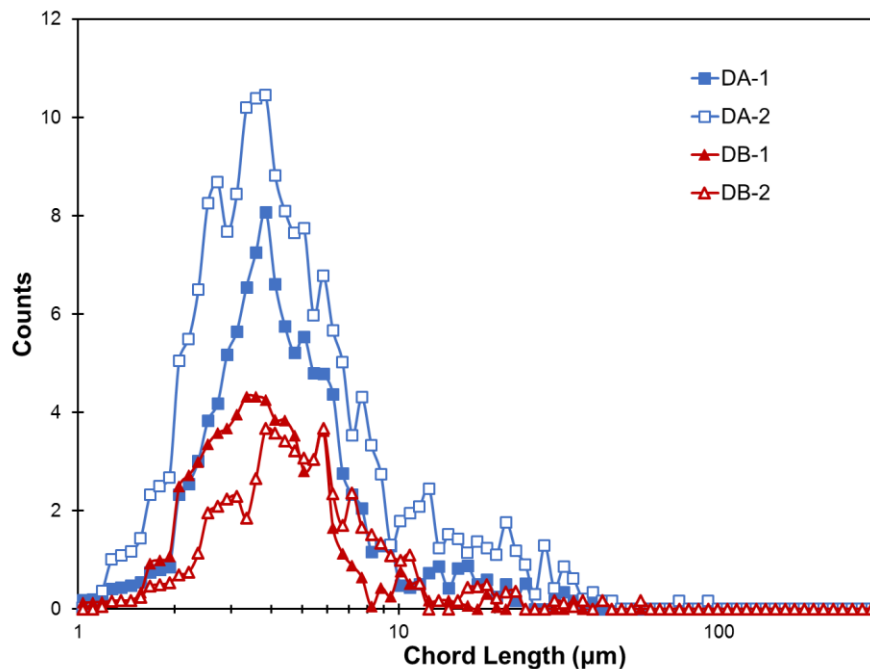


Figure 3-6: Chord Length Distribution of Dilbit Experiments after 5 min of Settling

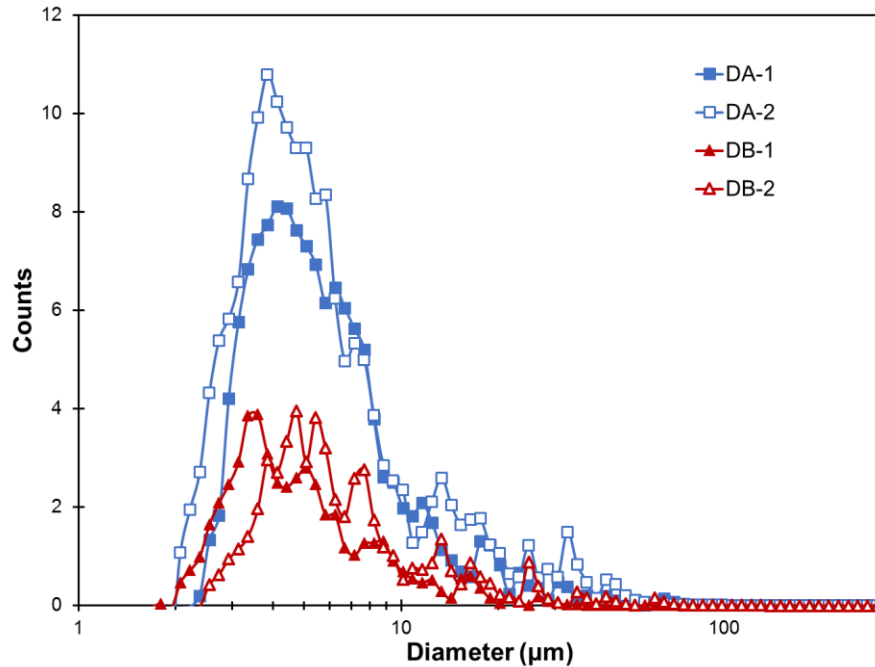


Figure 3-7: Calculated Drop Size Distribution after 5 min of Settling

To validate the use of the FBRM for froth, we sought to compare drop size distribution data collected with microscopy and image analysis to the drop size data from the FBRM. Microscopy and image analysis was used in a previous campaign to characterize settling in diluted bitumen (Leo, 2013). Figure 3-8 shows the drop size distribution at 5 minutes of settling as determined by the FBRM and chord length transformation, and as determined through microscopy and image analysis.

There is very little agreement between the two methods. The second method – microscopy and image analysis – is thought to be in error. More experiments will be conducted with special attention paid to the image quality and algorithm tuning parameters. Leo (2013) found a peak of droplets at 4 microns for most experiments conducted in dilbit.

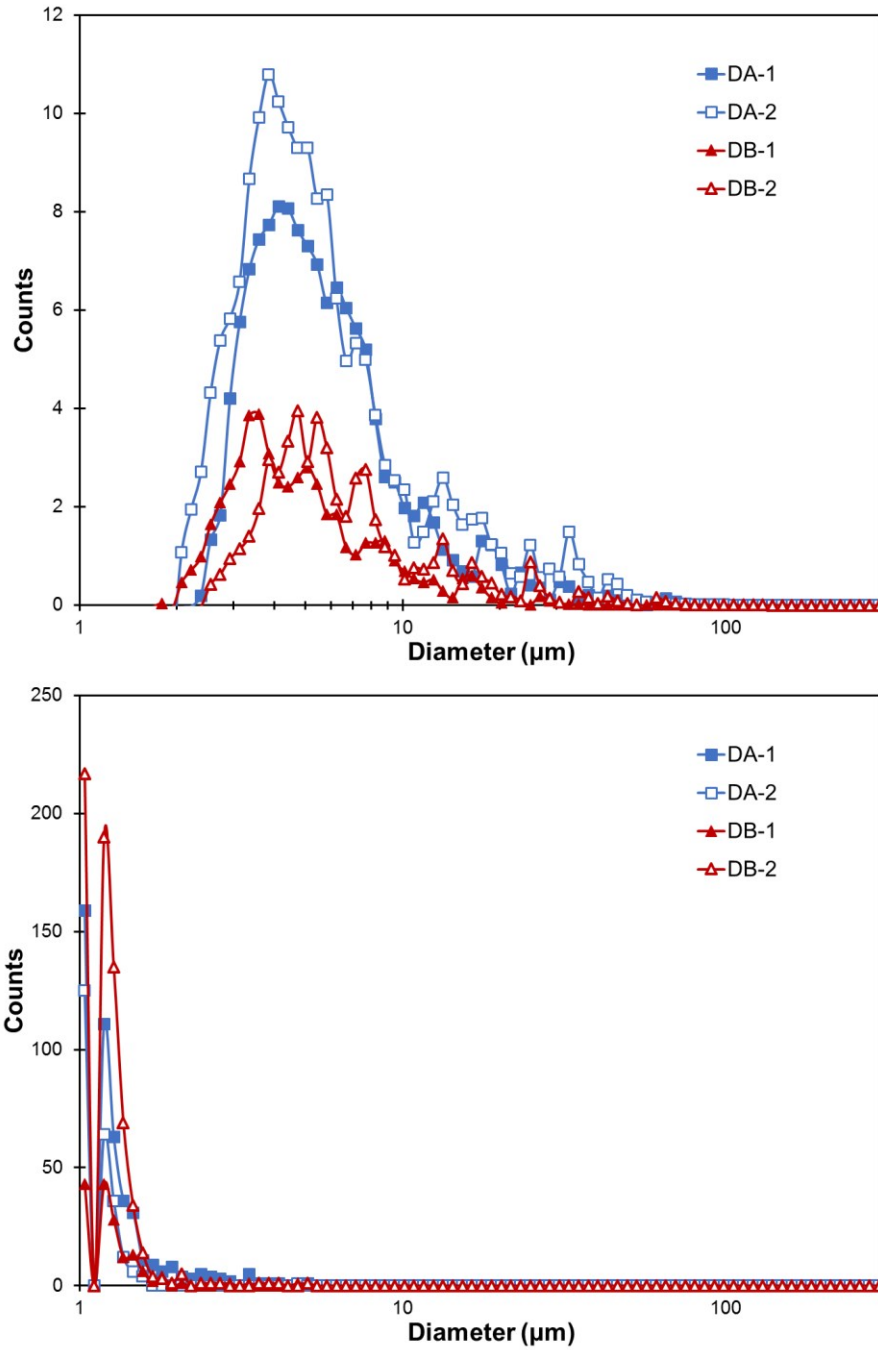


Figure 3-8: Drop size distribution for all experiments at 5 minutes settling time (a) transformed from CLD obtained from FBRM (b) using microscopy and image analysis.

Figure 3-9 and Figure 3-10 show the chord length counts in two size categories: fines, or chord lengths below 10 microns, and larger chord lengths between 10 and 100 microns. Figure 3-9 compares the results of the two replicates at good mixing conditions, while Figure 3-10 compares the results of two replicates at poor mixing. With good mixing, there is a clear upward trend of counts in the larger size range, indicating that there is flocculation or coalescence occurring. This hypothesis is further supported by the reduction of counts of fines. This is thought to be because of better dispersion of the demulsifier.

The demulsifier dispersion for the poor mixing case, shown in Figure 3-10, clearly lacks the same pattern. Rather than increasing, the counts of larger chords appears to decrease. Fines may be increasing slightly. This indicates a lack of flocculation or coalescence and is likely due to inadequate dispersion of demulsifier.

Although validation with micrograph data ultimately failed, this clear indication of a difference between the poor and good mixing cases is reassuring. This limited set of experiments shows that diluted bitumen is a feasible entry point for future studies into the use of the FBRM in diluted bitumen and bitumen froth systems. If the data for bitumen froth is difficult to interpret and analyze, further analysis in diluted bitumen could be used to enhance understanding.

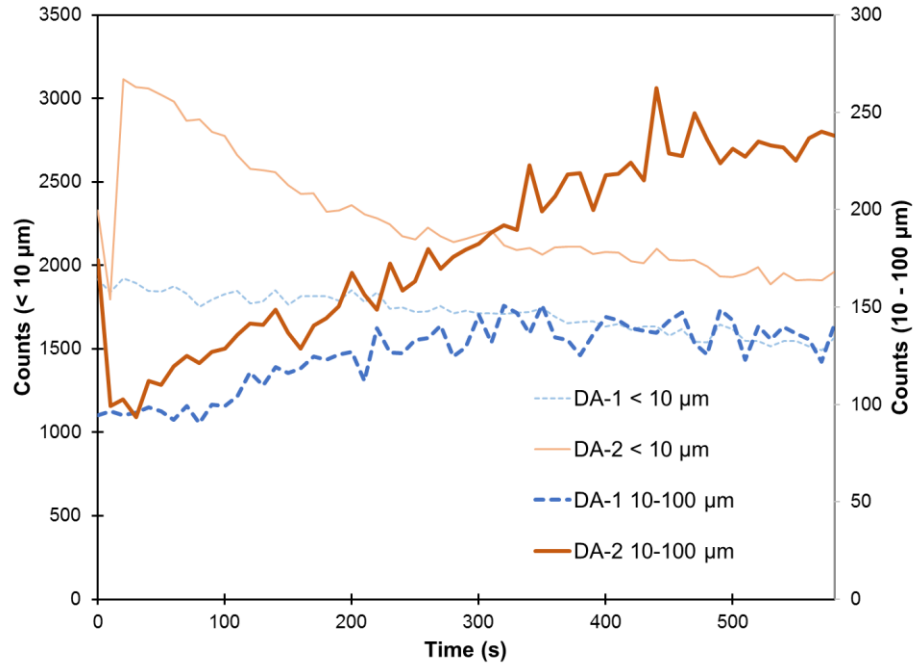


Figure 3-9: Chord length counts during demulsifier dispersion in diluted bitumen for *good mixing* (high J, low IC) cases

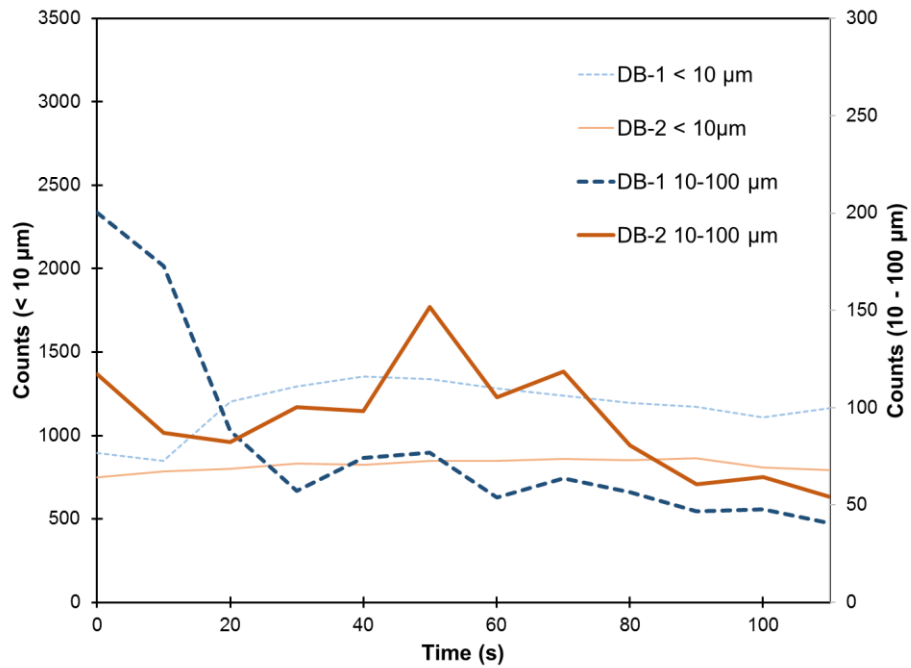


Figure 3-10: Chord length counts during demulsifier dispersion in diluted bitumen for *poor mixing* (low J, high IC) cases

Chapter 4: Optimizing Chemical Dosage in Low-Quality Froth

In processes where the mixing effects are poorly understood, varying the dosage of chemical additives may appear to be the only control variable available to target the desired process outcome. While adding more chemical often improves the process outcome, this can be subject to diminishing returns or even reduced performance at high dosage. In industry, this second phenomenon is often known as overdosing. Chemical additives are often costly, so alternative means of improving process outcomes can help processes achieve better economy and lower impact.

The first goal entering this campaign was to determine the optimal demulsifier dosage at which to study mixing effects. The ideal chemical dosage for this purpose would be the level at which poor mixing conditions (low mixing energy, high injection concentration) give a sub-optimal result, while good mixing conditions lead to an acceptable process result. These limits provide an experimental space over which the mixing variables have an effect that can be detected and studied. If the dosage is too low or too high, other effects may dominate, such as a lack of demulsifier with which to effect separation, or overdosing, which can make separation nearly impossible.

4.1 Experimental Design

Although previous studies have been done on bitumen froth, we had no clear basis for choosing the best operating point for chemical dosage for low-quality froth. The experimental design to discover the best operating point was simple: starting at a high dosage, an experiment is run with good mixing conditions, which are known to produce good separation with an adequate dose (Arora, 2016; Chong et al., 2016). If the separation is sufficient, lower the dosage and repeat. Once a point is reached at which

separation is inadequate, the dosage is returned to the last level at which good mixing conditions led to adequate separation and a new experiment is run with poor mixing conditions to verify that it leads to poor separation. The criterion for successful separation is no more than 1% water as determined by Karl Fischer titration at the topmost sampling point, height Z1, after 60 minutes of settling.

Experiments were begun at a bulk concentration of 200 ppm by weight of active ingredient per unit weight of naphtha-diluted froth. Previous experiments on average quality froth were done at a bulk concentration of 150 ppm (Arora, 2016), and it is hypothesized that low-quality froth would require more chemical to settle effectively. The BC was then reduced in 25 ppm steps. 6 steps were done to observe the trend. Repeats were done at the end of the campaign to verify results and to confirm the pattern with a more practiced experimental procedure. Some other runs were done for curiosity and for reference. Two trials were run with no demulsifier; one at high energy input ($J = 22778 \text{ J/kg}$) and one at low energy input (425 J/kg). One trial was done at a very high demulsifier dosage (200 ppm) to test for overdosing effects.

4.2 Results and Discussion

A full tabulated set of results (water content vs. time) is provided in Appendix A. Note that the sampling schedule changed from the one used by Arora (2016); it became obvious that the sampling schedule used in previous campaigns (with samples taken at minutes 3, 5, 7, 10, 30, 60) was not going to be adequate for these new experiments, as many of the experiments did not begin to settle until after 10 minutes. The new sampling schedule collects samples at 5, 10, 15, 20, 25, 30, 45, 60, 90, and 120 minutes.

Figure 4-1 shows all experiments done at an N:B (naphtha-to-bitumen ratio) of 0.7, with demulsifier, and good mixing conditions (i.e. low injection concentration, IC, and high mixing energy, J).

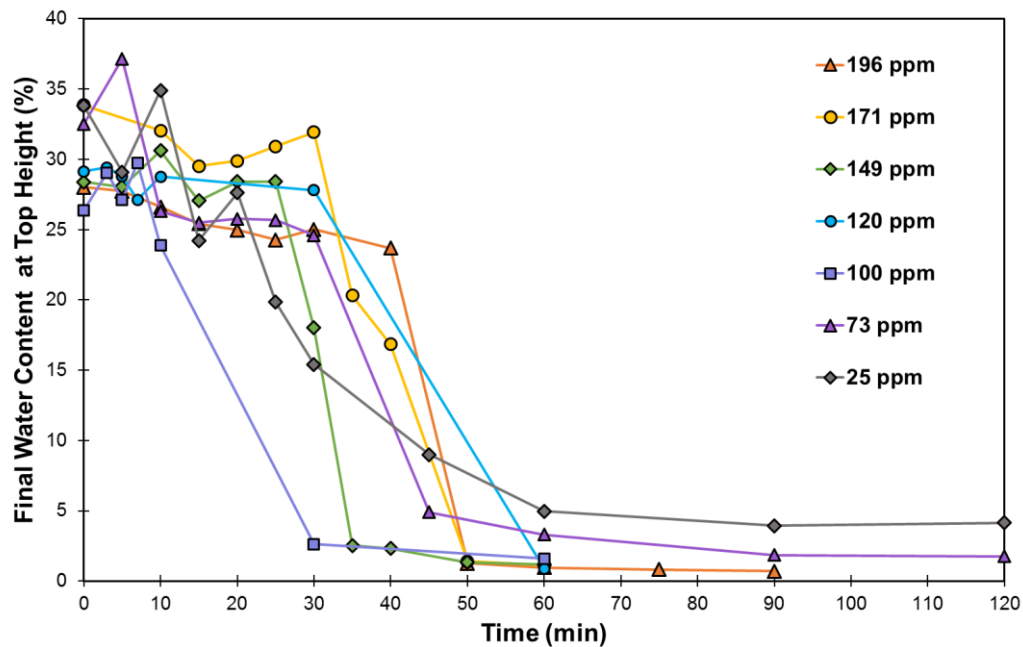


Figure 4-1: Water content over time for all experiments with demulsifier at N:B ratio of 0.7 and good mixing conditions, as determined by Karl Fischer titration

These experiments showed that reducing the demulsifier bulk concentration led to an increase in water content at height Z1 at 60 minutes. One notable exception is 120 ppm.

For these experiments, except for 100 ppm, significant settling does not begin until 20 – 40 minutes. This was termed an *induction time* and is discussed in more detail in the next section.

4.2.1 Induction Time

The presence of an induction time was a surprising finding from this campaign. Induction time is a delay before settling begins to happen at a significant rate; it is illustrated in Figure 4-2 below. In previous works (Arora, 2016; Chong, 2013), an induction time was not identified. In fact, good separation was associated with fast initial settling in the first 10 minutes, followed by slow settling over the course of the

following 50 minutes. These previous studies involved average-quality froth, unlike the low-quality froth used for this work.

In the pattern identified there was first a period of induction during which the very high water content stayed nearly constant. After the induction stage, there was a period of very fast settling (from >20% to less than 5%). The slope of this line changed between experiments, and is likely highly sensitive to sampling time. After reaching a value below 5%, a period of slow settling occurred during which the water content was reduced further.

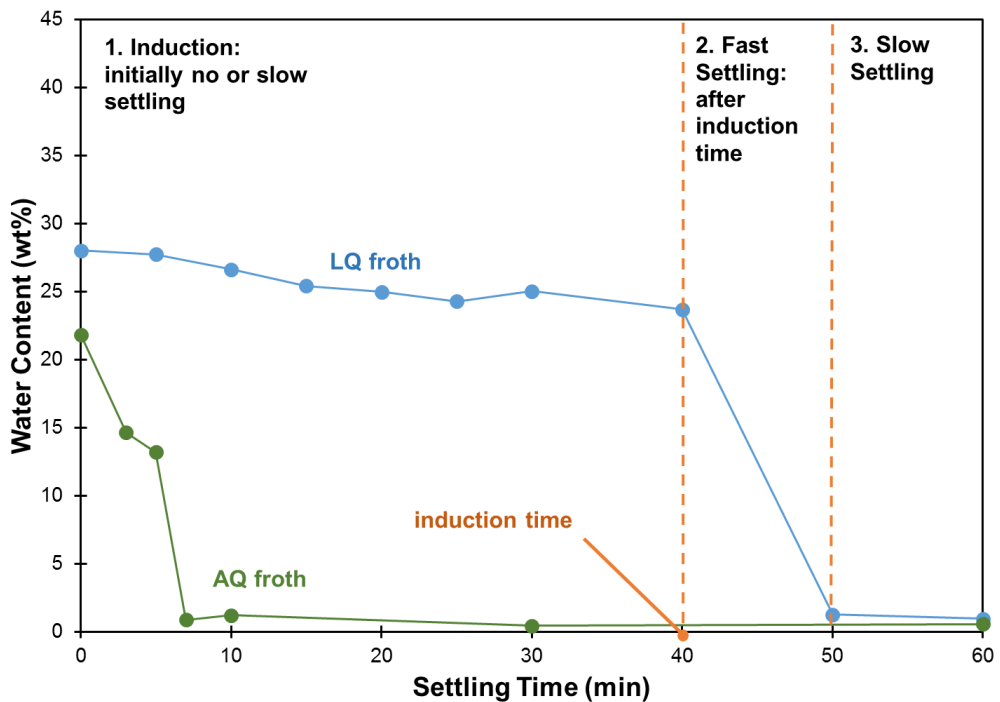


Figure 4-2: Illustration of settling process with 3 stages including significant induction time low quality (LQ) froth. Average quality (AQ) froth shown for comparison (Arora, 2016).

Figure 4-3 below compares the runs with demulsifier to those with no demulsifier added. Two experiments were done with no demulsifier: one with identical mixing energy to the experiments above, and one with low mixing energy.

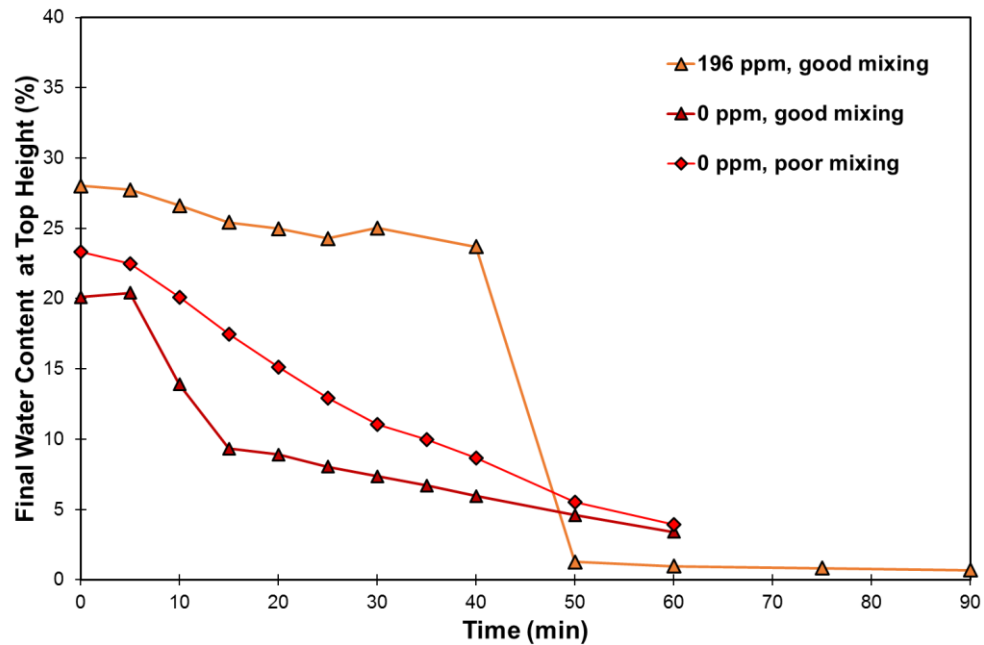


Figure 4-3: Comparison of no-demulsifier runs with a typical run with demulsifier

Runs with no demulsifier do not have the same pattern of a late induction time followed by fast settling and then slow settling. The run with no demulsifier and poor mixing settles slowly and steadily, while the run with no demulsifier and good mixing may have an induction time, but it is less than 10 minutes.

Suspecting that the induction time was indicative of poor settling, the final water content was plotted against induction time for several runs in Figure 4-4:

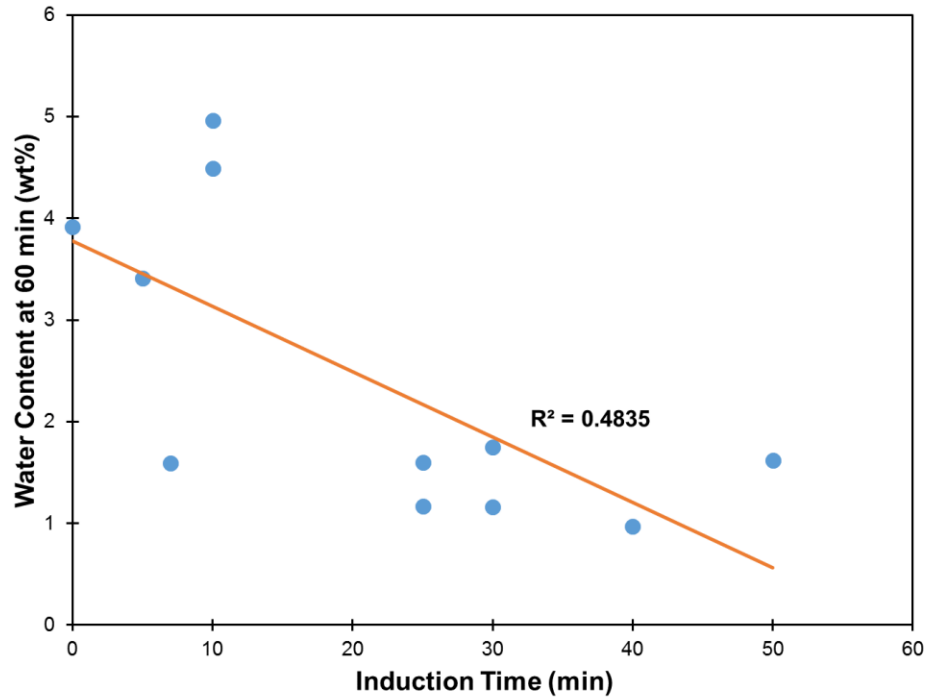


Figure 4-4: Final water content vs. Induction Time

The induction time was defined as the last point before there was a reduction in water of approximately 20%. Since the experiment conducted with no demulsifier and poor mixing settled slowly and evenly, its induction time was evaluated as 0. Long induction times were not associated with poor settling (high water content after 60 minutes at height Z1). In fact, induction times longer than 20 minutes were associated with better final separation.

4.2.2 Final Water Content

Figure 4-5 below shows the water content after 60 minutes of settling for all experiments with good mixing to illustrate how increasing bulk concentration improves the process outcome. Except for the experiments conducted with no demulsifier or at very high demulsifier dosage, more demulsifier leads to a lower water content at 60

minutes. Setting a criterion of < 1% final water content, 175 ppm produced a result very close. However, 200 ppm was chosen as an operating point for the second campaign.

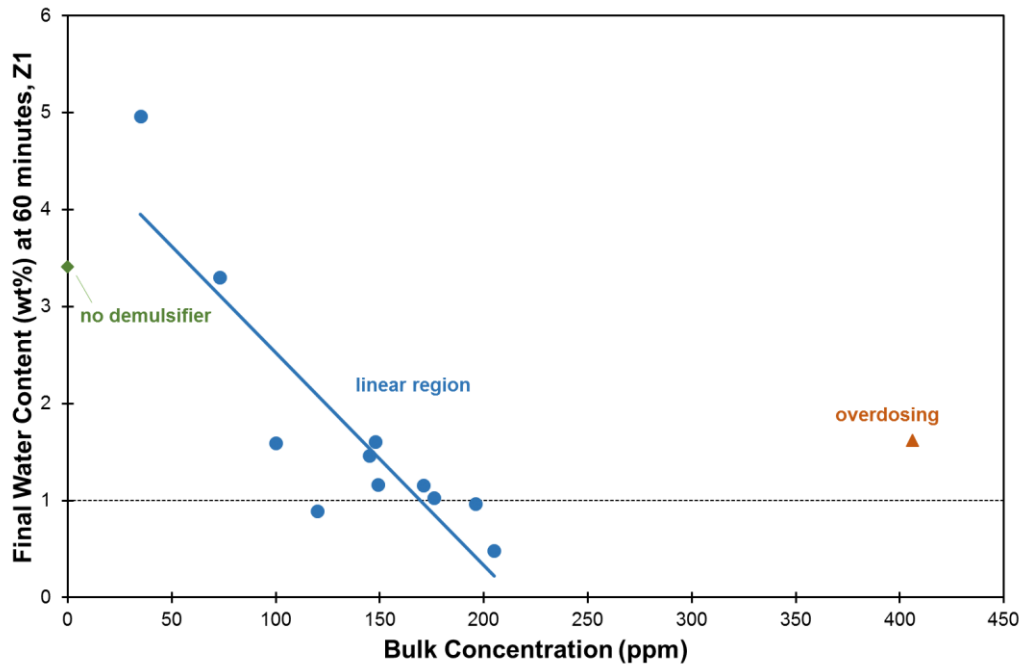


Figure 4-5: Final water content over bulk concentration (on naphtha-diluted froth basis). Water content of 1% (dashed line) considered successful.

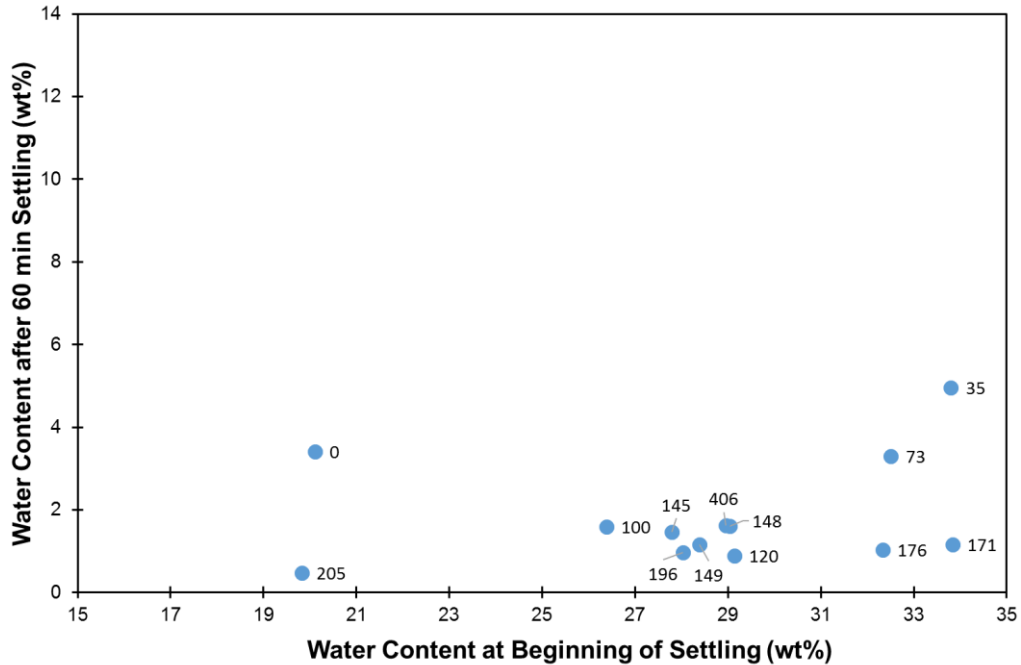


Figure 4-6: Final water content compared to water content at beginning of settling

All experimental runs conducted at good mixing conditions are shown on Figure 4-6 above, which plots the final water content on the y-axis and the water content at the beginning of settling on the x-axis. The points are tightly clustered around the bottom right of the graph. Two notable exceptions are the two runs with the lowest demulsifier dosage. Under good mixing conditions and bulk concentration at or close to the optimal level, high water-content at the beginning of settling is conducive to good water removal.

It seems there are large water droplets or flocs which take some time to settle: this may be indicative of sweep flocculation. The high water-content at the beginning may lead to larger flocs which then move like a filter through the fluid, capturing small particles and droplets as they settle themselves. Sweep flocculation acts as a mechanism to remove fine droplets which would otherwise remain in emulsion. However, the high surface area required for effective sweep flocculation would also slow settling by increasing drag on the agglomerate. The two runs at low demulsifier levels do not show this

behaviour: they have a higher water content at the end of settling, presumably because the bulk concentration of demulsifier was not sufficient to effect good settling.

The other two outliers are no demulsifier and the run with the highest N:B ratio (0.88, over 20% in excess of the target N:B ratio).

4.2.3 Verifying Chosen Condition

As an extra check that a level of 200 ppm was appropriate for further experimentation, this level was run again with poor mixing conditions. If the poor mixing conditions led to inadequate process performance, then 200 ppm is a level at which mixing effects can be studied. In Figure 4-7, the result of that experiment is compared to the experiment at 200 ppm and good mixing conditions, as well as one level lower of BC. The experiment done with 171 ppm of demulsifier was very close to the criterion of 1% and could also perhaps be used to study mixing effects:

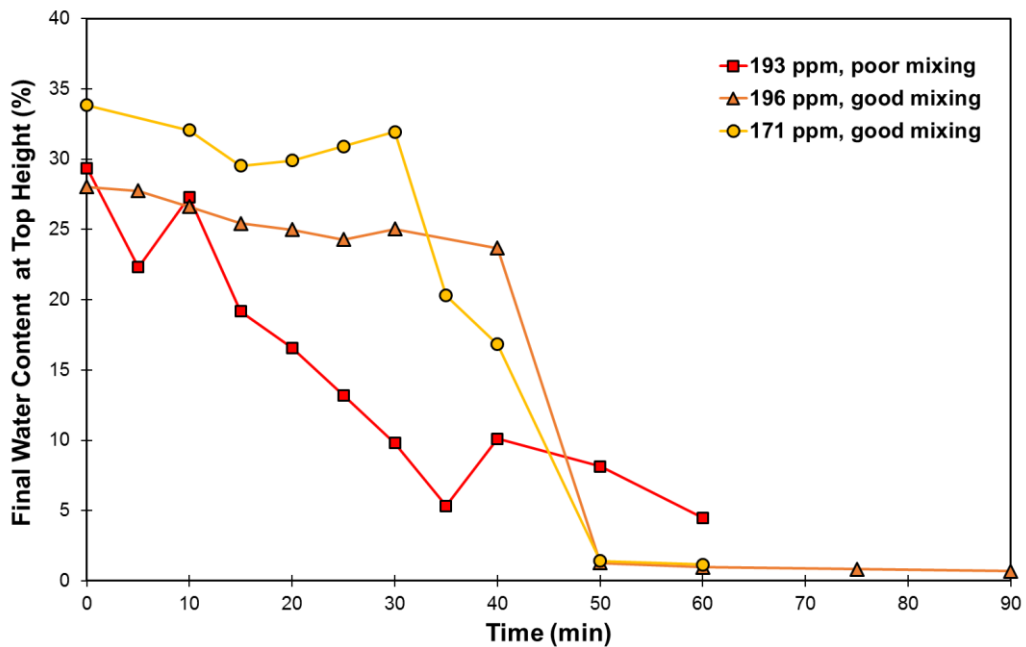


Figure 4-7: Verification experiment at chosen BC (200 ppm) and poor mixing conditions

While the two experiments done at good mixing conditions have the pattern identified in Figure 4-2, the experiment done at poor mixing conditions more closely resembles that of the runs with no demulsifier, as in Figure 4-3. The final water content is very high. It is apparent that 200 ppm is a suitable level at which to study mixing effects.

4.2.4 Other Runs

The remaining runs are shown in Figure 4-8 below. These include runs at high naphtha-to-bitumen ratio and one run under very high dosage.

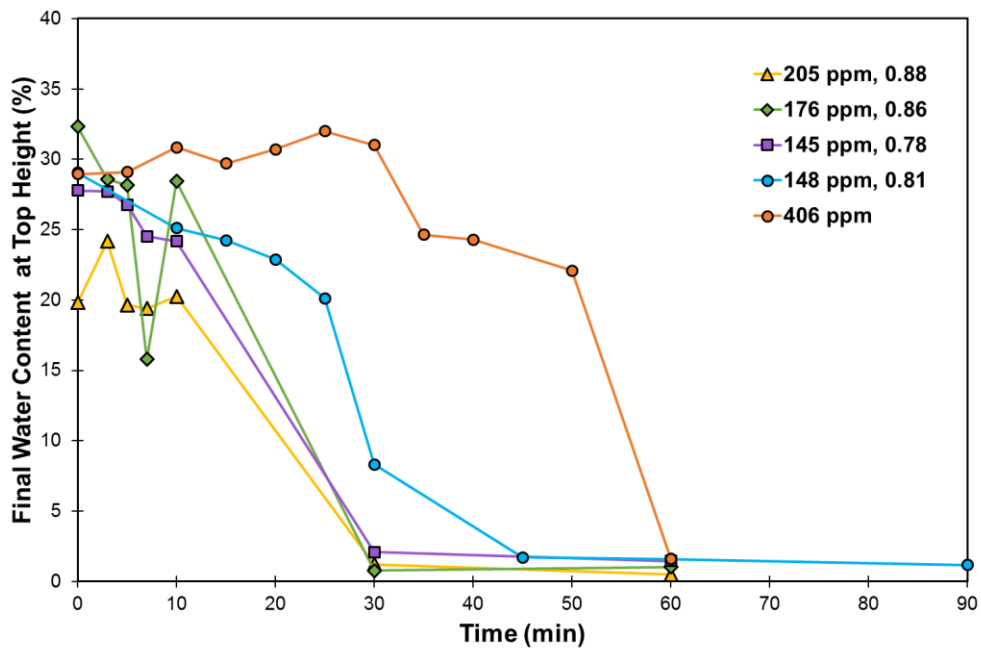


Figure 4-8: Runs at high naphtha-to-bitumen ratio and presumed overdosing condition. All runs under good mixing conditions.

The first three runs at high N:B ratio were done in error as the experimental procedure was being refined. They are notable for being the only 3 experiments with no induction time. It is unclear whether this is due to the high N:B ratio, due to the lack of points between 10 and 30 minutes (which means the actual induction time may have been later than 10 min but not observed), or for some reason unknown to the researcher. The

third experiment (145 ppm, 0.78 N:B ratio) was duplicated as closely as possible (148 ppm, 0.81 N:B ratio) to observe the behavior between 10 and 30 minutes. This experiment approached the induction time observed in the other experiments.

The overdosing experiment was done to observe the effect of very high dosage level. In industry “overdosing” is a phenomenon wherein increasing dosage leads to a worse process result. Indeed, the overdosed run had a very long induction time and a higher water content compared to runs at or near the chosen dosage level. It is possible that due to the very late induction time, the reason for high water content at 60 minutes is that the fast settling step has not yet finished.

These questions fall outside the scope of this study and were not pursued further.

4.3 Conclusions

An unexpected observation from many of the experiments in this campaign was the presence of an induction time, or a time before which the water content is nearly constant before then settling very quickly. The induction time was not associated with a lack of settling or poor settling.

A dosage of 200 ppm was chosen for further testing of mixing effects. A dosage of 200 parts per million is the mass of active ingredient of demulsifier added per mass of *naphtha-diluted froth*. Using an alternate definition based on the mass of froth alone, this dose is equivalent to 270 ppm (froth basis). The second definition is frequently used in industry for operational reasons.

Chapter 5: Mixing and Demulsifier Performance in Low-Quality Bitumen Froth Treatment

After determining the optimum level of chemical dosage (“bulk concentration”) at which to study mixing effects, the next task was to uncover the effect of the mixing variables *mixing energy* (J) and *injection concentration* (IC) on the performance of the demulsifier in low-quality froth. It was discovered in previous studies that these variables influence the performance of demulsifier in diluted bitumen (Chong, 2013; Laplante, 2011) and average-quality bitumen froth (Arora, 2016; Chong, 2013).

The second goal was to study the effects of these variables on the underlying mechanisms that promote or hinder settling. The interplay of the dynamics of mixing, injection concentration and demulsifier attachment, and the subsequent settling dynamics are expected to differ between runs, resulting in differences in the water and solids contents, particle size analysis, and FBRM chord length distribution.

5.1 Experimental Design

5.1.1 Replicated 2-Factor, 2-Level Design

The optimal bulk concentration for testing was determined in the first campaign (3.4): a level of 200 ppm of demulsifier on the basis of the weight of naphtha-diluted froth was chosen. The two remaining variables of interest are mixing variables: injection concentration and mixing energy. Injection concentration is denoted by the abbreviation IC, and is also known as pre-dilution of additive. It is the mass percentage

of active chemical in its carrier fluid (xylene) *before injection* into the system. A lower injection concentration at the same bulk concentration (the amount of active chemical on the basis of naphtha-diluted froth) necessitates a higher injection volume, due to the additional xylene used for dilution. Because the injection volume is small compared to the vessel volume it is presumed to be the pre-dilution itself which affects the system and not the additional xylene added to the system.

The mixing energy or energy input is denoted by the variable J. It is the product of the mixing power per unit mass (W/kg) and the mixing time (s) and is in units J/kg.

The experimental design chosen was a fully replicated factorial design of 2 factors (IC and J) each at 2 levels. The 2-level, 2-replicate factorial design allows for MANOVA (multivariate analysis of variance) using the contrast method as detailed in Montgomery & Runger (2007). Centre-points allow for a test of non-linear effects of each variable. However, only one centre point could be conducted due to supply limitations. The results of this centre run are presented but not used for quantitative analysis due to the lack of replication. The levels of each variable are shown below, and were chosen to be the same as Arora (2016) and Chong (2013):

Table 5-1: Factorial design variable levels

Factorial Factor Level (X)	-1	0	1
J (J/kg)	425	12164	22778
IC (wt%)	12	16.5	21

The factorial design levels X_J and X_{IC} can be related back to the physical variables J and IC by the following equations:

$$J \approx 12164 \frac{J}{kg} + X_J \times 11176 \frac{J}{kg}$$

$$IC = 16.5 \text{ wt\%} + X_{IC} \times 4.5 \text{ wt\%}$$

Nine experiments were conducted in total. The experiments are presented in Table 5-2 in the order in which they were run, which was randomized. The first run at each set of conditions was called the first replicate.

Table 5-2: Experiment codes and factorial design levels in randomized run order

Experiment Code	X _J	X _{IC}
FA-1	-	-
FC-1	-	+
FD-1	+	-
CP-1	0	0
FB-1	+	+
FD-2	+	-
FA-2	-	-
FB-2	+	+
FC-2	-	+

The factorial design levels are shortened to - and +, respectively denoting -1 and +1.

5.2 Results & Discussion

This section presents and discusses the data obtained from Karl Fischer titration (water content), FBRM (chord length distribution), Dean Stark extraction (oil, water, and solids content), and qualitative microscopy to probe the dynamics of mixing and settling that drive change in the system. Understanding these mechanisms would prove useful to design chemical aids and mixing protocols to drive water content lower. The experiments in the campaign continued to use 1% water content or less as a benchmark for success.

In such a complex system, I expected to find evidence of several mechanisms of combination and settling at work. These mechanisms are summarized here but discussed in more detail in Section 1.5. In addition to the simple Stokes settling and

hindered settling due to the loaded nature of the fluid, we look for evidence of more complex behaviour, including:

- Flocculation: the combination of droplets and solids into “flocs,” large aggregates that do not coalesce into larger droplets
- Coalescence: the combination of droplets into larger droplets. Because collisions occur between two droplets at a time, this is also called binary coalescence.
- Flocculation-Induced Coalescence: following flocculation, droplets may slowly coalesce due to prolonged contact.
- Sweep Flocculation: differential settling velocities or flow-through velocity can cause large droplets to capture smaller droplets or particles, or flocs to capture smaller items in their interstitial spaces. Sweep flocculation envisions flocs moving through the fluid as “moving filters,” removing small water droplets or solids that would otherwise remain stable or metastable
- Multiple Emulsion: multiple emulsions (oil in water in oil) were observed on microscope and proposed as a possible mechanism slowing settling. Because settling depends on density difference, having droplets of the generally continuous (oil in this case) fluid within the discontinuous (water) phase, the effective density difference has been reduced, reducing the driving force for settling.
- Compaction and Up-Flow: because of the very high loading of bitumen froth – water and solids together make up approximately 50% of low-quality bitumen froth – and because no free layer of water is resolved in bitumen froth treatment, Stokes settling and even hindered settling models may be inadequate to describe the settling. Instead, droplets of water and solids may compact slowly as random fluctuations in the fluid allow them to pack. Water droplets may be acting like particles due to interfacial “skins” that resist binary coalescence. The process of packing, or compaction, would in turn release pockets of interstitial fluid, which may flow upward and hinder the settling above.

- Consolidation and Structure Formation: droplet and solid particle interactions are major factors in the difficulty of processing waste streams of the oil sands process, most notably in the case of Mature Fine Tailings. These interactions are also present in bitumen froth, and in low-quality froth may be strong enough to influence settling operations.

All the data collected will be examined for evidence of these mechanisms at work. This discussion leads to the conclusion that several complex settling mechanisms are operating in the system.

5.2.1 Karl Fischer Results

Karl Fischer titration was the primary method of determining the water content in the vessel at different heights. Samples were taken at 52 mm, 96 mm, 140 mm and 184 mm below the liquid surface. These heights were called Z1, Z2, Z3, and Z4 respectively. Z1 is the highest while Z4 is the lowest. Z4 is 40 mm above the bottom of the vessel. The results are presented and discussed.

5.2.1.1 Select Comparisons of Replicated Data

There is considerable variance between the replicated datasets. For example, the estimated variance based on a MANOVA analysis at time 0 and height Z1 is 2.98 (wt\%)^2 , a standard deviation of 1.73 wt%. This value is based on the unexplained variance of all the factorial experiments.

If the data were normally distributed, this would mean that approximately 95% of the samples fell within $\pm 3.46 \text{ wt\%}$, a significant difference in a system that is approximately 30 wt% water.

Despite the considerable variance, there are still statistically significant patterns in the Karl Fischer data which will be explored in the following sections.

This estimate of the variance is high compared to the variance in the samples themselves; the variance in water content between different sample cans as determined by Dean Stark extraction by the industrial partner was only 0.66 (wt\%)^2 . It is also higher than the variation in samples taken for Karl Fischer titration; these were on the order of 0.5 (wt\%)^2 at higher water contents (approx. 30 wt%) and 0.01 (wt\%)^2 at low water contents (approx. 1 wt%).

To visualize the large variance, two sets of replicated data are presented below in Figure 5-1 and Figure 5-2:

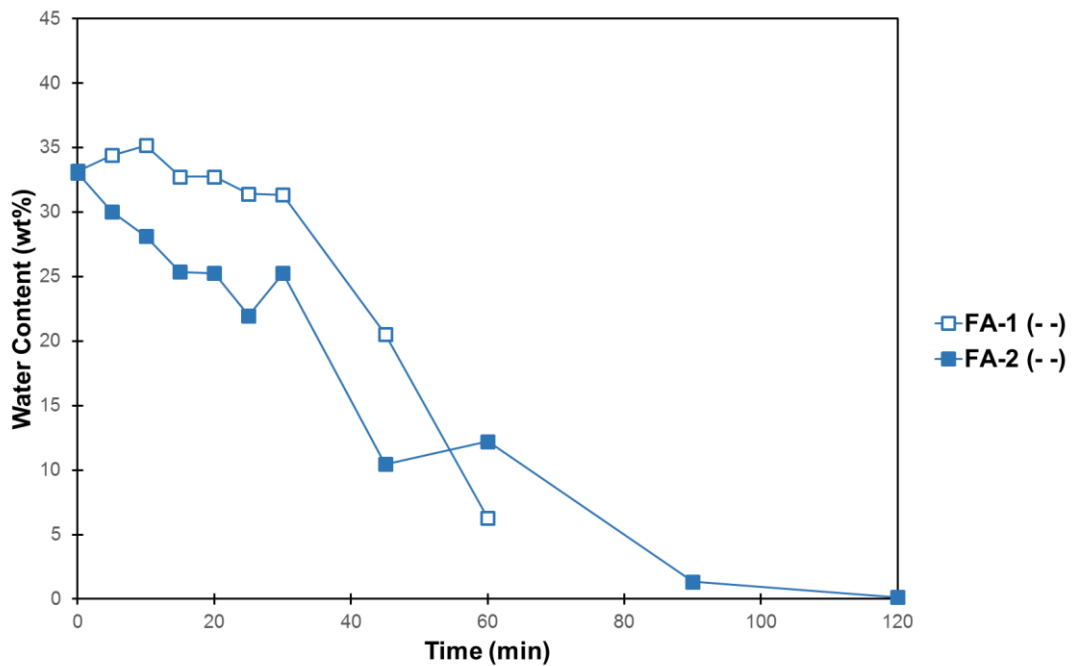


Figure 5-1: Comparison of Replicates at Z1 for low J, low IC condition

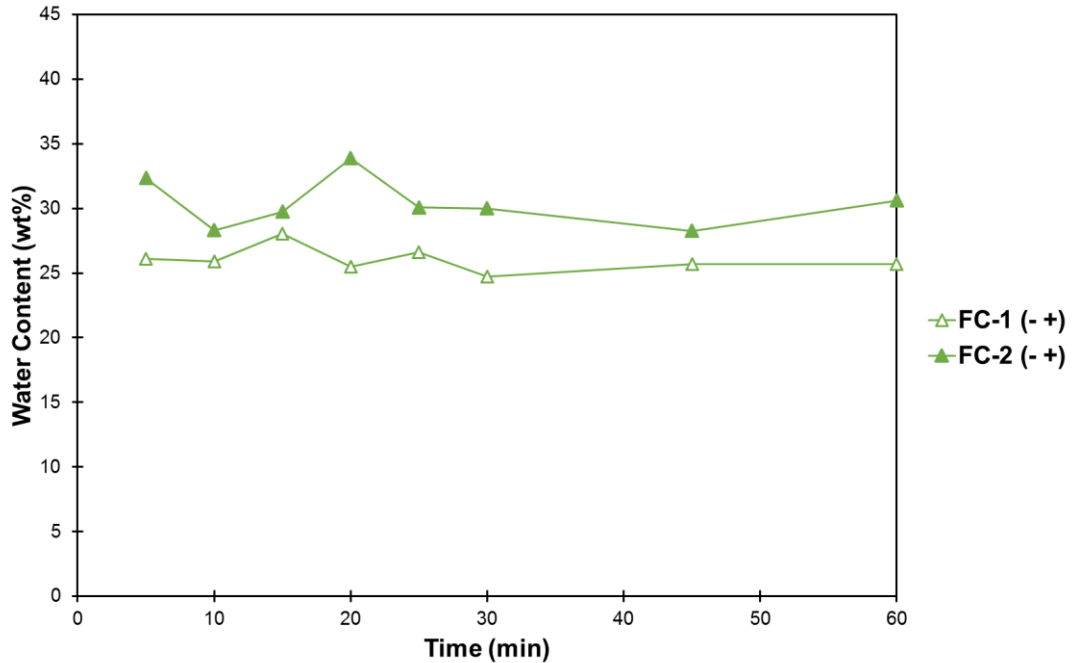


Figure 5-2: Comparison of Replicates at Z3 for low J, high IC condition

In a system wherein there are many complex components in high quantity – the bitumen froth with naphtha added still has approximately 27% water and 10% solids – a high level of variability is not surprising. The complex interplay of mechanisms could potentially lead to very unpredictable results.

5.2.1.2 Water Content vs. Time Trends

Water content was plotted against time for each height, starting with the topmost height, called Z1 ($z = 52$ mm below liquid surface). The full data set is tabulated in Appendix A. The data point at 0 min in Figure 5-3 corresponds to the sample taken at Z1 30 s before the end of demulsifier dispersion, and it is assumed that it is the same at the beginning of settling. Samples were taken at Z2 ($z = 96$ mm) between 5 and 120 minutes, and at Z3 ($z = 140$ mm) and Z4 ($z = 184$ mm) between 5 and 60 minutes.

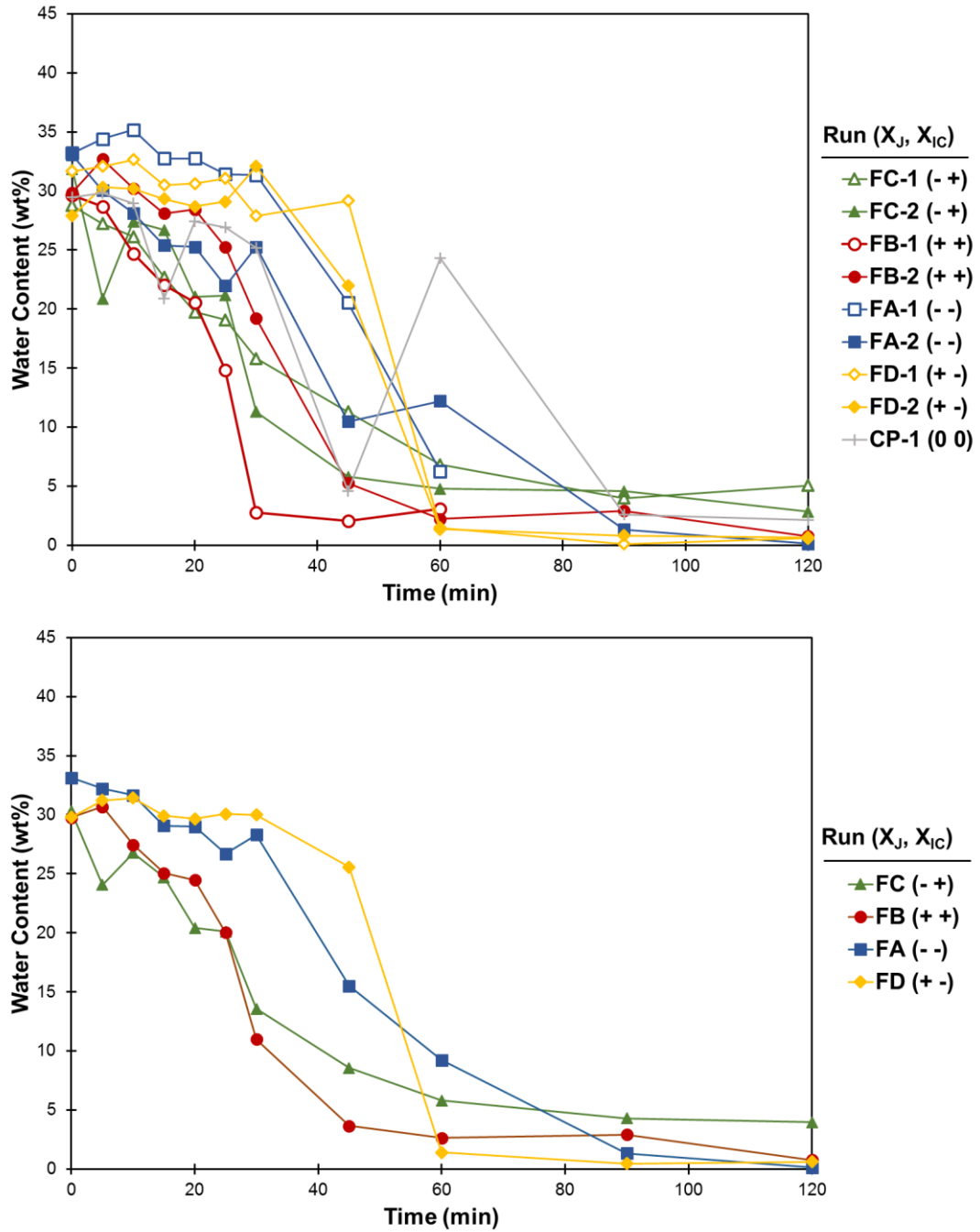


Figure 5-3: Water Content vs. Time at Z1 (topmost sampling point, 52 mm below surface), as determined by Karl Fischer titration (a) all runs including centre-point (b) data averaged between two replicates

The replicates at each condition look similar in shape, though there is variation between points at the same time. The runs with the best mixing conditions – high mixing energy (J) and low injection concentration (IC) – show the least difference between runs.

Using this graph, one can observe that most of the experiments can be described by the same three distinct stages identified in 3.4:

1. Induction

During the induction step, little to no settling is detected at the top sampling level. Something in the system is stopping or vastly slowing even large droplets from settling in significant numbers. The last time step wherein the water content is nearly the same as the initial water content is termed the induction time. Induction time is longer in experiments with low injection concentration.

Note that both experiments done at very poor mixing conditions (low J, high IC) do not follow this pattern. FC-1 has a clear induction point, but does not have a clear fast settling step. FC-2 behaves more like a system with no demulsifier, as found in Figure 4-3. The settling is slow but constant and does not lead to a satisfactory final value.

2. Fast Settling

After the induction time, there is a stage of relatively fast settling. The slope varies; there is some uncertainty in the inherent slope due to the time between data points. However, the slope seems steeper in cases of high mixing energy.

3. Slow Settling

After the fast settling stage, settling slows down significantly.

All experiments which were taken 120 minutes and had one or more variables corresponding to good mixing (i.e. high J or low IC or both) reached a final water content

of less than 1% at Z1. The only experiments which do not have less than 1% water content at time 120 minutes are FC-1 and FC-2. FC-1 and FC-2 occur at low J and high IC – the worst possible mixing condition. FA-1 and FB-1 cannot be evaluated because they were only allowed to settle for 60 minutes.

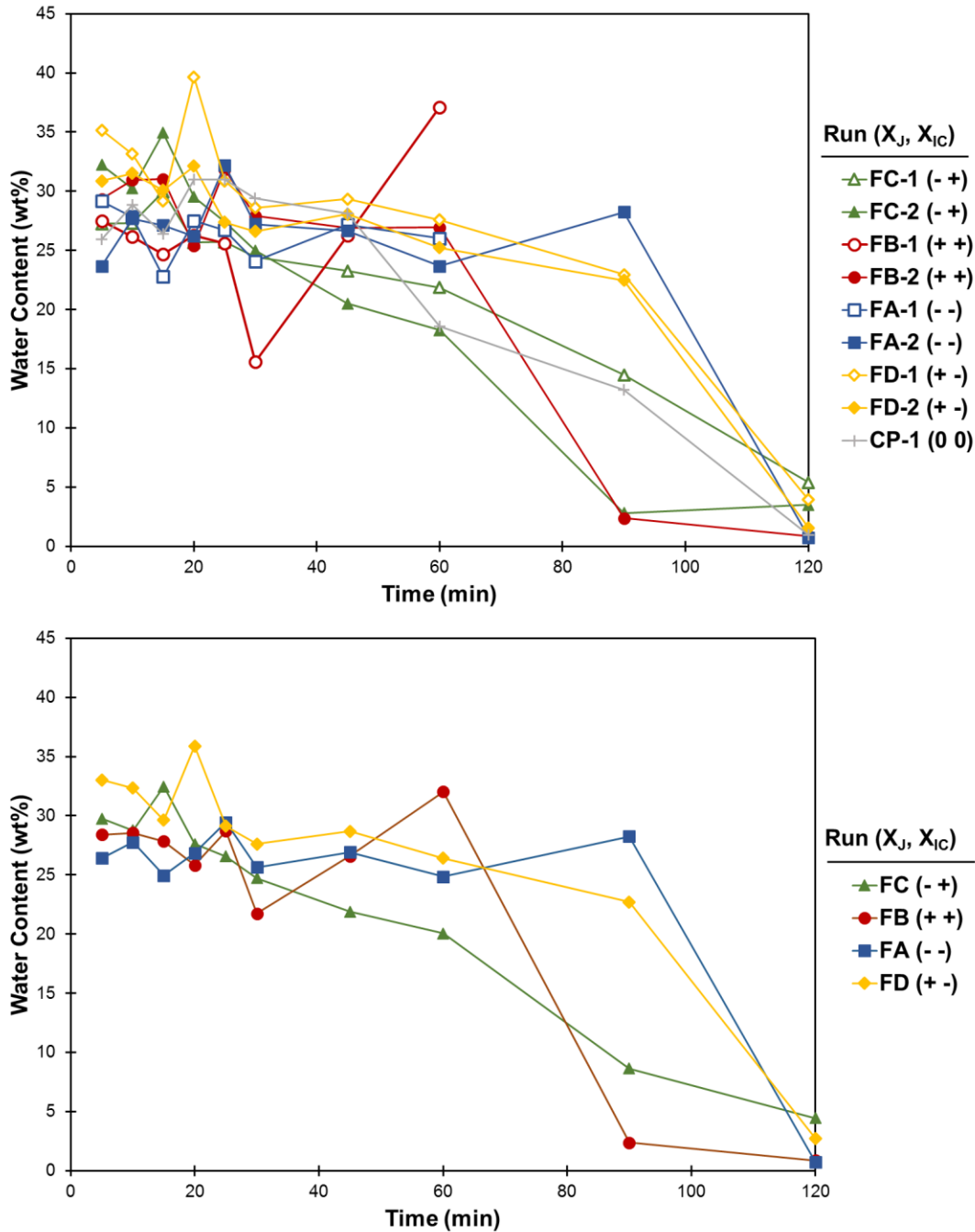


Figure 5-4: Water Content vs. Time at Z2 (96 mm below liquid surface) as determined by Karl Fisher titration (a) all runs including centre-point (b) data averaged between two replicates

The water content at Z2 resembles Z1 in that the water content starts at a high value and reduces over time. However, the pattern identified in height 1 (induction – fast settling – slow settling) is not evident here. Instead, most experiments show a steadier

reduction in the water content over time. Where there does appear to be an induction time, it lasts longer than at Z1.

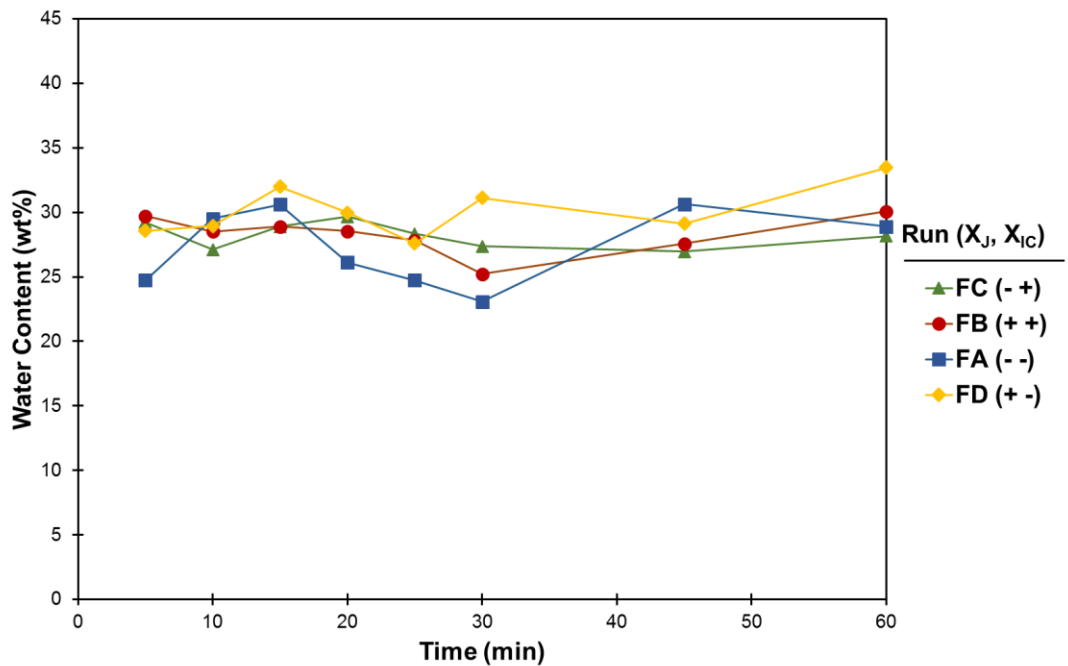
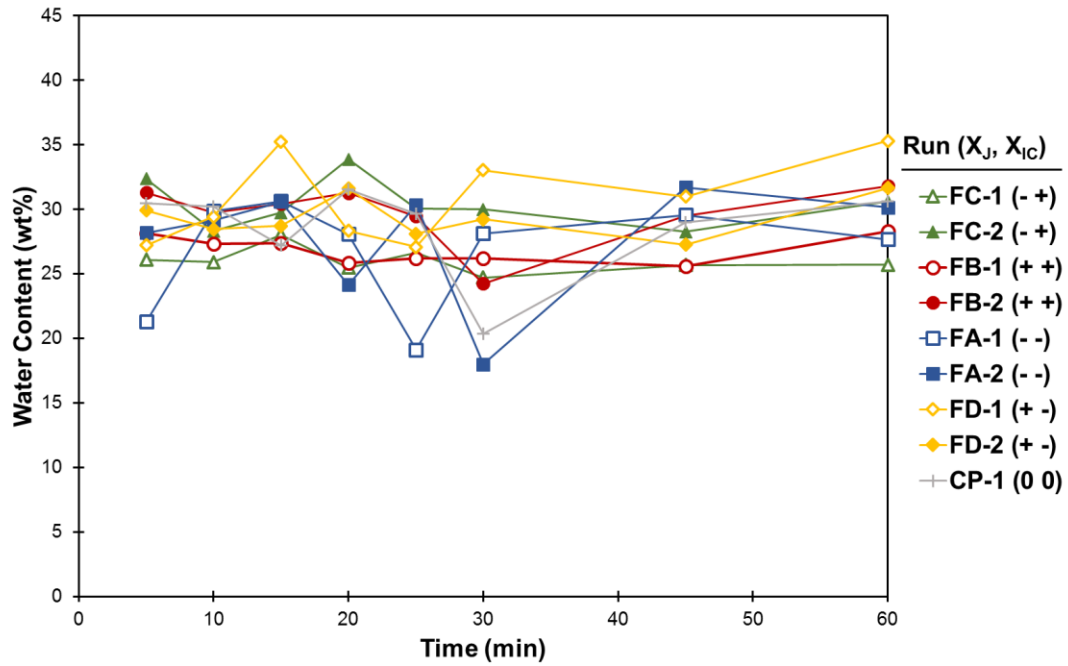


Figure 5-5: Water Content vs. Time at Z3 (140 mm below liquid surface) as determined by Karl Fischer titration for (a) all runs including centre-point (b) data averaged between two replicates

The water content at Z3 stays relatively constant over time. This means there is approximately the same amount of water settling into and settling out of this zone. Except for two experiments (both FA-1 and FA-2), the water content is higher at 60 minutes than at 45 minutes. This behaviour is consistent with a build up of a water-rich layer in the bottom of the CIST. Its front would eventually reach Z3 between 45 and 60 minutes. In other words, the tank below Z3 is slowly building up water and solids while naphtha and bitumen migrate upward. Clearly Z3 is in the bottoms layer at 60 minutes, and it is expected to continue to have high water content at 90 and 120 minutes. Analysis with Dean Stark extraction shows that this zone becomes very water rich by the end of settling – see Section 5.3 for more detail.

Figure 5-6 shows similar data for average-quality froth for comparison (Arora, 2016).

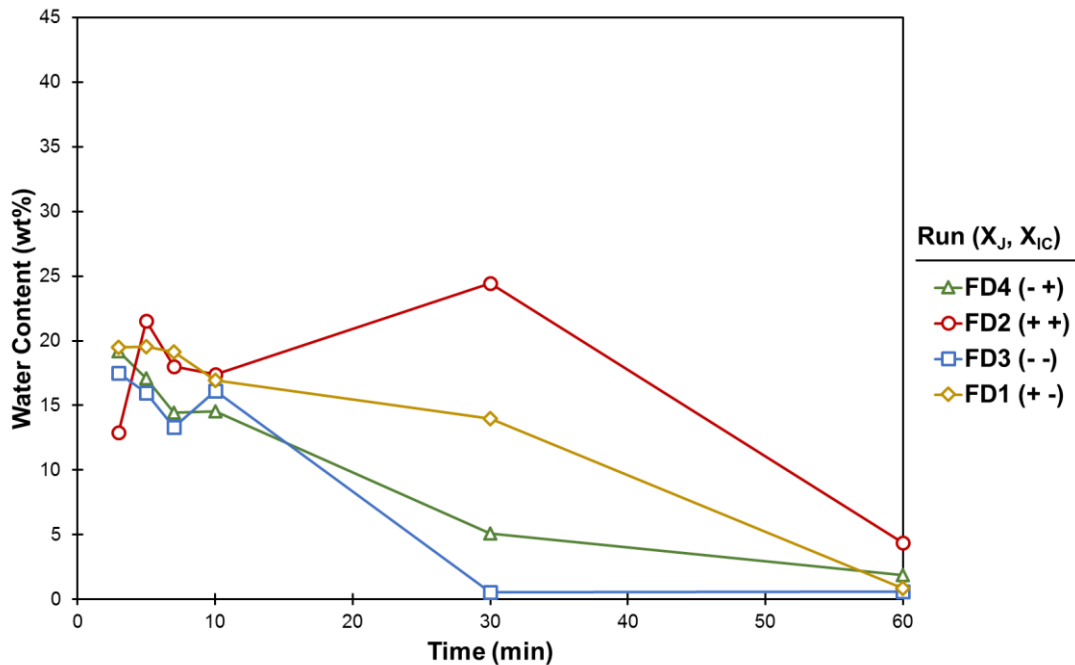


Figure 5-6: Water Content vs. Time at Z3 as determined by Karl Fischer titration for average-quality froth, produced from data collected by Arora (2016) with permission

The pattern of water content at Z3 in low quality froth differs greatly from average-quality froth. No matter the mixing conditions for average-quality froth, the water

content at Z3 was considerably lower than the water content at Z4, and much closer to the water content at Z1 and Z2 (Arora, 2016). Low-quality froth, by contrast, has a higher water content at Z3, much closer to the water content at Z4 by the end of settling.

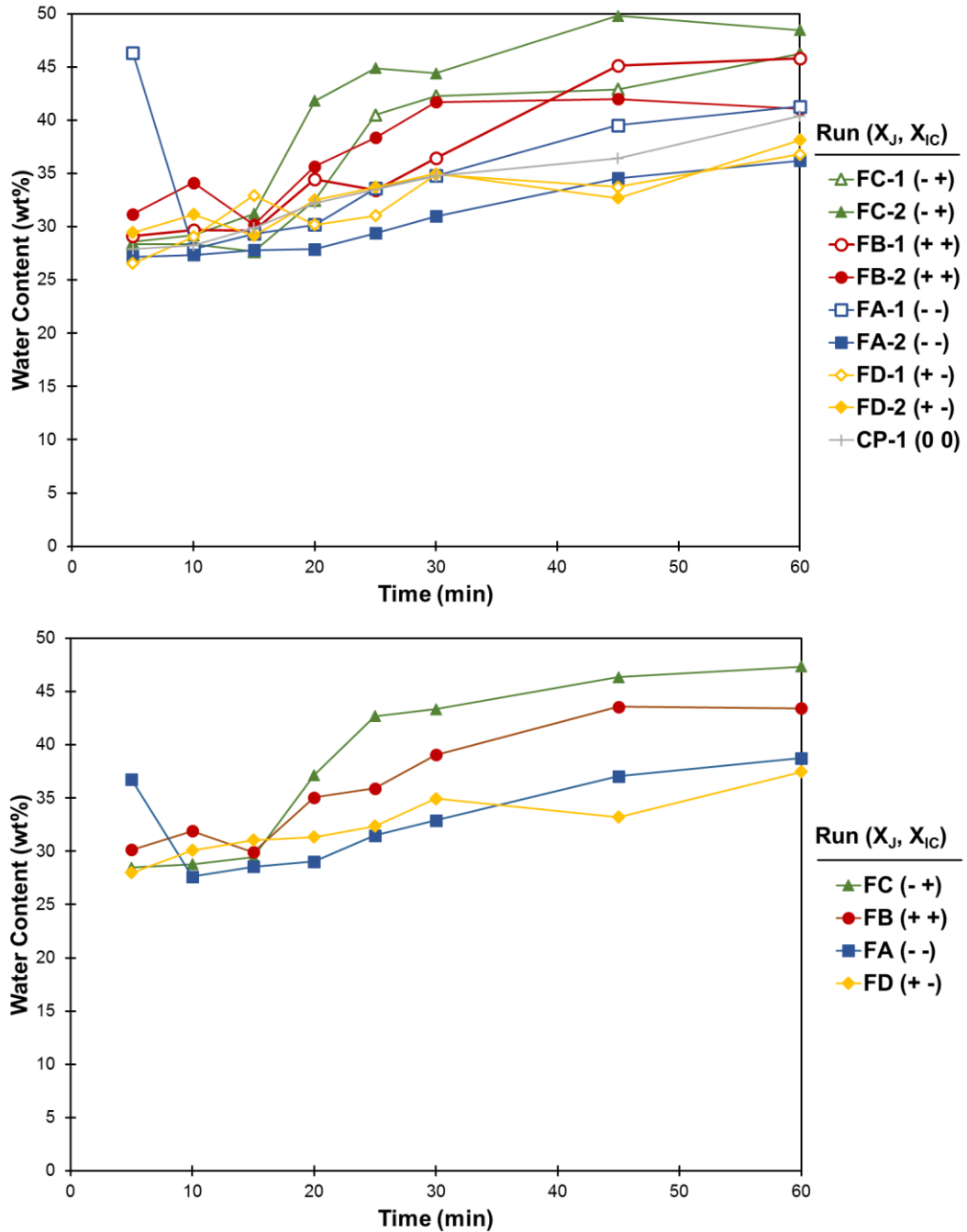


Figure 5-7: Water Content vs. Time at Height 4 (lowest sampling point) as determined by Karl Fischer titration for (a) all runs including centre-point (b) data averaged between two replicates

The water content at Z4 generally increases. At the high water content present in this zone, researchers have identified non-Newtonian behaviour and high viscosities owing to structural (i.e. interparticle interaction) effects or droplet crowding (Kokal, 2005). If

interparticle interactions are insignificant, then this is termed compression, otherwise it can be called consolidation.

This zone is hypothesized to slow the settling in the zones above it. This could be through compression or consolidation: fluid escaping the interstitial spaces has to flow upward, slowing the settling above it. Alternatively, the compression or consolidating may itself be the source of the induction time: the water content at Z1 cannot be reduced until the water-rich layer contracts until Z1 is no longer in it.

5.2.1.3 Final Settling Period

As in Figure 4-6, the water content at the beginning of settling and at the end of settling were graphed in Figure 5-8.

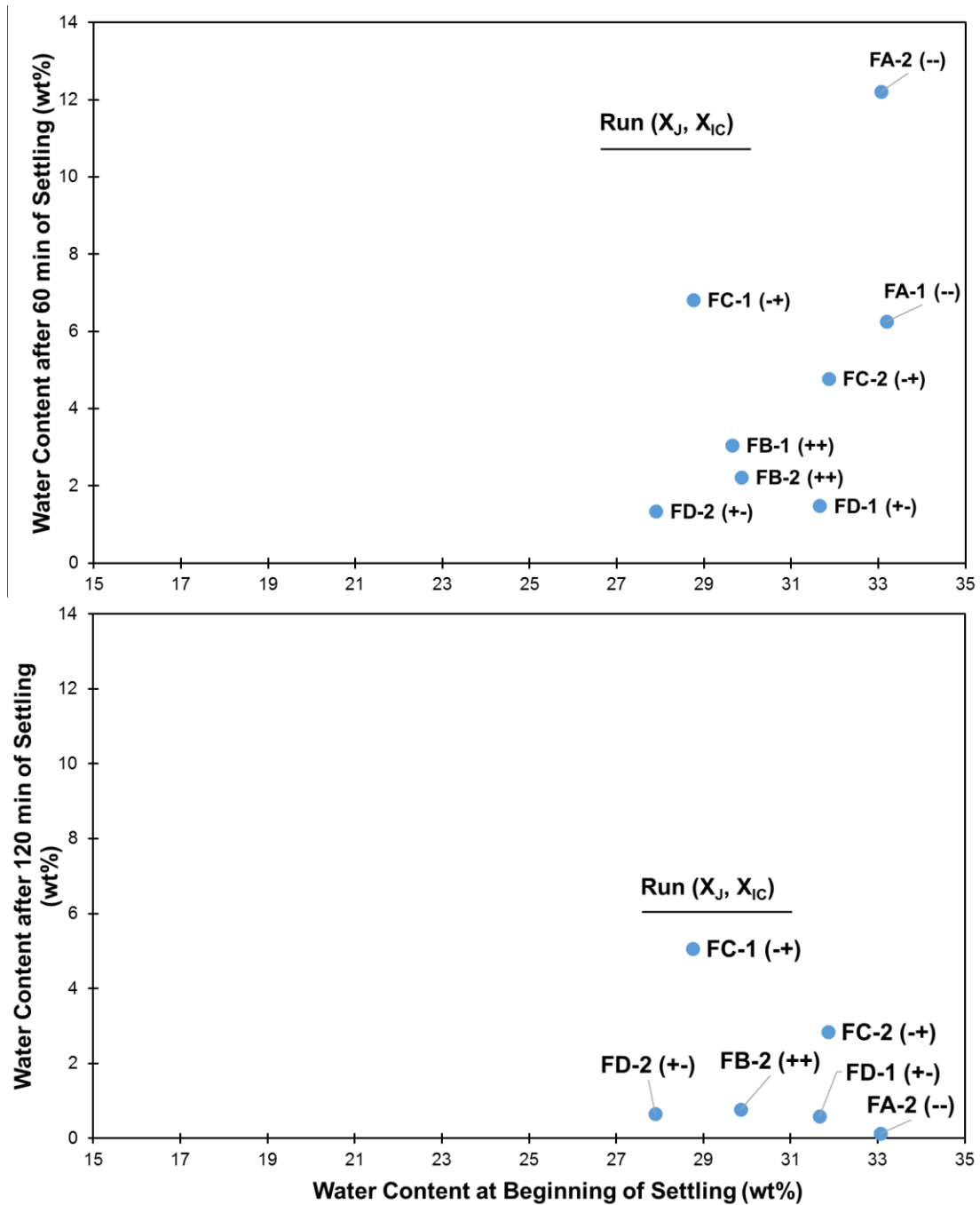


Figure 5-8: Comparison of Water Content at Beginning of Settling and After (a) 60 min and (b) 120 min

In Figure 5-8a, all the experiments with a high J condition had a water content less than 4% after 60 minutes, while all those at low J had a water greater than 4%. This suggests

that the energy input has made a large difference at this stage, and that higher energy input leads to lower water content at 60 minutes.

To support this claim, a multivariate analysis of variance (MANOVA) analysis was conducted. The results are in Table 5-3. The analysis indicates that the variation due to J is significant at a 95% confidence level.

Table 5-3: MANOVA table for factors at height Z1, 60 minutes

Variation	SS	d.f.	MS	F _o	p
J	60.22	1	60.22	11.93	0.026
IC	2.43	1	2.43	0.4815	0.526
J*IC	10.87	1	10.87	2.153	0.216
Error	20.19	4	5.047		
Total	93.7	7			

Unlike Figure 4-6, which graphed all runs under good mixing conditions, the data is not tightly clustered on the bottom right, indicating that high initial water content is no longer a good predictor for low water content after 60 minutes. No relationship between these two values can be detected.

Graphing the same information at 120 minutes in Figure 5-8b, the clean division between low and high J no longer exists. It seems that after 120 minutes a favourable IC condition (i.e. low IC) can compensate for a poor J condition (low J) or vice versa.

5.2.1.4 Comparison of Effects of Mixing Energy and Injection Concentration

A factorial design was used to provide a broad overview of the important control variables – mixing energy J and injection concentration IC – on the water content at all sampled heights and times, as determined by Karl Fischer titration. This is the first time data has been collected at four heights for a low-quality froth.

Since each experiment had the same 35 samples, the contrast method was run 35 times in MATLAB. The centre-point experiment was not replicated and thus not used for this

section. The coefficients and confidence intervals at 90 and 120 minutes were calculated using a different procedure using only 4 experiments.

The goal of finding these coefficients is not to propose a predictive model but rather to uncover the important effects. The underlying model used for this analysis is:

$$C(t, h) = \beta_0 + \beta_J X_J + \beta_{IC} X_{IC} + \beta_{J*IC} X_J X_{IC}$$

Wherein each time and height has its own set of coefficients (β) and the X variables are the factorial levels of the variables of interest, as shown in Table 5-1. The coefficients are graphed with 95% confidence intervals for each time and height. Figure 5-9 below shows the coefficients for all times at height 1.

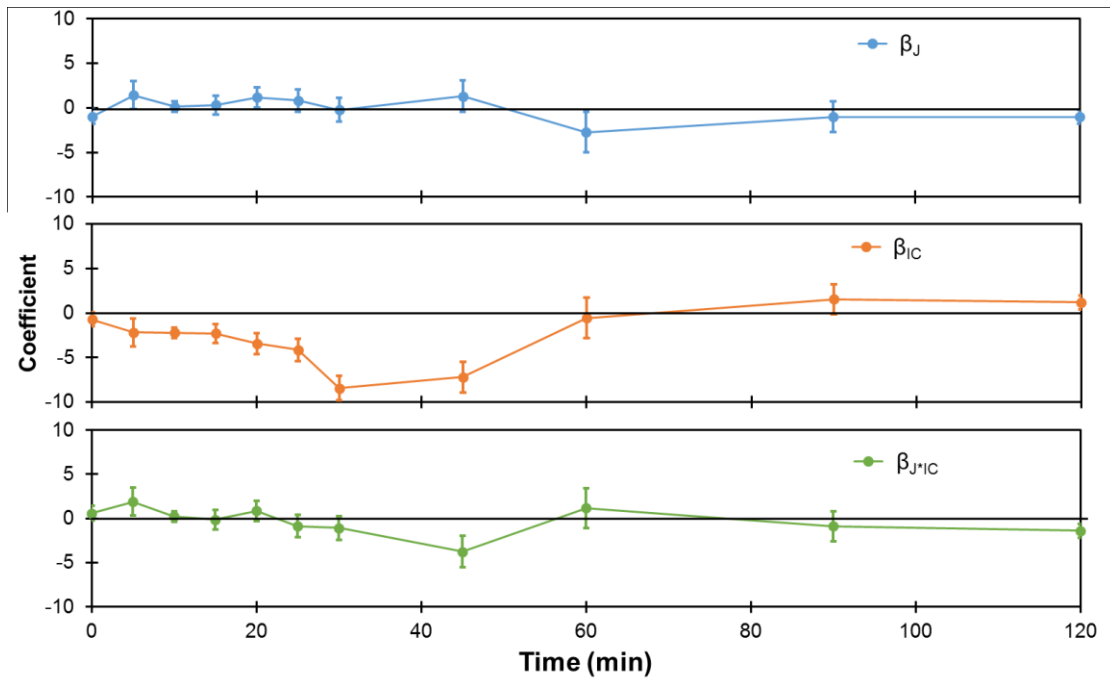


Figure 5-9: Coefficients for Water Content at Z1 over Time

Previous studies in froth disagree on the effect of mixing energy J . Arora (2016) found in average-quality froth that J correlated positively with water content for minutes 3, 5, and 7, and negatively during minutes 10, 30, and 60. Chong (2013) found in high-solids froth that J negatively correlated with water content at height 1 at all sample times.

High J may be associated with high water content (the opposite of expectations) at the beginning but crosses the axis, so that by 60 minutes high J is associated with low water content as expected.

The finding on the effect of injection concentration also vary. Chong (2013) – who used a froth with high solids content but average water content – found that injection concentration was negatively correlated with water content at height 1 at minutes 5, 7, and 10 but then positively correlated toward the end of settling. Arora (2016), who used average-quality froth, showed that low IC was correlated with less water content at height 1 throughout the experimental time.

The data collected during this campaign showed a pattern like that in Chong's (2013) data. Injection concentration was negatively correlated with water content until 60 minutes; the negative correlation persisted much longer. This is a very important finding; if a 60-minute settling time is desired, low injection concentration may have the opposite of the intended effect.

Between 60 and 90 minutes, the coefficient becomes positive although its confidence interval extends over 0, meaning the effect is not significant within a 95% confidence level at this time point. By the end of settling, low IC may be correlated with less water content.

Previous studies (Arora, 2016; Chong, 2013) have shown that high mixing energy and low injection concentration (over the ranges studied) leads to favourable settling by the end of settling. The available evidence shows that this is true for low-quality froth as well.

There is no significant interaction effect at most time points.

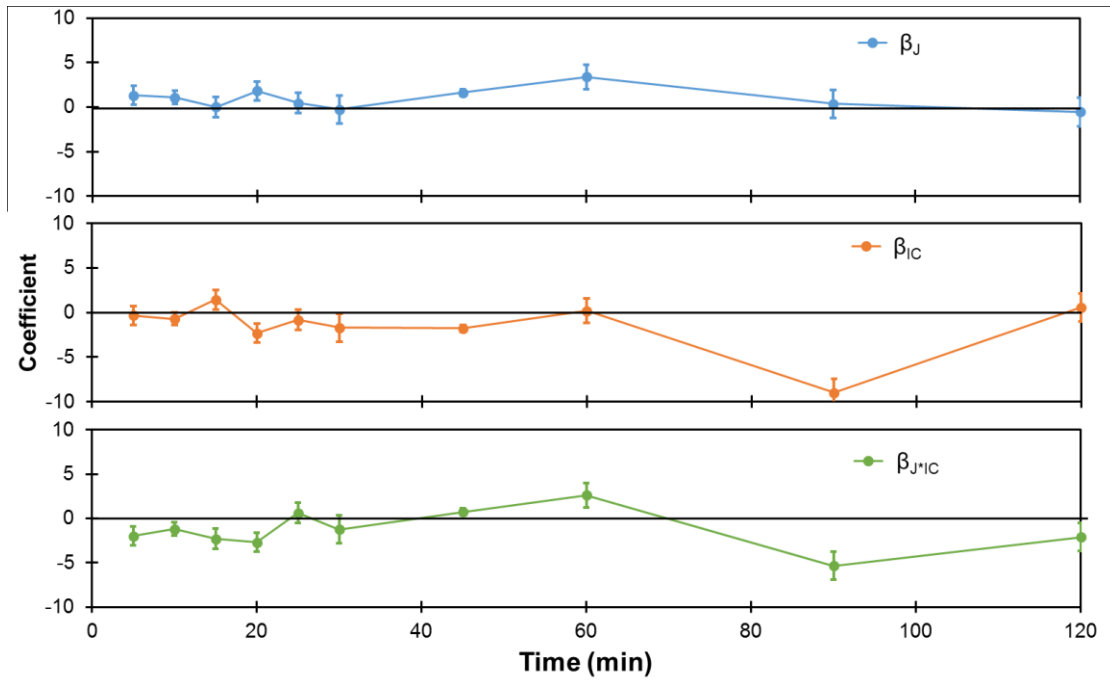


Figure 5-10: Coefficients for Water Content at Z2 over Time

At Z2 the trends are similar to those at Z1. There is a very strong negative relationship between injection concentration and water content until it becomes positive late in the settling. This is similar to Z1 but the change in the sign occurs later than at Z1. This may indicate that the phenomenon we saw at Z1, above Z2, is repeated at Z2, but later: an intuitive result. The trend for mixing energy also seems to follow the Z1 result, but later. However, the confidence intervals cross the x-axis at many of the points, indicating that the relationship can not be detected as significant at a 95% confidence level.

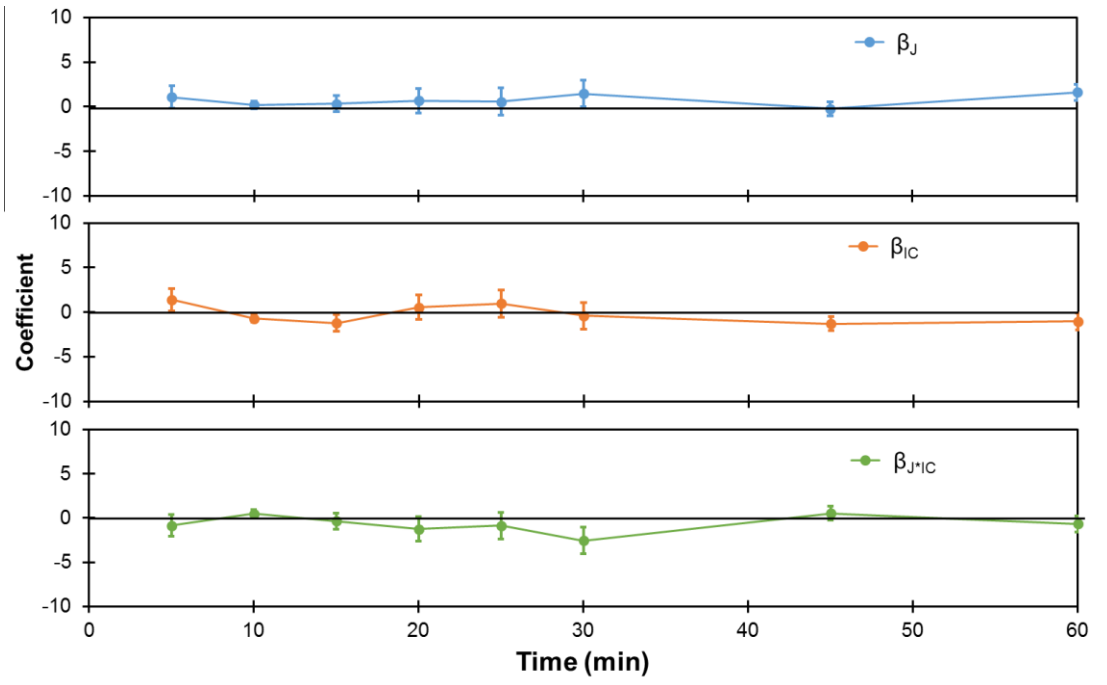


Figure 5-11: Coefficients for Water Content at Z3 over Time

Z3 and Z4 are considered a part of the bottom layer, owing to their high water-content. In the bottom layer, high water-content is more desirable less product loss to the waste stream. Data were only collected until 60 minutes for these two heights.

There are few significant results detected at Z3 because there was little variation in water content.

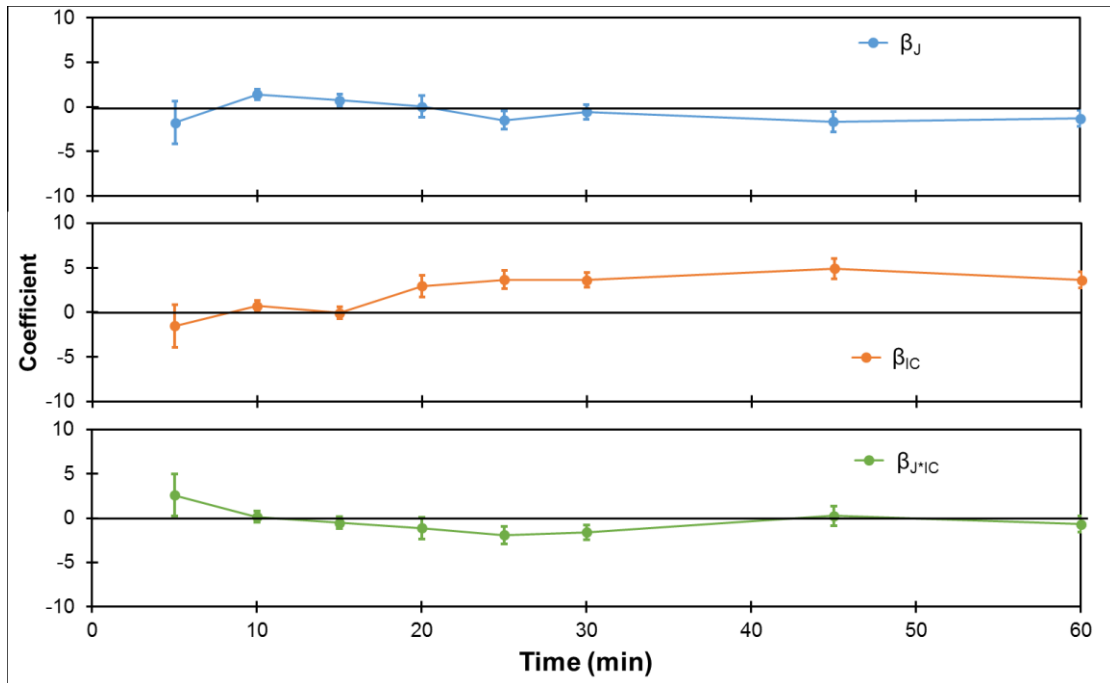


Figure 5-12: Coefficients for Water Content at Z4 over Time

At Z4 there are significant effects. Injection concentration shows a strong positive correlation with water content after 15 minutes, indicating that high water content at the lowest sampling level is associated with high injection concentration. This is not consistent with the hypothesis that low injection concentration leads to better settling.

The effect of J at this height is also unexpected: from 25 minutes onward, high water content is associated with low J.

Low injection concentration and high mixing energy are associated with lower water content at the top two heights; by mass balance, this implies that the bottom zone (the water-rich layer) is larger at 60 minutes.

If the effects are the same sign at 90 and 120 minutes as at 60 minutes, it would be desirable to reduce the amount of product or diluent loss to the underflow by having a higher IC or lower J or to balance this criterion against the purity of the product stream. This unexpected result may also give a hint about the settling mechanisms at play.

Long induction time is associated with high J and low IC, as will be discussed in the next section. The slow contraction of the water-rich layer, either due to compression or consolidation, may be causing the induction time. Since long induction times were also associated with low water contents at the high levels, it may be that the compression or consolidation assists water and solids removal, or some factor contributes to both effects.

5.2.1.5 Induction Time

To see if induction time could act as a predictor of final water content, the final water contents at 60 minutes (for all 9 experiments) and 120 minutes (for the 7 experiments which include this data) were graphed:

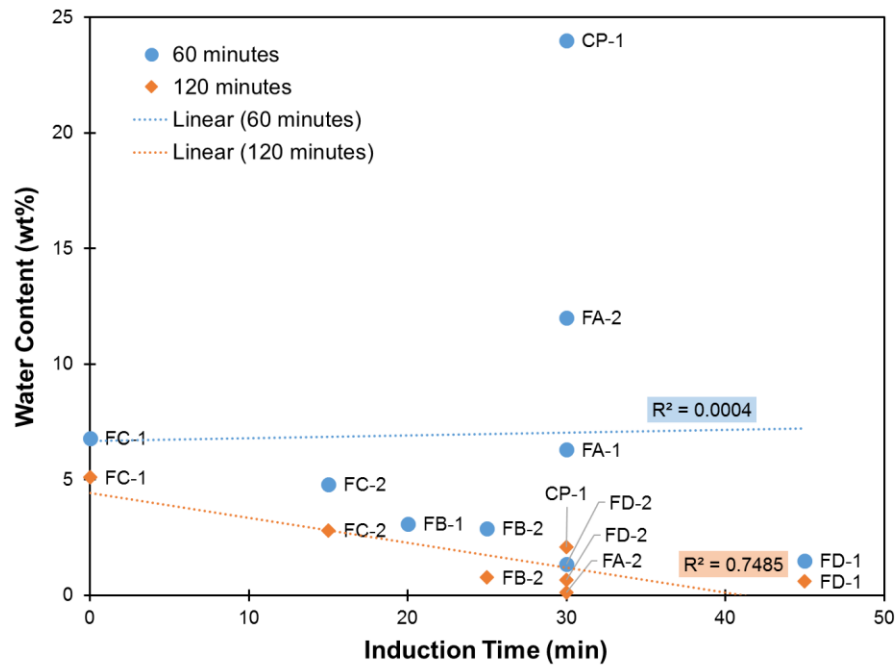


Figure 5-13: Induction Time compared to Water Content at 60 and 120 min

The induction time does not correlate with the water content at 60 minutes. At 120 minutes, there is a clear negative relationship. The experiments at this time are also organized on this line in approximately the order of the favourability of their mixing

conditions. The worst mixing condition (FC, low J high IC) produces a high final water content and very little induction time. The best mixing condition (FD, high J low IC) produces two of the higher induction times (30 and 45 minutes) and two of the lower water contents at 120 minutes (0.6% and 0.66%).

5.2.2 Mass Balance

A simple mass balance of water was conducted on the vessel using water content data obtained with sampling and Karl Fischer titration. The estimation used the water content at the four sample points, assumed the top was the same water content as at Z1, and the bottom was the same water content as at Z4. A schematic of this is presented in Figure 5-14 for one experiment (FD-2). The top of the vessel has the lowest water content, and each lower height is higher in water content. To estimate the water content over the whole of the vessel, we take the area to the left of the line. Since height is dimensionless, this approximates the overall water content.

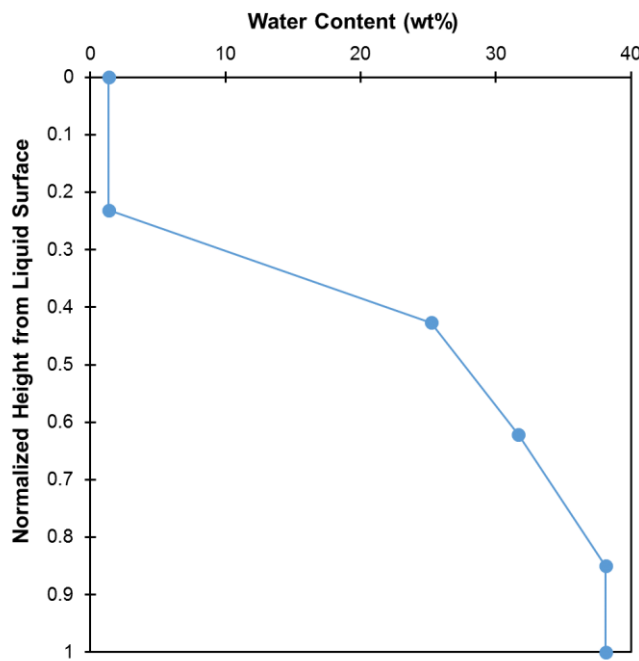


Figure 5-14: Water content (wt%) vs. height for FD-2 at 60 minutes. Top and bottom points are assumed.

Note that data points were not taken at the lower heights Z3 and Z4 after 60 minutes. This estimation was conducted at all time points between 5 and 60 minutes inclusive for all experiments.

The estimated overall water content tended to fall over time, even though the water content should stay the same, or even increase (since hydrocarbon components are more volatile than water).

Table 5-4 shows the estimated water content at 5 min and 60 minutes. Except for the centre-point, all experiments had a lower estimated water content at 60 minutes than at 5 minutes. The amount of water unaccounted for varied from 1.5 – 9.4 wt%, or 5-28% of the water content present at 5 minutes. No relationship between the water loss and the mixing variables could be detected.

Table 5-4: Estimate of overall water content for select times.

Experiment (X _J X _{ic})	FC (- +)		FB (+ +)		FA (- -)		FD (+ -)		CP
Replicate	1	2	1	2	1	2	1	2	
Water Content – 5 min (wt%)	27.3	27.6	28.4	31.3	33.7	27.6	30.2	30.1	28.7
Water Content - 60 min (wt%)	24.2	24.4	26.3	23.6	23.9	24.6	23.1	22.1	28.8
Water Loss (wt%)	2.7	2.7	1.5	7.2	9.4	2.8	6.6	7.5	-0.2
Water Loss (%)	10	10	5	23	28	10	22	25	-1%

15% of the volume of the vessel lies below Z4. It could be that this zone becomes more water-rich over the settling time and thus has most of the water that is unaccounted for. However, OWS analysis (discussed in more detail in Section 5.3) shows that the water content in this zone is approximately 42% for all experiments except for FB-2. This does not match with the amount of water that is unaccounted for by a mass balance.

Attempting to apply a common correction method to every experiment does not yield to more consistent results. It is hypothesized that the inconsistencies arise from the exact location of the interface between low- and high-water zones, which could be highly variable between runs but difficult to pinpoint with only four sample locations.

5.2.3 FBRM Results

The FBRM was inserted into the CIST before the beginning of naphtha blending and collected chord length data during naphtha blending, demulsifier dispersion and settling. For discussion these are separated into different sections. Other values are monitored by the FBRM or can be calculated from the data, such as average diameter or square-weighted mean diameter. However, the counts and chord length distributions changed little between experiments, so the discussion is confined to these metrics.

5.2.3.1 Data Overview

FBRM data was collected in all 9 experiments. Many of these experiments had a very high fouling index – an indication of the degree to which the window of the probe is covered in stagnant material. Because of this high fouling index, the data from many experiments were not used in the following discussion. The runs are shown in order of date conducted in Table 5-5, which also shows which runs provided good data. An important observation made during the campaign was that the window treatment lasted for 2 experiments before failing.

We eventually overcame the fouling with the use of a surface treatment to repel oil and water from the probe window. Five experiments were conducted with this treatment. Experiment FB-1 was eliminated because the probe was placed too high in error, and the level of liquid quickly evaporated to below the probe window.

For more discussion on the challenges associated with the use of the FBRM in bitumen froth and the solutions which were used in the lab, see Section 2.2.

Table 5-5: FBRM Data Collection Summary

Experiment	X _J	X _{IC}	Useable	Notes
FA-1	-1	-1	No	Failed: high fouling index
FC-1	-1	+1	No	Failed: high fouling index
FD-1	+1	-1	Yes	Data to 30 min
CP-1	0	0	Yes	Data to 30 min
FB-1	+1	+1	No	Failed: high fouling index
FD-2	+1	-1	Yes	Data to 30 min
FA-2	-1	-1	Yes	Data to 30 min
FB-2	+1	+1	No	Failed: erroneous placement of probe
FC-2	-1	+1	No	Failed: high fouling index

5.2.3.2 FBRM Counts During Naphtha Blending

The naphtha blending step was isolated, and chord counts collected into three size categories to observe general trends over time. The naphtha blending step was designed to be as similar as possible between experimental treatments; the mixing time was held constant, and a constant power input was maintained by running the impellers with higher power number at lower RPM. Figure 5-15 and Figure 5-16 show trends for two experiments.

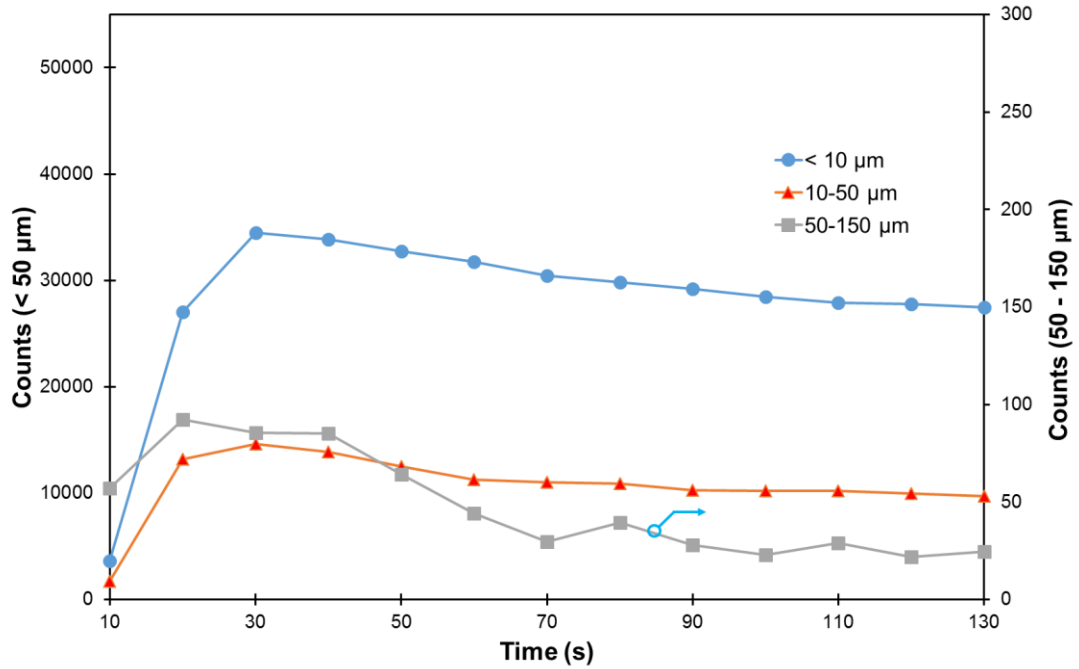


Figure 5-15: FBRM Counts during Naphtha Blending for FA-2 ($X_J = -1$, $X_{IC} = -1$)

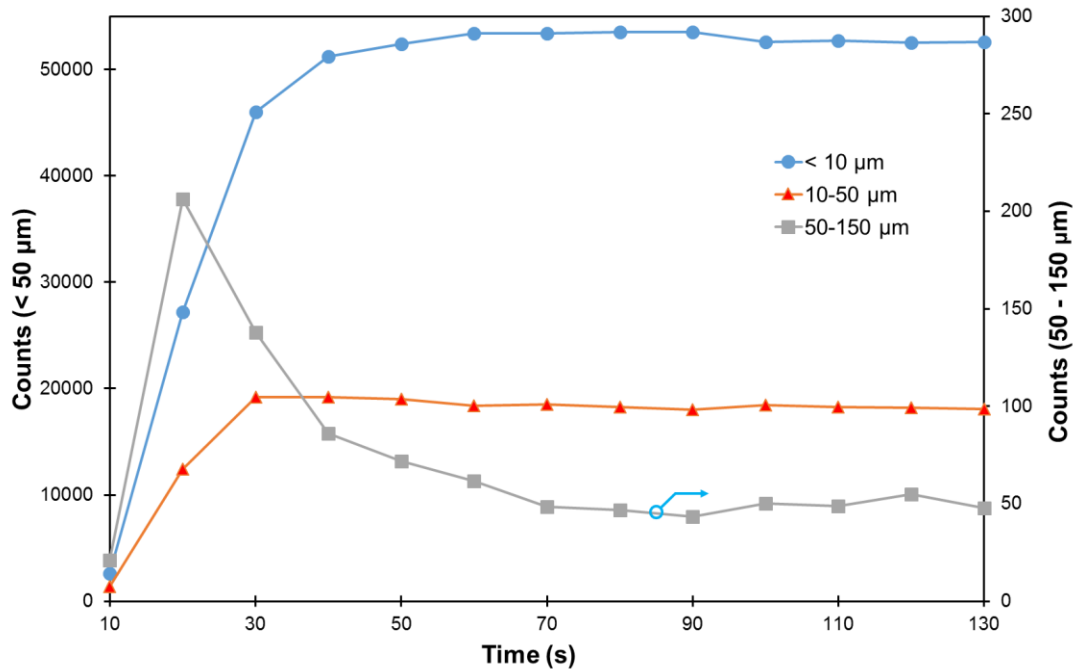


Figure 5-16: FBRM Counts during Naphtha Blending for FD-1 ($X_J = +1$, $X_{IC} = -1$).

All available data sets show a rapid increase in counts followed by a quick levelling off. The rapid increase in counts is presumably from droplets and particles being suspended

after having been settled or partially settled. The rapid levelling-off is good indication that the naphtha blending is working as intended. In fact, for all experiments, within 1 minute the counts in each channel are within 15% of their value at the end of naphtha blending.

The only difference noted between runs was that Run FA-2 had considerably fewer counts in all three size categories than the other three runs – CP-1, FD-1, and FD-2. The main difference between runs was the impeller. The results from CP-1 and FD-1 were very similar to FD-2.

5.2.3.3 FBRM Counts During Demulsifier Dispersion

Mixing energy and injection concentration were varied during demulsifier dispersion. These factors have been shown to affect the settling step. The same factors may also have a detectable effect on the chord lengths detected by the FBRM during demulsifier dispersion. We will examine and discuss the chord length data collected during this step of the process.

Note that because mixing time varies between runs (10 minutes for the high J case, 2 minutes for low J, and 5.25 minutes for the centre point), the number of points (which are always 10s apart) varies as well. The axis limits are set to the same values as in the previous section to allow easy comparison, and the counts of larger droplets and particles are on the secondary Y axis.

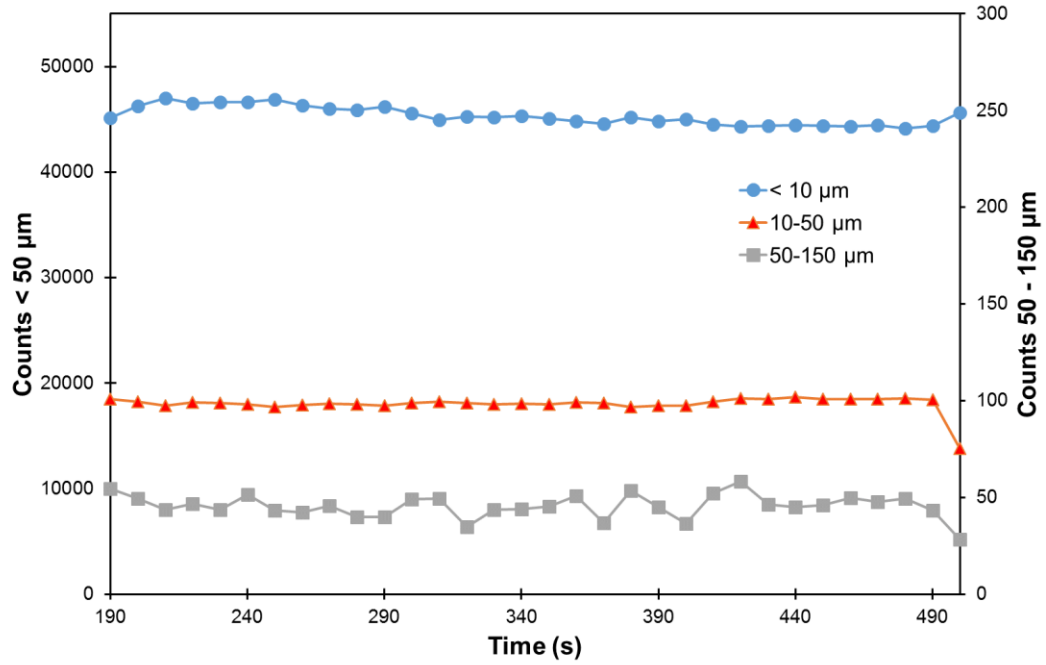


Figure 5-17: FBRM Counts during Demulsifier Disp. for Experiment CP-1 ($X_J = 0$, $X_{IC} = 0$). Similar to results from FD-1, FD-2.

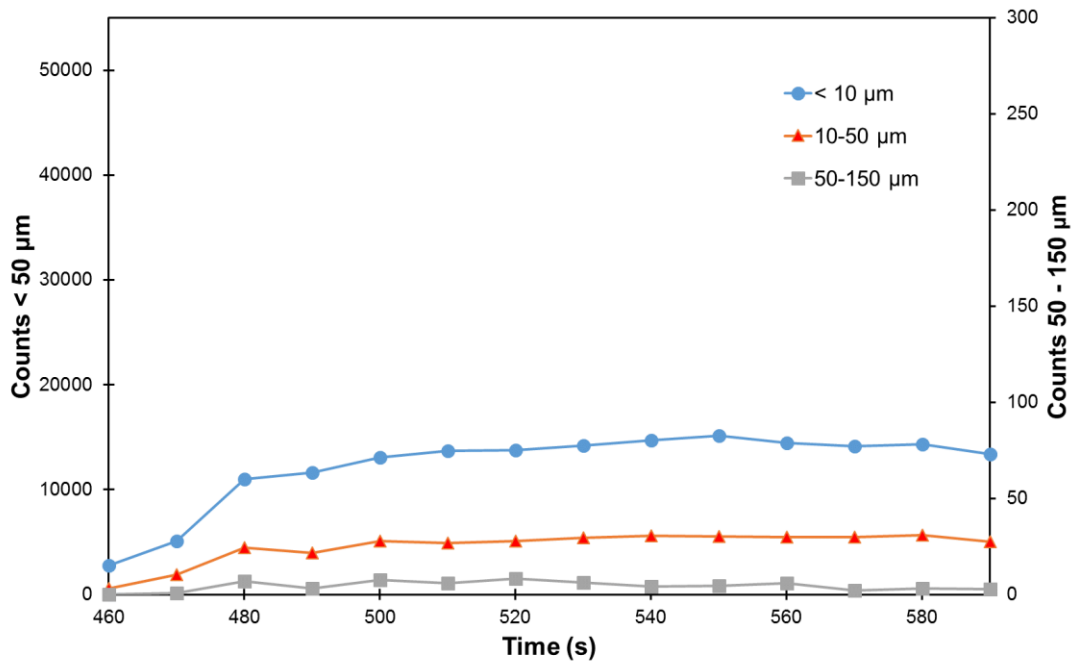


Figure 5-18: FBRM Counts during Dem. Disp. for Experiment FA-2 ($X_J = -1$, $X_{IC} = -1$)

The most significant finding of the time trends of chord counts is that they do not show a gradual change over the whole period of demulsifier dispersion; instead there is only a rapid change at the beginning as the impellers are turned on. If there were significant coalescence or flocculation of particles below 50 μm during demulsifier dispersion, there would be a reduction in counts of these trends as either the larger droplets or flocs either moved to the larger bin sizes (50-150 μm or higher) or settled to below the level of the FBRM. A reduction in counts in any size category could have also pointed to breakup outpacing coalescence or flocculation, especially if were accompanied by a growth in counts in the lowest size category.

As before, experiment FA-2 had considerably fewer counts than the other experiments. This experiment had low J: it may be that the mixing energy was no sufficient to lift particles from the bottom of the vessel. The results of FD-1, FD-2, and CP-1 were again very similar.

5.2.3.4 FBRM Counts During 30 minutes of Settling

The counts are captured in Figure 5-19 and Figure 5-20 for the first 30 minutes of the settling process. Most of this 30 minutes is considered induction time; the KF titration shows very little change in the water content at the top sampling point. In contrast, the FBRM data does show a change in counts for many experiments.

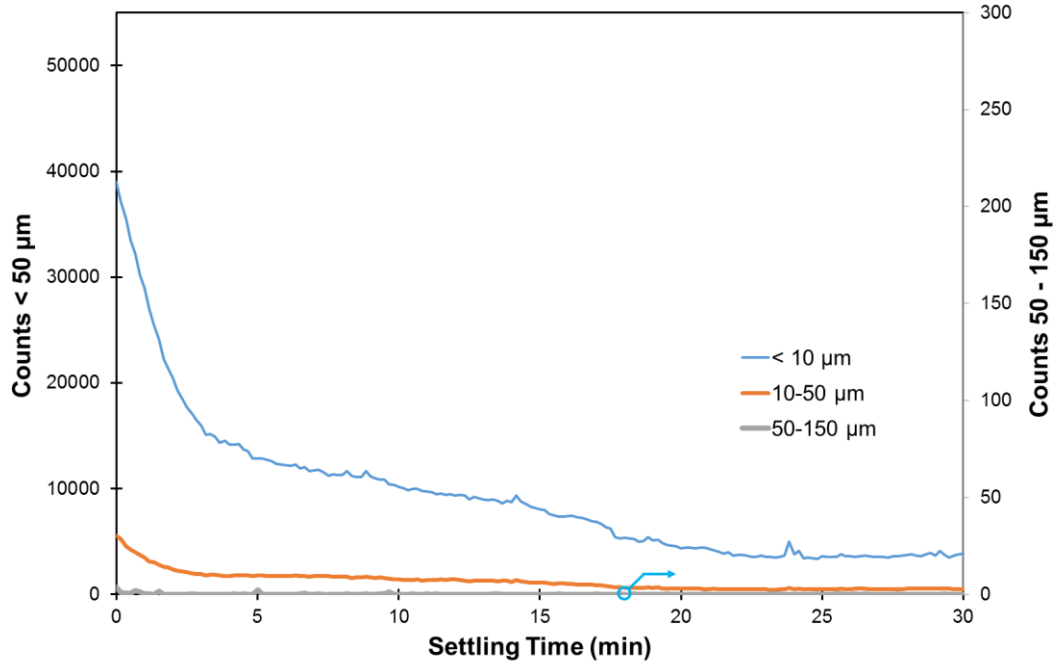


Figure 5-19: FBRM Counts during 30 minutes of Settling for CP-1 ($X_J = 0$, $X_{IC} = 0$)

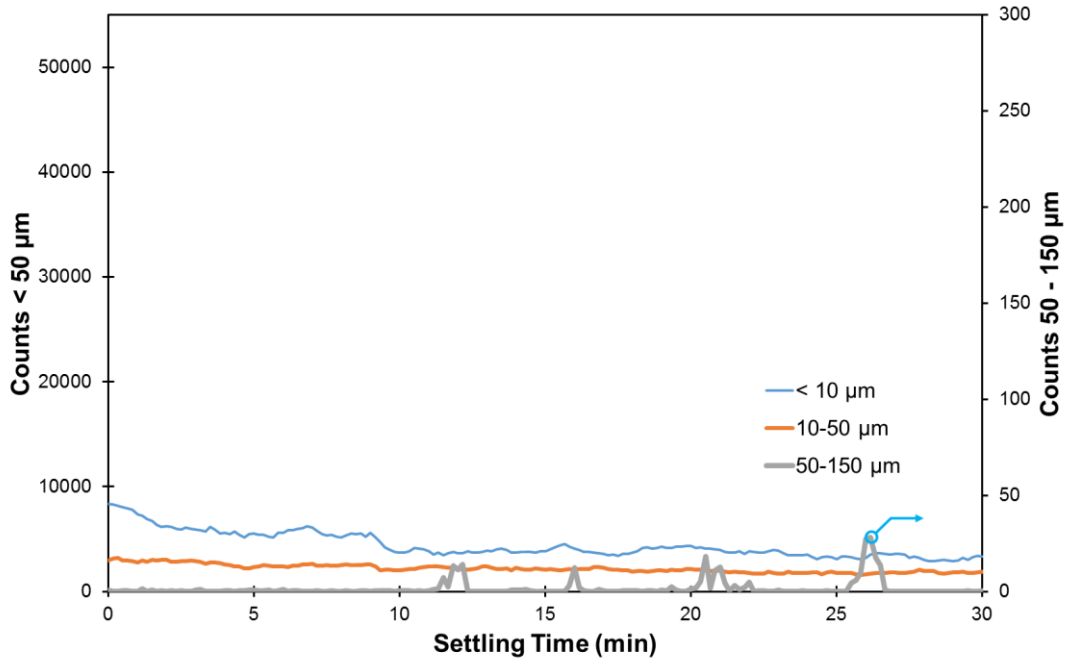


Figure 5-20: FBRM Counts during 30 minutes of Settling for FA-2 ($X_J = -1$, $X_{IC} = -1$)

Experiment FA-2, run at low J and low injection concentration, starts from a base of much lower counts of particles and droplets in the $< 10 \mu\text{m}$ range, and yet its final

number of counts is comparable to that of the other experiments (3300 counts compared to 3800 for CP-1, 2500 for FD-1 and 2800 for FD-2). The final counts of 10 – 50 μm species is significantly higher at the end of FA-2 as well (1900 compared to approximately 500 for all three other experiments).

A very notable difference between FA-2 and the remaining experiments is the initially high rate of removal of fines. This is followed by a removal rate that is much slower, though still faster than that of FA-2. The same is true of 10 – 50 μm to a lesser extent.

5.2.3.5 Chord Length Distributions of Naphtha Blending

Figure 5-15 and Figure 5-16 show chord length distributions that were collected during naphtha blending for FA-2 and FD-1, respectively. FD-2 and CP-1 were similar to FD-1 and not shown here.

The chord length distribution shows the whole profile of sizes which were detected in the fluid. This may give more information than the trends in each size category and allow us to spot mechanisms of settling and combination. The chord length distributions will be examined for evidence of the mechanisms which were discussed at the beginning of this chapter.

An unweighted chord length distribution will tend to be dominated by fines. Depending on the process, it is common practice to use weighted means or size distributions. The right-hand set of distributions in the chord length distributions is this weighted distribution. The weighting is further detailed in Section 2.1.2; it weights the counts in each bin according to the square of the bin size, emphasizing larger lengths in the distribution.

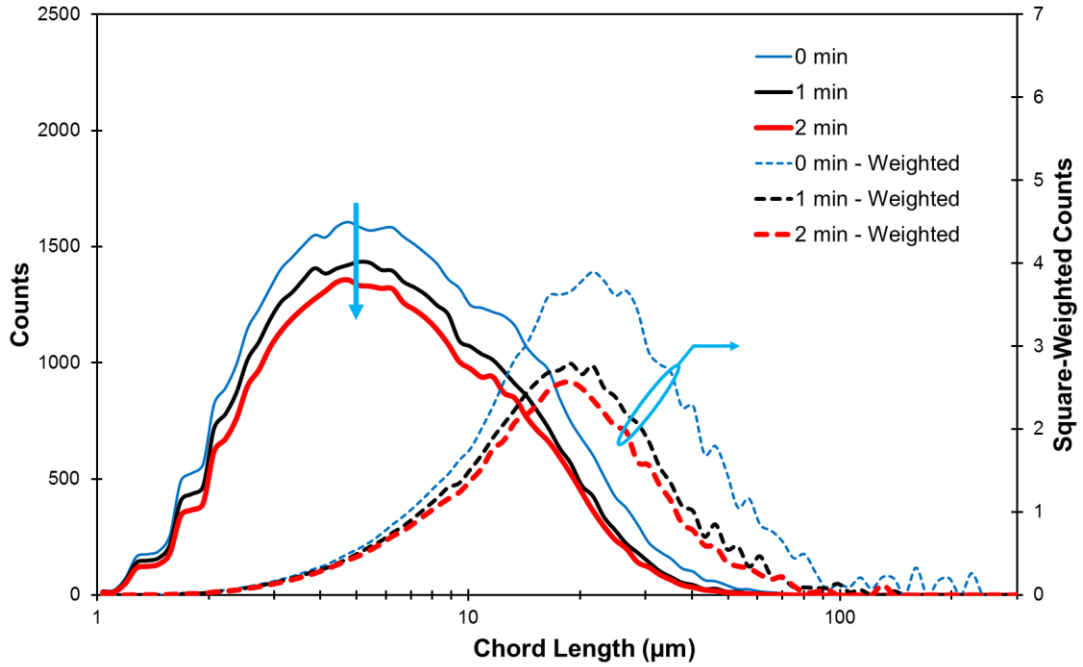


Figure 5-21: Chord Length Distributions for Naphtha Blending of FA-2 ($X_j = -1$, $X_{IC} = -1$)

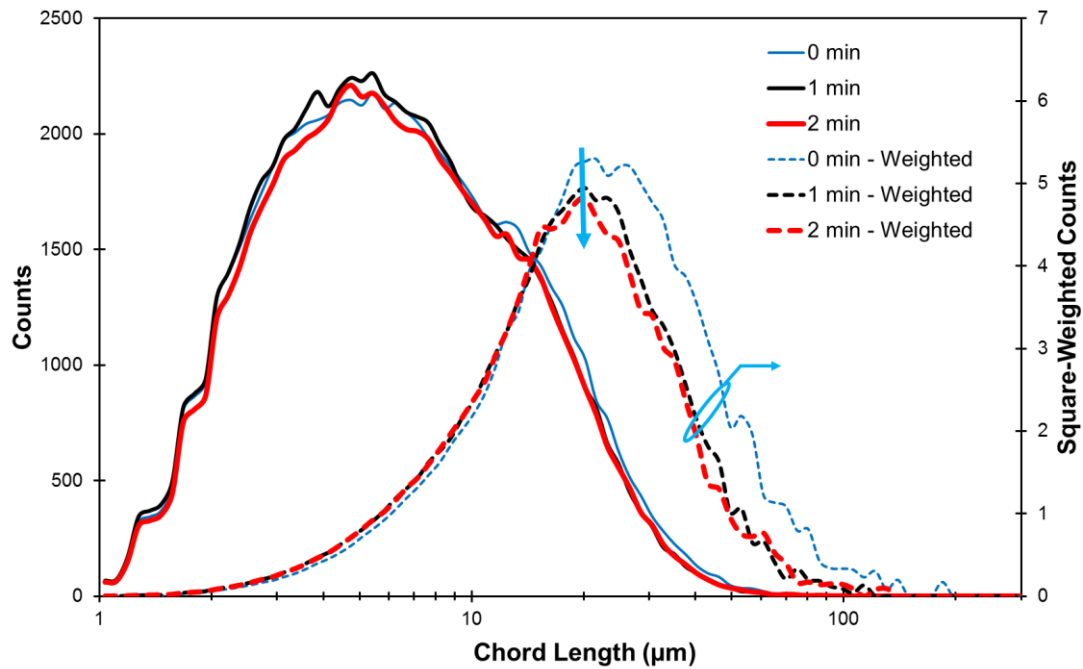


Figure 5-22: Chord Length Distributions for Naphtha Blending of FD-1 ($X_j = +1$, $X_{IC} = -1$)

As in Section 5.2.3.2, there is little difference between CP-1, FD-1, and FD-2. Only FD-1 is shown here. In these three it seems that large droplets are disappearing, shifting the square-weighted distribution down and to the right. The peak of the large distribution is approximately 20-25 μm , so each large droplet that breaks up into smaller droplets will not make an appreciable difference to the count of smaller particles.

The results from FA-2 are quite different: in both the unweighted and square-weighted distributions there is a loss of counts. This would indicate that despite the running impellers, there is significant disappearance of all sizes of species.

5.2.3.6 Chord Length Distributions of Demulsifier Dispersion

As in the previous section, chord length distributions are compared between experimental conditions. In the case of demulsifier dispersion, the mixing time varies between runs. A low J condition (as in FA-2) corresponds to 2 minutes, while the middle and high conditions of J correspond to 5.25 minutes and 10 minutes respectively.

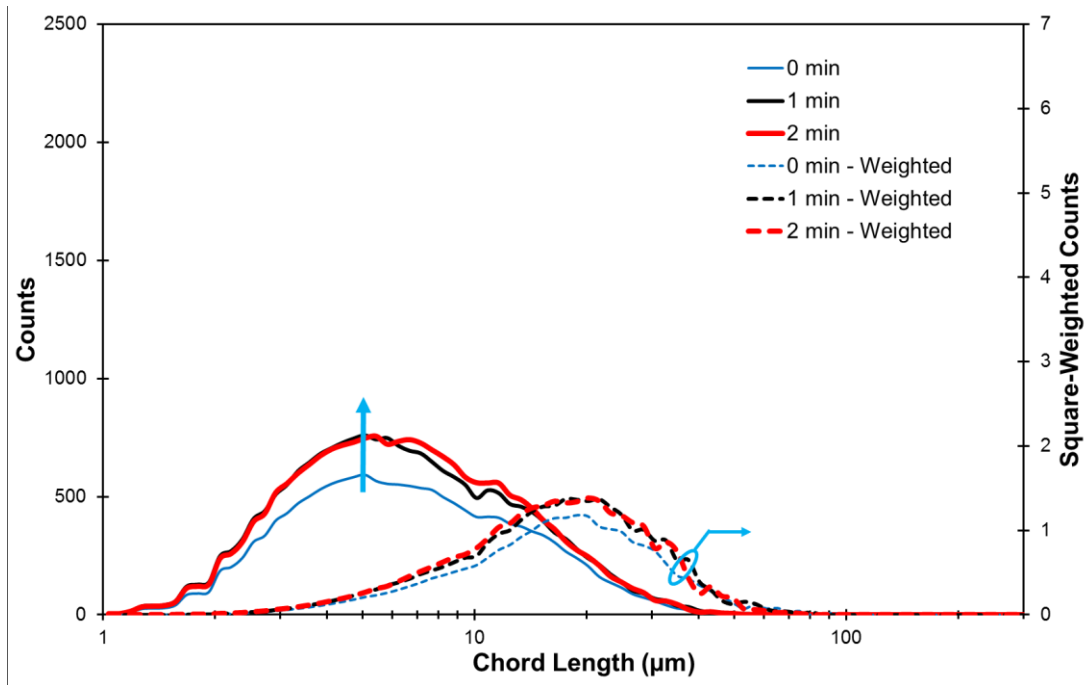


Figure 5-23: Chord Length Distributions for Demulsifier Disp. of FA-2 ($X_j = -1$, $X_{IC} = -1$)

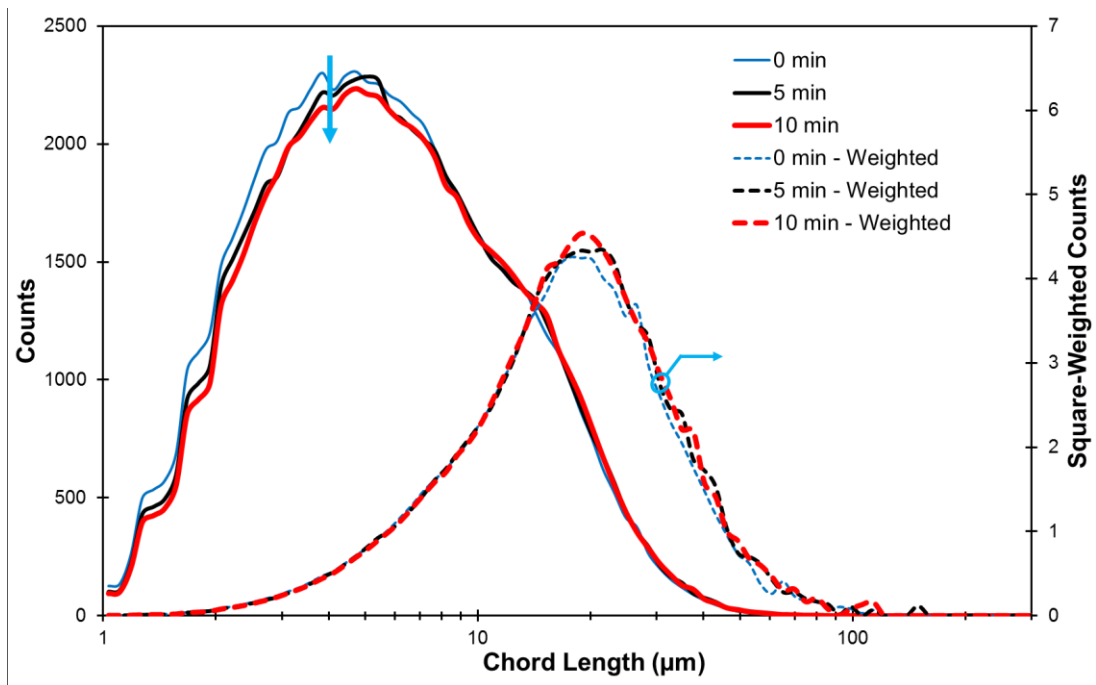


Figure 5-24: Chord Length Distributions for Demulsifier Disp. of FD-1 ($X_j = +1$, $X_{IC} = -1$)

An important observation is that the chord lengths do not change substantially in any of the experiments, despite the addition of demulsifier. It is apparent that whatever coalescence or flocculation behaviour the demulsifier promotes is offset by the turbulence induced by the impellers.

There is some change during demulsifier dispersion in FA-2, but by comparison with Figure 5-18 we can see that this is probably because this experiment reached steady state slower than the other experiments which ran at high impeller speed.

FA-2 again has considerably less counts than the other 3 experiments, though the distribution is similar in terms of the dominant sizes. It is possible that the mixing provided is inadequate to lift all the water and solids from the bottom of the vessel. If the difference was due to the different power input or flow distribution a different distribution of sizes would be expected.

5.2.3.7 Chord Length Distributions of Settling

Figure 5-25 and Figure 5-26 depict the chord length distributions over settling for 3 points: the beginning (with a small offset to eliminate a spike in data that occurs when the impellers are turned off), then at 15 minutes of settling and 30 minutes of settling. The data was truncated at this point because at some point after 30 minutes there is significant fouling measured by the instrument (refer to the beginning of Section 5.2.2 for further detail). The chord length distributions will be analyzed for hints of the mechanisms and discussed.

CP-1 and FD-2 have very similar trends to FD-1 and so are not shown.

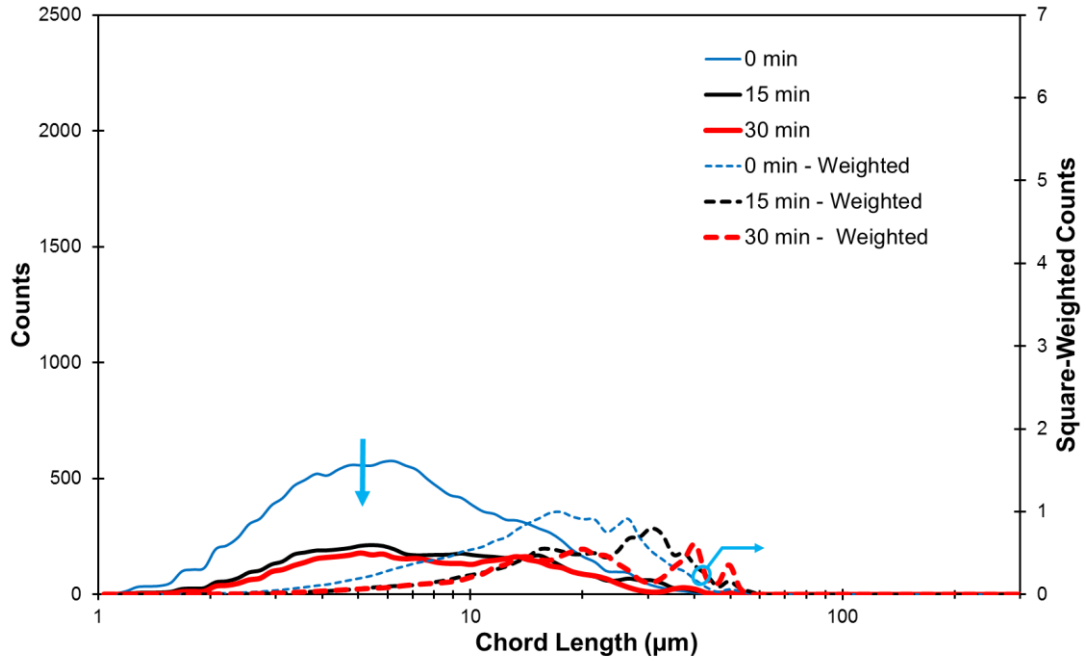


Figure 5-25: Chord Length Distributions for Settling of FA-2 ($X_j = -1$, $X_{IC} = -1$)

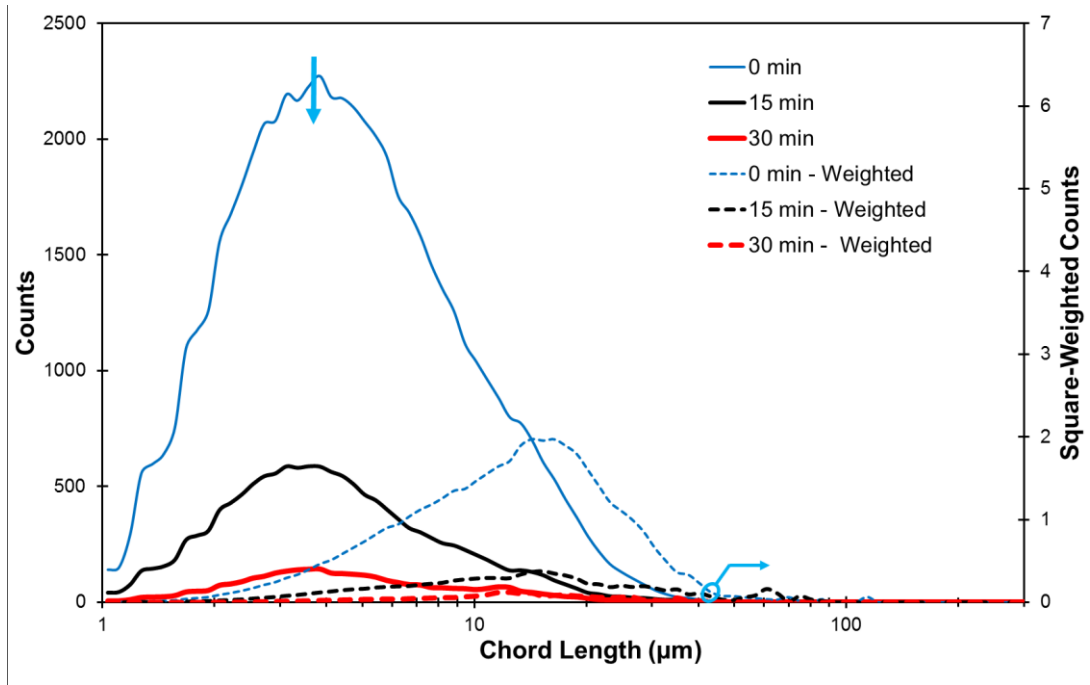


Figure 5-26: Chord Length Distributions for Settling of FD-1 ($X_j = +1$, $X_{IC} = -1$)

Both the weighted and unweighted distributions show a significant reduction – by a factor of 3 or more – in counts by 15 minutes. This seems to be in direct contrast with the Karl Fischer data, which shows very little difference in the water content before 30 minutes.

Despite starting from a lower peak, it seems that FA-2 has not yet settled to the extent that the other experiments do. For some reason, very large flocs or droplets are persisting at the top heights.

Perhaps the extra mixing time or reduced injection concentration has an effect, despite not being detectable during demulsifier dispersion. Either mechanism may be responsible for better distributing the demulsifier chemical, so that as the components settle in the tank they better flocculate with other components. If the bulk of flocculation or coalescence occurs as large droplets or flocs settle in the tank, it may not be captured at the level of the FBRM (30 mm below the liquid surface), which is above the level of the first impeller (38 mm below liquid surface for the Rushton impellers, 50 mm for the Intermigs) and the first syringe-sampling point (52 mm) due to space restrictions.

Notably, experiment FA-2 has considerably fewer fines than the other experiments. It is also the only experiment of the 4 conducted at the lower energy input J . It is possible that the high level of turbulence in the other three cases created a lot of fines that are nonetheless removed – as evidenced by their lower fines counts by 30 minutes of settling.

5.3 Dean Stark OWS Data

Large samples of 100 mL were collected at the end of settling time at relative heights of 0.1, 0.5, and 0.9 (as measured from the top of the liquid at the beginning of sampling). These were sent to the industrial partner for analysis using the Dean Stark method of

extraction to determine the levels of oil, water, and solids (OWS). The results at the top height are shown in Figure 5-27.

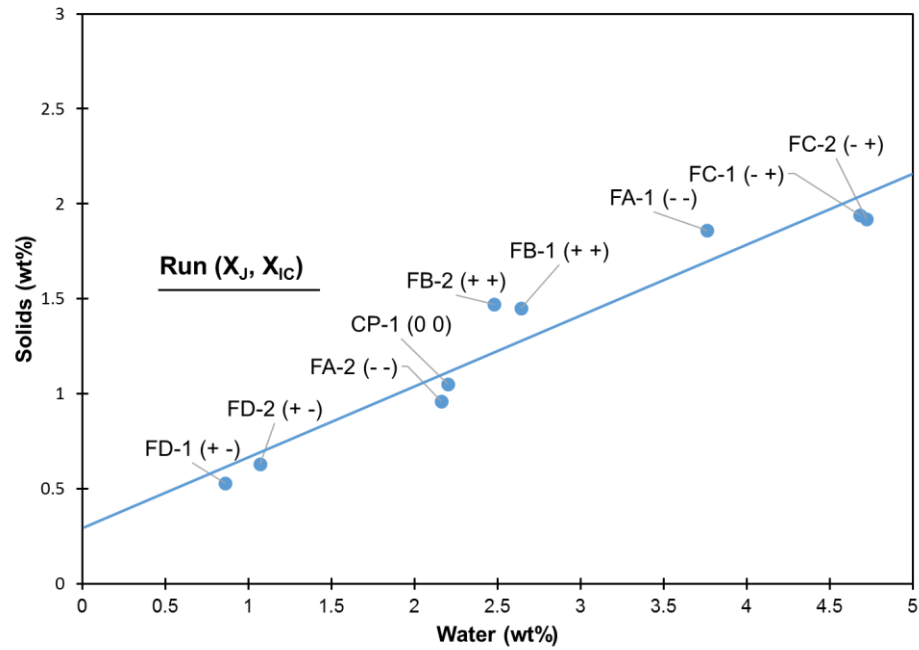


Figure 5-27: Water and solids content at top height ($h/H = 0.1$) for all experiments

As in average quality froth (Arora, 2016), the level of water and solids at the top layer are tightly related. In this case, mixing under the best conditions (FD: $X_j = 1, X_{ic} = -1$) produced the lowest water and solids content while the worst conditions (FC, $X_j = -1, X_{ic} = 1$) produced the higher water and solids content. All other experiments are between these extremes. It is worth noting that FA-1 and FB-1 only settled for 60 minutes while all others settled for 120 minutes, so their position may not be representative of the settling after 120 minutes.

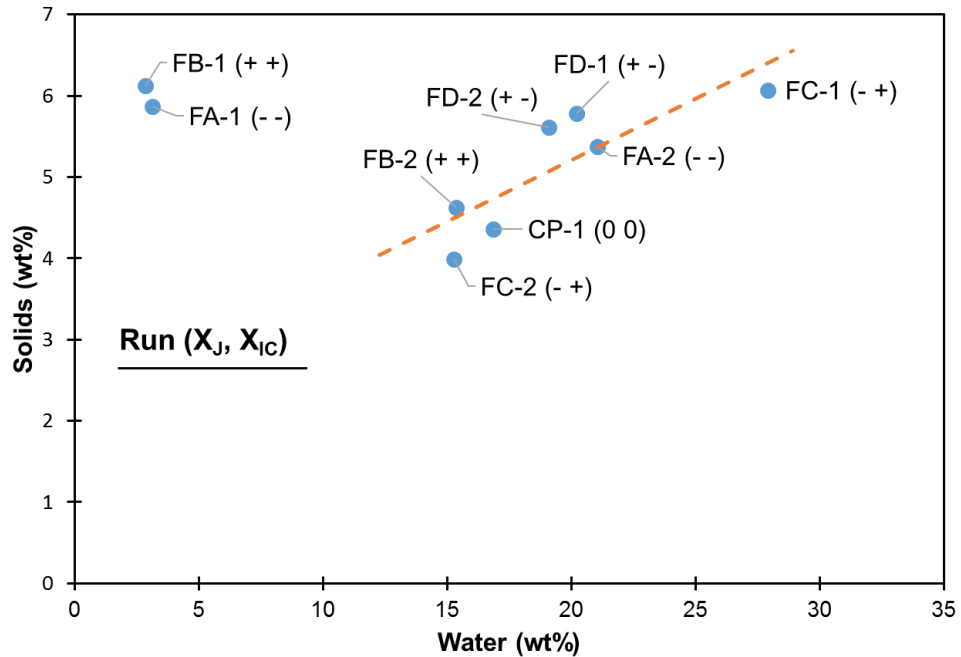


Figure 5-28: Water and solids content at middle height ($h/H = 0.5$) for all experiments

At the middle height, runs done at the same conditions are no longer clustered together, except for FD-1 and FD-2. This is especially true for FA-1 and FB-1, though this is probably because they settled for half the time - 60 min rather than 120 min. These disparities between different runs with the same experimental conditions – of which FC is the widest – may reflect the fact the middle zone is the most likely to have multiple mechanisms at work and thus be more random in nature.

One can see however that there is a relationship between solids content and water content, as above in Figure 5-27, indicating that they tend to settle together, suggesting that the flocculation of water and solids together is an important mechanism.

5.3.1 Effects Using Dean Stark Data

The Dean Stark data is subjected to multivariate analysis of variance (MANOVA) in a similar manner to the Karl Fischer data in Section 5.2.1 to uncover the important effects.

This analysis is shown for the top height in Table 5-6 and Table 5-7 for water content and solids content respectively. At the top height (the top 10% of the vessel), the effects of both mixing energy and injection concentration are significant at a 95% confidence level. This is true with respect to both the water content and the solids content at the top height.

Table 5-6: Multivariate Analysis of Variance for the Solids Content at $z/H = 0.1$

Source of Variation	Sum of Squares	d.f.	Mean Square	f_0	p-Value
J	0.8450	1	0.845	8.24	4.5%
IC	0.9800	1	0.980	9.55	3.7%
J*IC	0.0648	1	0.065	0.63	47.1%
Error	0.4104	4	0.103		
Total	2.3002	7			

Table 5-7: Multivariate Analysis of Variance for the Water Content at $z/H = 0.1$

Source of Variation	Sum of Squares	d.f.	Mean Square	f_0	p-Value
J	8.55	1	8.549	25.99	0.7%
IC	5.56	1	5.561	16.91	1.5%
J*IC	0.0105	1	0.011	0.03	86.7%
Error	1.35	4	0.329		
Total	15.4	7			

The detected effects on water in the top 10% of the vessel agree with the findings at Z1 in the Karl Fischer data – that high J and low IC lead to lower water content. They also agree with previous studies in the group (Arora, 2016; Chong et al., 2016; Laplante et al., 2015) in both bitumen froth and diluted bitumen. The same studies also showed that solids content trends with water content as it did in this analysis.

At the middle height, no effects were detected at the same 95% significance level for either solids or water. The analysis is shown for water in Table 5-8. The lack of effects may reflect the fact that the interface between low and high water contents is somewhere in this region, leading to unpredictability in the exact water content. In

average-quality bitumen froth, the middle height was similar to the top height – it had low water content and low solids content (Arora, 2016).

Table 5-8: Multivariate Analysis of Variance for the Water Content at $z/H = 0.5$

Source of Variation	Sum of Squares	d.f.	Mean Square	f_0	p-Value
J	12.2	1	12.2	0.152	71.6%
IC	0.536	1	0.536	0.007	93.9%
J*IC	201	1	201	2.52	18.8%
Error	320	4	79.9		
Total	533	7			

Each sample was taken at the end of settling, but the first two experiments FA-1 and FB-1 were only allowed to settle for 60 minutes while all the other experiments settled for 120 minutes. Perhaps the settling at the top height is mostly finished but at the mid height is still proceeding. FA-1 and FB-1 (the two which were collected at 60 minutes) had the lowest water contents by a significant margin: their average water content is 3.00 wt% while the remaining experiments have an average water content of 19.4 wt%. It is hypothesized that over the course of the last 60 minutes of settling, the tightly-compacted bottoms layer builds up through settling until it reaches approximately $z/H = 0.5$. This supports the assertion that for low-quality froth it is crucial to allow the settling step to continue for 120 minutes. Interestingly, the solids content does not show a similar discrepancy. The average solids content is 6.00 wt% for the first two experiments and 5.11 wt% for all the rest.

A similar MANOVA could not be done at $z/H = 0.9$ because one data point could not be collected at this height. The graph of solids content vs. water content is shown in Figure 5-29:

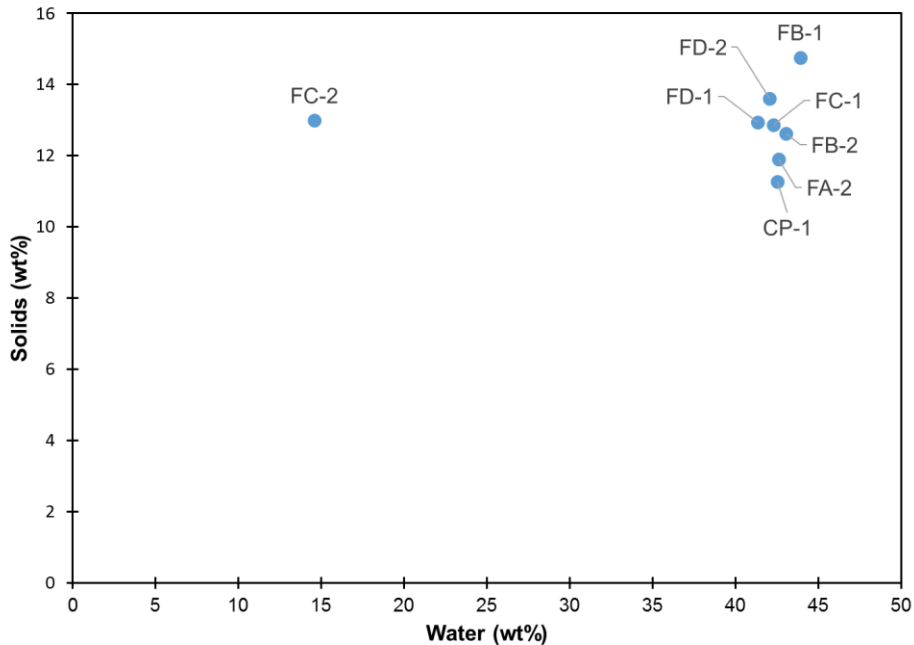


Figure 5-29: Water and solids content at $z/H = 0.9$ for all experiments

Aside from one outlier, the water content is tightly clustered around 42 wt%, while the solids content varies from 11-15% with no discernable pattern between runs.

5.4 Selected Microscope Data

Samples were taken and applied to microscope slides to make qualitative observations. Previous works in the group have also applied quantitative analysis to micrographs from dilbit (Leo, 2013) and average-quality froth (Arora, 2016). However, the micrographs taken of low-quality froth were qualitatively very different from dilbit and average-quality froth and not conducive to image analysis using protocols known to the group. Qualitative analysis is also difficult as patterns between runs are difficult to identify; even runs under the same conditions seem to look different.

Nevertheless, the micrographs can help interpret the FBRM data and Karl Fisher data by giving visual information on the quantity, size, and morphology of water droplets, solid particles, and flocs.

The induction time was also observable on microscope data. Some examples are highlighted in Figure 5-30 and Figure 5-31 (Xu, 2016):

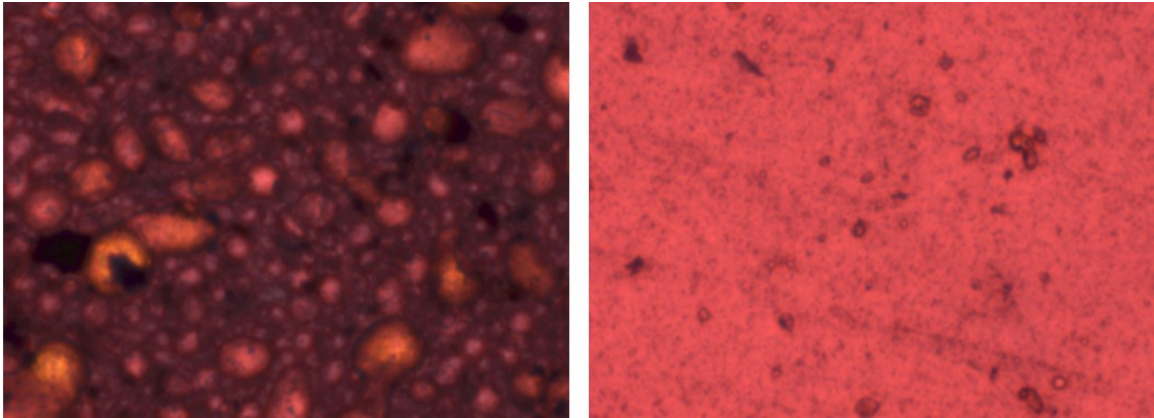


Figure 5-30: Micrographs showing difference in fluid before and after induction for experiment FA-2 (at 30 min and 45 min, respectively)

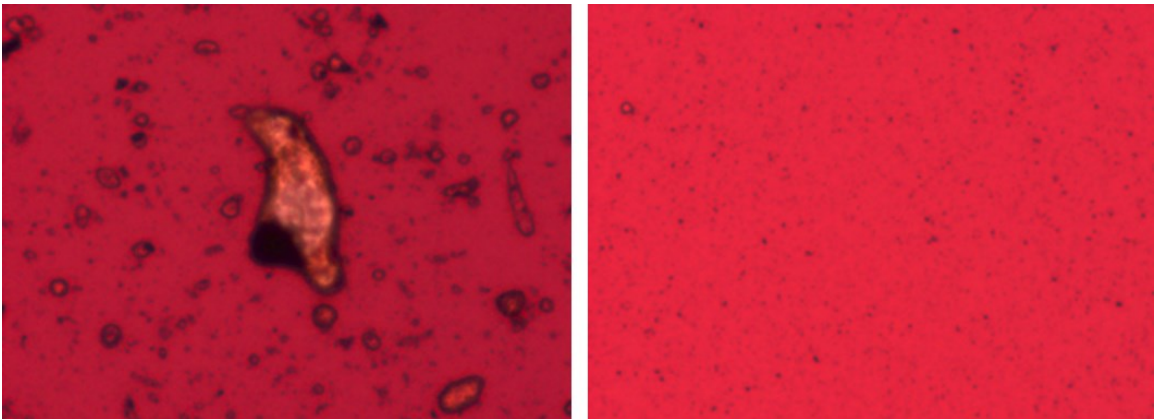


Figure 5-31: Micrographs showing difference in fluid before and after induction for experiment FD-1 (at 45 min and 60 min, respectively)

Figure 5-30 and Figure 5-31 show some examples of the fluid before and after the induction time. In each experiment, there is a considerable difference between the microscope slides before and after the induction time. Water droplets are smaller and less abundant. These figures show that even large water droplets persist at the top heights of the vessel well into the induction time; it is not a high quantity of small droplets.

Figure 5-30 and Figure 5-31 also show typical morphologies of water in low-quality bitumen froth: water is rarely present in small spherical droplets, unlike in dilbit (Leo, 2013) or average-quality bitumen froth, in which it is present at some heights and times (Arora, 2016). Instead, non-spherical droplets dominate at all heights and times with a significant amount of water. The size and shape varies considerably between experiments but attempts to characterize the differences based on the mixing conditions failed.

Most of the droplets have complex surfaces and in many cases entrained solids or oil. These large droplets are not conducive to analysis using the clustering algorithm developed by Arora (2016).

Notably absent from the microscope images are flocs of solids and spherical droplets. These were present in average-quality bitumen froth (Arora, 2016), so there is a qualitative difference between these two froths. This may be caused by high loading, the nature of the bitumen itself (such as the minerals making up the solids), or by the demulsifier.

5.4.1 Comparison with Average-Quality Froth

Low-quality froth is different quantitatively from average-quality froth; while average-quality froth contains approximately 60% bitumen, 30% water, and 10% solids, the low-quality froth used for this work had approximately 50% bitumen, 37% water, and 13% solids. Since the processing steps are largely the same for these two bitumen ores, there must be underlying properties of the bitumen that contribute to the higher percentages of water and solids. Low-quality bitumen froth treated under naphthenic froth treatment also looks qualitatively different under the microscope. Arora (2016) found that many of the samples taken from average-quality froth treated with NFT in the lab had flocs of spherical water droplets and solids. Figure 5-32 shows a sample microscope image from average-quality froth. In contrast to Figure 5-30 and Figure 5-31, there are

spherical water droplets aggregated into a cluster. It was observed with low-quality bitumen froth microscope data that spherical droplets are relatively rare, and they do not form clusters like those found in average-quality froth.

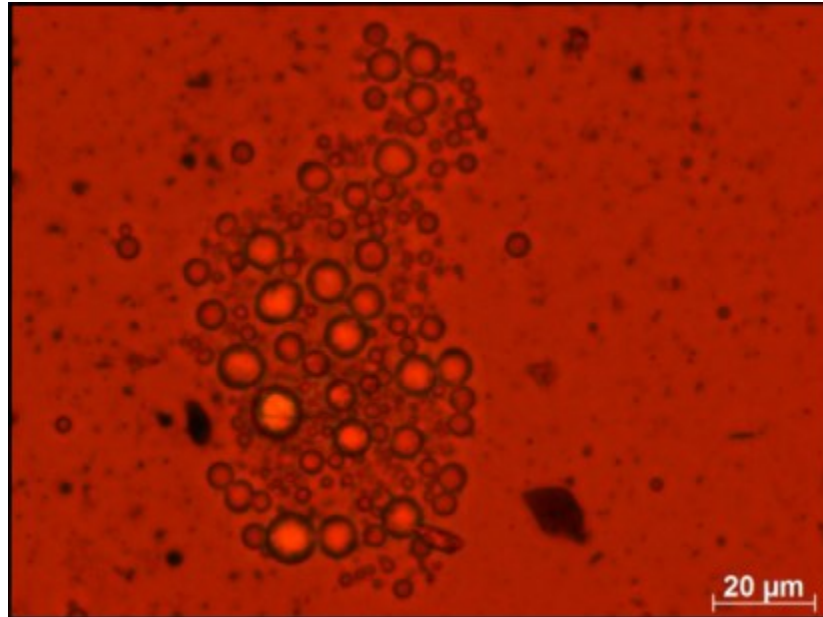


Figure 5-32: Microscope image of average-quality froth during laboratory naphthenic froth treatment, showing spherical water aggregate (Arora, 2016)

5.5 Conclusions

The experiments conducted and data analyzed in this chapter show some patterns and hint at the underlying mechanisms involved in dewatering low-quality bitumen froth.

Dewatering and removing solids from low-quality bitumen froth can be described in three stages: induction, fast settling, and slow settling. The induction time is unique to low quality froth; for some reason, settling is delayed considerably in this type of bitumen froth.

Even large water droplets, which are expected to settle quickly, are observable through microscopy at the top heights of the vessel. According to Stokes Law or hindered

settling models, these large droplets should have settled quickly, yet something is preventing or considerably slowing their settling.

The three stages identified in Chapter 3 – induction, fast settling, and slow settling – are necessary for low water content at the top height in low-quality froth; very unfavorable mixing conditions lead to slow, steady settling that never arrives at a satisfactory end, like a system with no demulsifier added. Long induction time correlated with effective separation after 120 minutes of settling.

Having one of the mixing variables at its “good” level – either low injection concentration or high energy dissipation – is sufficient to get effective separation by 120 minutes. However, only by setting optimal levels of both variables were we able to deliver effective separation by 60 minutes.

Good mixing – high mixing energy and/or low injection concentration – was also associated with low water content in the bottoms layer, where it would be better to form a water-rich layer with less bitumen. This has two interesting implications:

1. The loss of bitumen to tailings may need to be balanced against the quality of the product stream.
2. By mass balance, this implies the water-rich zone is bigger. The induction time may be related to slow contraction of the water-rich zone.

More FBRM data could be used to make more conclusions about the system. It is not clear why there is significant loss of chord counts during settling and no corresponding large water reduction in the Karl Fischer data until later. This seems contradictory and should be explored further.

5.6 Future Work

5.6.1 Induction Time

The induction time is so far unique to low-quality froth and further study could uncover why it happens and how it can be harnessed to improve water removal or avoided to improve settling time. Two possibilities are suggested to account for the induction time and the presence of large water at the top height 20-40 minutes into settling time:

1. Large droplets are not settling until the induction time is over. Something may be preventing droplets. It is perhaps a structure to the fluid, or flow escaping upward during compaction or consolidation to slow or stop normal settling.
2. Large droplets are settling very slowly. Large droplets are continually being replaced by large droplets from above until the induction time. Thus the induction time is the time at which the top-most large droplets pass the level where the induction time is detected.

In addition to multiple emulsion, the very high loading of both solids and water and the nature of the emulsified water may be contributing to compaction effects or viscous effects due to inter-particle adhesion. Water droplets do not resolve with a free layer but rather sit at the bottom of the vessel in tightly packed collections of large non-spherical water droplets and flocs. Even as more droplets continue to settle onto the top of this packed layer, the interstitial space between these large water droplets will be reduced due to the weight above. As the interstitial spaces close, the fluid that occupied them must flow upward. This effect is negligible in most systems but at the high loading present in low-quality bitumen froth it is hypothesized that this up-flow delays settling of the layers above until the rate of compaction or consolidation slows.

5.6.2 Extend FBRM Data Set

The first path for future work is to use the FBRM to get a more complete data set, as was the intention of this work.

By utilizing the surface repellency treatment discussed in 2.2.1 collecting data over a full experimental space, such as that which was done for KF results, more trends can be identified that may in turn allow us to identify the mechanisms of mixing and settling that dominate the system.

A few key variables could be chosen from the FBRM data and tested statistically to determine the effects of the mixing variables presented here.

5.6.3 PVM for Further Analysis and Interpreting FBRM Data

The particle video microscopy (PVM) probe should also be used in future experiments. This probe is only available in a larger form factor than the FBRM, so it is challenging to use in the CIST vessel, which has a small diameter (3"). To prevent fouling and obtain useful data, a similar window treatment to that used for the FBRM can be used for the glass window of the PVM. The PVM could help interpret the FBRM data, especially if quantitative image analysis can be performed and compared to the data from the FBRM. Qualitatively, the PVM could still help choose between the macro and primary modes on the FBRM and help resolve the current discrepancy between FBRM counts (which drop significantly during the first 15-30 minutes of settling) and water content as determined by Karl Fischer titration (which stays very high until 20-40 minutes).

5.6.4 Vessel Redesign

The FBRM may be able to gather more relevant data at lower levels in the tank.

Currently it must be inserted through the top of the tank, restricting the depth to which

it can be inserted. It may be easier to identify sweep flocculation or other complex mechanisms lower in the tank. Vessel design is a challenge, however; the combination of 4 sampling ports, a heating jacket, and an FBRM port may strain the limits of what is possible with the glass vessel. At the very least, a major design will be needed if future experiments are to get FBRM or PVM data from lower in the vessel.

One possibility is to abandon the conventional fluid heating jacket. In its place, another type of heating which allows for easier installation of ports could be used. Perhaps this could be a simple heating blanket with temperature control, or another type of jacket that does not cover the vessel fully, allowing ports to be installed between.

5.6.5 Settling Time and Pre-Settling

Over the course of the campaign it became clear that 120 minutes was often needed to obtain water contents below 1%. It is clear in Figure 5-3 that many experiments done at the chosen dosage are not finished settling at 60 minutes, even with good mixing conditions.

The industrial partner, however, uses a settling time of 60 min, and settling times higher than this would turn bitumen froth treatment into a plant bottleneck. Several possibilities have been discussed but not yet explored in the lab. Chief among these is pre-settling; this would split the settling operation into two. The first settling step would happen in the absence of demulsifier; free water would be allowed to settle and the upper phase would be collected and sent on to the normal settling operation, with demulsifier. This may achieve better settling in the residence time available and may also allow for less demulsifier usage.

References

- Anthieren, G., 2003. Eulerian-Lagrangian Model of Turbulent Mixing for Silver Halide Precipitation. University of Alberta.
- Arora, N., 2016. Mechanisms of Aggregation and Separation of Water and Solids from Bitumen Froth using Cluster Size Distribution. University of Alberta.
- Arora, N., Awosemo, A., Machado, M.B., Kresta, S.M., 2015a. Comparison of Sampling Orientation for Water/Solids Settling Experiments in a Diluted Bitumen System, in: European Conference on Mixing.
- Arora, N., Awosemo, A., Machado, M.B., Kresta, S.M., 2015b. Comparison of Sampling Orientation for Water/Solids Settling Experiments in a Diluted Bitumen System, in: European Conference on Mixing.
- Bittorf, K.J., Kresta, S.M., 2000. Active volume of mean circulation for stirred tanks agitated with axial impellers. *Chem. Eng. Sci.* 55, 1325–1335. doi:10.1016/S0009-2509(99)00403-0
- Bloemen, H.H.J., De Kroon, M.G.M., 2005. Transformation of Chord Length Distributions into Particle Size Distributions Using Least Squares Techniques. *Part. Sci. Technol.* 23, 377–386. doi:10.1080/02726350500212996
- Boxall, J. a., Koh, C. a., Sloan, E.D., Sum, A.K., Wu, D.T., 2010. Measurement and calibration of droplet size distributions in water-in-Oil emulsions by particle video microscope and a focused beam reflectance method. *Ind. Eng. Chem. Res.* 49, 1412–1418. doi:10.1021/ie901228e
- CanmetENERGY, 2016. Froth Treatment | Natural Resources Canada [WWW Document]. *Nat. Resour. Canada*. URL <http://www.nrcan.gc.ca/energy/oil-sands/5873> (accessed 2.22.16).
- Chen, F., Finch, J. a., Xu, Z., Czarnecki, J., 1999. Wettability of fine solids extracted from bitumen froth. *J. Adhes. Sci. Technol.* 13, 1209–1224. doi:10.1163/156856199X00884
- Chen, Z., Peng, J., Ge, L., Xu, Z., 2015. Demulsifying water-in-oil emulsions by ethyl cellulose demulsifiers studied using focused beam reflectance measurement. *Chem. Eng. Sci.* 130, 254–263. doi:10.1016/j.ces.2015.03.014
- Chong, J.Y., 2013. University of Alberta Mixing Effects on Chemical Demulsifier Performance in Diluted Bitumen and Froth Master of Science in Chemical Engineering Chemical and Material Engineering. University of Alberta.

- Chong, J.Y., Machado, M.B., Bhattacharya, S., Ng, S., Kresta, S.M., 2016. Reduce Overdosing Effects in Chemical Demulsifier Applications by Increasing Mixing Energy and Decreasing Injection Concentration. *Energy & Fuels* acs.energyfuels.6b00621. doi:10.1021/acs.energyfuels.6b00621
- Crittenden, J.C., Trussell, R.R., Hand, D.W., Howe, K.J., Tchobanoglous, G., 2012. *MWH's water treatment: principles and design*, 3rd ed. John Wiley & Sons, Inc., Hoboken, New Jersey.
- Czarnecki, J., Tchoukov, P., Dabros, T., 2012. Possible role of asphaltenes in the stabilization of water-in-crude oil emulsions. *Energy and Fuels* 26, 5782–5786. doi:10.1021/ef300904a
- Eley, D.D., Hey, M.J., Symonds, J.D., 1988. Emulsions of water in asphaltene-containing oils 1. Droplet size distribution and emulsification rates. *Colloids and Surfaces* 32, 87–101. doi:10.1016/0166-6622(88)80006-4
- FBRM Method of Measurement [WWW Document], n.d. . Mettler Toledo. URL <http://www.mt.com/ca/en/home/library/videos/automated-reactors/Lasentec-FBRM-Method-of-Measurement.html>
- Gray, M., Xu, Z., Masliyah, J., 2009. Physics in the oil sands. *Phys. Today* March, 31–35. doi:10.1063/1.3099577
- Johnson, M., Peakall, J., Fairweather, M., Biggs, S., Harbottle, D., Hunter, T.N., 2016. Characterization of Multiple Hindered Settling Regimes in Aggregated Mineral Suspensions. *Ind. Eng. Chem. Res.* 55, 9983–9993. doi:10.1021/acs.iecr.6b02383
- Kasperski, K.L., 1992. A Review of Properties and Treatment of Oil Sands Tailings. *AOSTRA J. Res.* 8, 12–42.
- Khan, A., 2011. Froth Handling, in: Czarnecki, J., Masliyah, J., Xu, Z., Dabros, M. (Eds.), *Handbook on Theory and Practice of Bitumen Recovery from Athabasca Oil Sands, Vol 1: Theoretical Basis*. Kingsley Publishing Services, pp. 199–210.
- Kirpalani, D.M., Matsuoka, A., 2008. CFD approach for simulation of bitumen froth settling process - Part I: Hindered settling of aggavy oil aggregates are formed when bitumen emulsions, consisting of emulsified water droplets dispersed solids and precipitated asphaltenes, are treated with a. *Fuel* 87, 380–387. doi:10.1016/j.fuel.2007.05.018
- Kokal, S., 2005. Crude Oil Emulsions: A State-Of-The-Art Review. *SPE Prod. Facil.* 20, 5–13. doi:10.2118/77497-PA
- Komrakova, A.E., Liu, Z., Machado, M.B., Kresta, S.M., 2017. Development of a zone flow model for the confined impeller stirred tank (CIST) based on mean velocity and turbulence measurements (submitted). *Chem. Eng. Res. Des.*

- Kresta, S., Kukukova, A., Aubin, J., 2009. Measurement of mixing using three dimensions of segregation 14–17.
- Kresta, S.M., Etchells, A.W., Dickey, D.S., Atiemo-Obeng, V.A., 2015. *Advances in Industrial Mixing*, 1st ed. John Wiley & Sons, Inc., Hoboken, New Jersey.
- Kukukova, A., Aubin, J., Kresta, S.M., 2009. A new definition of mixing and segregation: Three dimensions of a key process variable. *Chem. Eng. Res. Des.* 87, 633–647. doi:10.1016/j.cherd.2009.01.001
- Laplante, G.P., 2011. On Mixing and Demulsifier Performance in Oil Sands Froth Treatment. *Dep. Chem. Mater. Eng. Master of*, 30–31.
- Laplante, P., Machado, M.B., Bhattacharya, S., Ng, S., Kresta, S.M., 2015. Demulsifier performance in froth treatment: Untangling the effects of mixing, bulk concentration and injection concentration using a standardized mixing test cell (CIST). *Fuel Process. Technol.* 138, 361–367. doi:10.1016/j.fuproc.2015.05.028
- Leng, D.E., Calabrese, R. V., 2004. Immiscible Liquid – Liquid Systems, *Handbook of Industrial Mixing: Science and Practice*.
- Leo, S., 2013. Measurement and Analysis of Changes in Drop Size Distribution during Bitumen Clarification using Image Analysis. *Dep. Chem. Mater. Eng. Master of*.
- Long, Y., Dabros, T., Hamza, H., 2004. Structure of water/solids/asphaltenes aggregates and effect of mixing temperature on settling rate in solvent-diluted bitumen. *Fuel* 83, 823–832. doi:10.1016/j.fuel.2003.10.026
- Long, Y., Dabros, T., Hamza, H., 2002. Stability and settling characteristics of solvent-diluted bitumen emulsions. *Fuel* 81, 1945–1952. doi:10.1016/S0016-2361(02)00132-1
- Machado, M.B., Bittorf, K.J., Roussinova, V.T., Kresta, S.M., 2013. Transition from turbulent to transitional flow in the top half of a stirred tank. *Chem. Eng. Sci.* 98, 218–230. doi:10.1016/j.ces.2013.04.039
- Machado, M.B., Kresta, S.M., 2013. The confined impeller stirred tank (CIST): A bench scale testing device for specification of local mixing conditions required in large scale vessels. *Chem. Eng. Res. Des.* 91, 2209–2224. doi:10.1016/j.cherd.2013.06.025
- Masliyah, J.H., Czarnecki, J., Xu, Z., 2011. *Handbook on Theory and Practice of Bitumen Recovery from Athabasca Oil Sands, Volume I: Theoretical Basis*. Kingsley Knowledge Publishing, Canada.
- Mettler Toledo, 2013. *Inline Particle Measurement: Optimize Process Development*.
- Montgomery, D.C., Runger, G.C., 2007. *Applied Statistics and Probability for Engineers*,

- Fourth. ed. Wiley, Hoboken, NJ.
- Muñoz, V. a., Kasperski, K.L., Omotoso, O.E., Mikula, R.J., 2003. The Use of Microscopic Bitumen Froth Morphology for the Identification of Problem Oil Sand Ores. *Pet. Sci. Technol.* 21, 1509–1529. doi:10.1081/LFT-120023225
- Patterson, G.K., Paul, E.L., Kresta, S.M., Etchells, A.W.I., 2004. Mixing and Chemical Reactions, in: Paul, E.L., Atiemo-Obeng, V.A., Kresta, S.M. (Eds.), *Handbook of Industrial Mixing: Science and Practice*. John Wiley & Sons, Inc., Hoboken, New Jersey.
- Peña, A.A., Hirasaki, G.J., Miller, C.A., 2005. Chemically Induced Destabilization of Water-in-Crude Oil Emulsions. *Ind. Eng. Chem. Res.* 44, 1139–1149. doi:10.1021/ie049666i
- Rao, F., Liu, Q., 2013. Froth Treatment in Athabasca Oil Sands Bitumen Recovery Process: A Review. *Energy & Fuels* 27, 7199–7207. doi:Doi 10.1021/Ef4016697
- Rocha, J.A., Baydak, E.N., Yarranton, H.W., Sztukowski, D.M., Ali-Marcano, V., Gong, L., Shi, C., Zeng, H., 2016. Role of Aqueous Phase Chemistry, Interfacial Film Properties, and Surface Coverage in Stabilizing Water-in-Bitumen Emulsions. *Energy and Fuels* 30, 5240–5252. doi:10.1021/acs.energyfuels.6b00114
- Romanova, U.G., Valinasab, M., Stasiuk, E.N., Yarranton, H.W., 2006. The Effect of Bitumen Extraction Conditions on Froth Treatment Performance. *J. Can. Pet. Technol.* 45, 36–45. doi:http://dx.doi.org/10.2118/2004-028-EA
- Romanova, U.G., Yarranton, H.W., Schramm, L.L., Shelfantook, W.E., 2004. Investigation of oil sands froth treatment. *Can. J. Chem. Eng.* 82, 710–721. doi:10.1002/cjce.5450820410
- Rondón, M., Bouriat, P., Lachaise, J., Salager, J.L., 2006. Breaking of water-in-crude oil emulsions. 1. Physicochemical phenomenology of demulsifier action. *Energy and Fuels* 20, 1600–1604. doi:10.1021/ef060017o
- Safari Alamuti, F., 2016. Transformation of dynamic Chord Length Distribution into Drop Size Distribution.
- Sarafinas, A., Teich, C.I., 2016. Scale-Up Using the Bourne Protocol: Reactive Crystallization and Mixing Example, in: Kresta, S.M., Etchells, A.W.I., Dickey, D.S., Atiemo-Obeng, V.A. (Eds.), *Advances in Industrial Mixing*. John Wiley & Sons, Inc., Hoboken, pp. 479–490.
- Seville, J., Wu, C.-Y., 2016. Particles in Fluids, in: *Particle Technology and Engineering*. Butterworth-Heinemann, Oxford, UK, pp. 67–81.
- Shelfantook, W.E., 2004. A perspective on the selection of froth treatment processes. *Can. J. Chem. Eng.* 82, 704–709.

- Stokes, G.G., 1850. On the Effect of the Internal Friction of Fluids on the Motion of Pendulums. *Trans. Cambridge Philos. Soc.* 9, 8.
doi:10.1017/CBO9780511702242.005
- Sullivan, A.P., Kilpatrick, P.K., 2002a. The Effects of Inorganic Solid Particles on Water and Crude Oil Emulsion Stability. *Ind. Eng. Chem. Res.* 41, 3389–3404.
doi:10.1021/ie010927n
- Sullivan, A.P., Kilpatrick, P.K., 2002b. The Effects of Inorganic Solid Particles on Water and Crude Oil Emulsion Stability. *Ind. Eng. Chem. Res.* 41, 3389–3404.
doi:10.1021/ie010927n
- Xu, A., 2016. Qualitative Microscope Analysis (internal report). Edmonton AB.
- Xu, Y., Wu, J., Dabros, T., Hamza, H., Venter, J., 2005. Optimizing the polyethylene oxide and polypropylene oxide contents in diethylenetriamine-based surfactants for destabilization of a water-in-oil emulsion. *Energy and Fuels* 19, 916–921.
doi:10.1021/ef0497661
- Yeung, a., Dabros, T., Masliyah, J., Czarnecki, J., 2000. Micropipette: A new technique in emulsion research. *Colloids Surfaces A Physicochem. Eng. Asp.* 174, 169–181.
doi:10.1016/S0927-7757(00)00509-4
- Zhou, G., Kresta, S.M., 1996. Impact of tank geometry on the maximum turbulence energy dissipation rate for impellers. *AIChE J.* 42, 2476–2490.
doi:10.1002/aic.690420908

Appendix A: Experimental Data

Table A-1: Time Series Karl-Fischer Determined Water Content (wt%) for Chapter 4. All data provided are an average of at least 3 titrations.

BC (ppm)	N:B	Mixing	Settling Time (min) and Water Content (wt%)											
			0	5	10	15	20	25	30	35	40	50	60	
406	0.72	good	0	5	10	15	20	25	30	35	40	50	60	
			28.96	29.09	30.86	29.71	30.71	32.01	31.02	24.63	24.29	22.08	1.62	
205	0.88	good	0	3	5	7	10	30	60					
			19.82	24.18	19.64	19.40	20.25	1.23	0.48					
196	0.71	good	0	5	10	15	20	25	30	40	50	60	75	90
			28.03	27.74	26.61	25.42	24.97	24.27	25.02	23.68	1.28	0.97	0.83	0.69
193	0.72	poor	0	5	10	15	20	25	30	35	40	50	60	
			29.36	22.31	27.29	19.17	16.57	13.19	9.80	5.32	10.10	8.14	4.49	
176	0.86	good	0	3	5	7	10	30	60					
			32.33	28.57	28.19	15.78	28.44	0.78	1.03					
171	0.72	good	0	10	15	20	25	30	35	40	50	60		
			33.84	32.05	29.52	29.89	30.91	31.94	20.30	16.84	1.41	1.16		
149	0.74	good	0	5	10	15	20	25	30	35	40	50	60	
			28.39	28.05	30.61	27.07	28.41	28.41	18.02	2.52	2.32	1.34	1.17	
148	0.81	good	0	10	15	20	25	30	45	60	90	120		
			29.04	25.10	24.26	22.89	20.11	8.32	1.71	1.60	1.17	0.77		
145	0.78	good	0	3	5	7	10	30	60					
			27.79	27.70	26.79	24.51	24.18	2.07	1.46					
120	0.70	good	0	3	5	7	10	30	60					
			29.14	29.42	28.80	27.14	28.78	27.80	0.89					
100	0.74	good	0	3	5	7	10	30	60					
			26.38	29.04	27.11	29.74	23.88	2.61	1.59					
73	0.71	good	0	5	10	15	20	25	30	45	60	90	120	
			32.51	37.15	26.30	25.48	25.78	25.68	24.60	4.89	3.30	1.86	1.75	
25	0.71	good	0	5	10	15	20	25	30	45	60	90	120	
			33.80	29.09	34.90	24.22	27.61	19.85	15.42	8.99	4.96	3.93	4.15	
0	0.72	good	0	5	10	15	20	25	30	35	40	50	60	
			20.11	20.40	13.89	9.32	8.90	8.03	7.37	6.71	5.95	4.60	3.41	
0	0.71	poor	0	5	10	15	20	25	30	35	40	50	60	
			23.35	22.49	20.11	17.48	15.14	12.94	11.06	9.99	8.67	5.51	3.92	

Table A-2: Time Series Karl-Fischer Determined Water Content (wt%) for Chapter 5. All data provided are an average of at least 3 titrations.

Run Code & Variable Levels (X_i , X_{ic})	Sampling Height	Water Contents (wt%) by Settling Time (min)									
		5	10	15	20	25	30	45	60	90	120
FA-1 (-1, -1)	Z1	34.40	35.17	32.73	32.73	31.41	31.34	20.53	6.25		
	Z2	29.16	27.83	22.79	27.51	26.72	24.09	27.17	26.03		
	Z3	21.29	29.88	30.63	28.07	19.11	28.14	29.56	27.66		
	Z4	46.29	27.88	29.33	30.19	33.58	34.79	39.51	41.28		
FB-1 (+1, +1)	Z1	28.68	24.70	22.03	20.54	14.84	2.77	2.08	3.06		
	Z2	27.47	26.14	24.66	26.25	25.58	15.58	26.27	37.08		
	Z3	28.13	27.31	27.35	25.84	26.18	26.20	25.61	28.31		
	Z4	29.11	29.66	29.62	34.44	33.45	36.42	45.11	45.82		
FC-1 (-1, +1)	Z1	27.22	26.13	22.70	19.75	19.07	15.82	11.29	6.82	4.00	5.07
	Z2	27.26	27.30	29.96	25.67	25.72	24.44	23.26	21.86	14.48	5.38
	Z3	26.10	25.90	28.04	25.47	26.63	24.72	25.67	25.72		
	Z4	28.37	28.36	27.67	32.48	40.47	42.28	42.90	46.20		
FD-1 (+1, -1)	Z1	32.08	32.65	30.49	30.62	31.04	27.90	29.17	1.48	0.11	0.60
	Z2	35.16	33.13	29.16	39.66	30.86	28.61	29.33	27.59	22.96	3.92
	Z3	27.21	29.44	35.22	28.33	27.08	33.03	30.98	35.30		
	Z4	26.54	29.04	32.92	30.18	31.03	34.90	33.72	36.79		
CP-1 (0, 0)	Z1	29.81	28.95	20.86	27.43	26.91	25.17	4.58	24.29	2.58	2.14
	Z2	25.96	28.85	26.39	30.97	30.98	29.41	28.13	18.59	13.20	0.98
	Z3	30.49	30.22	27.19	31.54	29.65	20.35	28.98	30.60		
	Z4	27.93	28.21	29.91	32.19	N/A	34.76	36.40	40.38		
FD-2 (+1, -1)	Z1	30.33	30.18	29.31	28.68	29.09	32.09	21.96	1.35	0.82	0.66
	Z2	30.87	31.52	30.08	32.12	27.36	26.60	28.05	25.22	22.47	1.57
	Z3	29.91	28.47	28.73	31.60	28.11	29.23	27.25	31.66		
	Z4	29.45	31.14	29.17	32.52	33.70	34.98	32.67	38.13		
FA-2 (-1, -1)	Z1	30.03	28.11	25.37	25.26	21.97	25.25	10.46	12.21	1.33	0.13
	Z2	23.66	27.68	27.13	26.19	32.19	27.22	26.65	23.68	28.24	0.75
	Z3	28.19	29.15	30.57	24.16	30.34	18.00	31.70	30.15		
	Z4	27.17	27.35	27.80	27.88	29.38	30.99	34.56	36.18		
FB-2 (+1, +1)	Z1	32.69	30.22	28.09	28.42	25.22	19.21	5.25	2.23	2.91	0.77
	Z2	29.34	30.96	31.04	25.39	31.83	27.91	26.90	26.95	2.38	0.87
	Z3	31.29	29.74	30.42	31.26	29.46	24.24	29.50	31.81		
	Z4	31.18	34.12	30.19	35.66	38.37	41.69	41.99	41.04		
FC-2 (-1, +1)	Z1	20.88	27.39	26.69	21.05	21.14	11.30	5.80	4.78	4.57	2.84
	Z2	32.24	30.22	34.94	29.53	27.42	25.00	20.49	18.25	2.82	3.50
	Z3	32.36	28.30	29.75	33.87	30.06	30.00	28.27	30.61		
	Z4	28.57	29.19	31.19	41.83	44.89	44.41	49.80	48.45		

Table A-3: Pre-Settling Karl-Fischer Determined Water Content (wt%) for Chapter 5. All data provided are an average of at least 3 titrations.

Experiment	<i>Sample (Code)</i>		
	Premixing (P)	Naphtha Blending (A)	Demulsifier Dispersion (B)
FA-1	36.9	38.9	33.2
FB-1	31.0	23.0	29.6
FC-1	37.3	27.6	28.8
FD-1	37.6	29.8	31.7
CP-1	40.9	37.6	29.5
FD-2	35.9	31.5	27.9
FA-2	35.7	29.4	33.1
FB-2	37.2	30.2	29.9
FC-2	36.3	31.6	31.9

Table A-4: OWS Data for Chapter 5, as determined by industrial partner using Dean Stark extraction

Run Code	Height (z/H from top of liquid)	X _l	X _{ic}	Bitumen (%)	Water (%)	Solids (%)	Naphtha (by balance, %)
FA-1	0.1	-1	-1	58.78	3.76	1.86	35.6
	0.5	-1	-1	40.64	3.14	5.87	50.35
FB-1	0.1	1	1	62.8	2.64	1.45	33.11
	0.5	1	1	41.79	2.85	6.13	49.23
	0.9	1	1	24.36	43.91	14.76	16.97
FC-1	0.1	-1	1	57.94	4.68	1.94	35.44
	0.5	-1	1	39.77	27.93	6.07	26.23
	0.9	-1	1	26.21	42.3	12.87	18.62
FD-1	0.1	1	-1	61.18	0.86	0.53	37.43
	0.5	1	-1	44.9	20.21	5.78	29.11
	0.9	1	-1	27.48	41.34	12.94	18.24
CP-1	0.1	0	0	58.16	2.2	1.05	38.59
	0.5	0	0	47.33	16.85	4.36	31.46
	0.9	0	0	27.12	42.54	11.27	19.07
FA-2	0.1	-1	-1	58.33	2.16	0.96	38.55
	0.5	-1	-1	43.8	21.05	5.38	29.77
	0.9	-1	-1	27.97	42.61	11.91	17.51
FB-2	0.1	1	1	56.45	2.48	1.47	39.6
	0.5	1	1	48.22	15.37	4.63	31.78
	0.9	1	1	26.44	43.03	12.63	17.9
FC-2	0.1	-1	1	55.76	4.72	1.92	37.6
	0.5	-1	1	47.52	15.27	3.99	33.22
	0.9	-1	1	24.41	14.57	12.99	48.03
FD-2	0.1	1	-1	59.1	1.07	0.63	39.2
	0.5	1	-1	44.81	19.09	5.61	30.49
	0.9	1	-1	26.84	42.05	13.6	17.51

Appendix B: Select Standard Operating Procedures

B.1 Bitumen Froth Experiments (Low Quality Froth with FBRM)

Main Hazards

- Hot bitumen: skin irritant
- Hot hydrocarbon products: high vapour pressure & flammable gases. Should be handled under the fume hood at all times and respirator should be worn.

Experiment Preparation

- Froth Can:
 - Ensure froth can is more than 860 g (which will fill the vessel to approx. 1L). If not, heat a froth can, run premixing step, then pour into other froth cans until they are.
 - Turn can upside down one or two days before experiment, with tissue underneath. Ensure lid is secure.
- Needles
 - Silanize
 - Chop pipette tips using the plate with a standard whole (1.5 mm diameter)
 - Mark needles for insertion depth (4.5 cm for $r/R = 0.9$)
 - Attach needles to pipette tips using duct tape
- Silanize and label microscope slides
- Label and weigh sample bottles (See Table 1).
- End-of-run OWS/CPA samples
 - Label bottles (See Table 1)
 - Cut plastic tubing for various sampling depths (1 each @ 58, 150, 242 mm)
- Attach tubing to 100ml glass syringe with duct tape
- CIST preparation
 - Install septa inside sampling ports, making sure they do not buckle
 - Screw in Teflon plugs over sampling ports
 - Put baffles and Teflon bearing at the bottom of CIST
 - Prepare demulsifier at 12 wt% ($X_{IC}=-1$), 16.5 wt% ($X_{IC}=0$) or 21 wt% ($X_{IC}=+1$)

On Experiment Day

- Take the upside down can out of fridge and keep in fume hood in same orientation.
- Turn the Ethylene Glycol bath on.
- Install impellers (Rushton, Intermig or A310) in CIST with motor driver.
- Set CIST in fumehood and secure against back support plate using Velcro.
- Load demulsifier in syringe and prepare pump. Enter injection rate and volume. (ID = 32.43 mm)
- Mark insertion depth = 8.6cm on demulsifier injection tubing

Premixing

- Heat Premixing Ethylene Glycol bath to 82°C for at least 1 hour.
- Measure the weight of froth can and based on N/B=0.7 (by mass), fill naphtha in another can.
- Heat froth can for 1.5 hours. Froth should heat up to 70°C.
- Install CIST in fumehood and start EG circulation and heating to 80°C.
- Once froth reaches 70°C, do premixing using PBT impeller at 1000 rpm for 15 minutes. Froth should heat up to 80°C at the end of premixing.
- Heat Naphtha can to 80°C for half an hour. Both froth premixing and naphtha should be ready for transferring to CIST at same time.

Naphtha Blending

- Remove naphtha from bath, dry and weigh
- Transfer heated Naphtha to CIST first using thermal glove, then weight empty beaker
- Remove froth can from bath, dry and weigh
- Transfer heated froth to CIST using thermal glove and weight empty can
- Check the liquid level in CIST in comparison to 1L mark.
- Set impeller speed (rpm) and time (min) as per Table 3.
- Set up FBRM to be above impeller/below feed pipe location.
- Blend for 2 min by hitting "Run", take a sample at the end of naphtha blending (Table 1).

Demulsifier dispersion

- Set motor to appropriate time/speed and hit run
- Inject demulsifier using syringe pump (Table 3) after motor is running
- Take samples as per sampling schedule (Table 1)

Batch settling

- Once the impellers stop, start the timer
- Take samples accordingly to sampling schedule (Table 1). For runs with 4 heights, each person takes 1 sample (e.g. Z1 and Z3) at 10 s before the nominal time, and one sample 10 s after the nominal time. This is to reduce the chance of an accident and to improve the quality of sampling.
- For Syncrude samples (OWS/CPA), start sampling from top and then move down

Table 5-9: Sampling schedule and labelling criteria

Label	Time	Location	Analysis	No of samples
P	End of premixing	Just below the liquid surface	KF	1
A	End of Naphtha blending	Z1 mm below the liquid surface	KF, Microscope	1
B	During demulsifier dispersion (30 s before mixing ends)	Z1 and Z4	KF, Microscope	2
3, 5, 7, 10, 30, 60	During settling	(Z1,Z4) or (Z1, Z2, Z3,Z4)	KF, Microscope	12 or 24
DS_1, DS_5, DS_9	End of settling	At z/H = 0.1, 0.5, 0.9	OWS (DS, CPA): 100 ml each	3

Table 2: Variable range for bitumen froth experiments

	Regression Coefficient, X		
	-1	0	1
BC (wppm)	150		
J (J/kg)	425	12164	22778
IC (wt%)	12	16.5	21

Table 3: Low Quality Froth Trials Operating Conditions

Run/Code	X _J	X _{IC}	Impeller	Naphtha Blending	Demulsifier Dispersion	Dem. Injection Rate (mL/hr), Volume (mL)	
FA-1	-1	-1	Intermig	1060 rpm/2 min	400 rpm/2 min	125.1	1.7
FB-1	+1	+1	Rushton	600 rpm/2 min	600 rpm/10 min	634.7	0.9
FC-1	-1	+1	Intermig	1060 rpm/2 min	400 rpm/2 min	125.1	0.9
FD-1	+1	-1	Rushton	600 rpm/2 min	600 rpm/10 min	634.7	1.7
CP-1	0	0		600 rpm/2 min	600 rpm/5.25 min	634.7	1.2
FD-2	+1	-1	Rushton	600 rpm/2 min	600 rpm/10 min	634.7	1.7
FA-2	-1	-1	Intermig	1060 rpm/2 min	400 rpm/2 min	125.1	1.7
FB-2	+1	+1	Rushton	600 rpm/2 min	600 rpm/10 min	634.7	0.9
FC-2	-1	+1	Intermig	1060 rpm/2 min	400 rpm/2 min	125.1	0.9

B.2 Receiving Test Material from Syncrude

Syncrude provides some of the test fluid: this includes naphtha for dilution, demulsifier chemical, diluted bitumen (dilbit), and bitumen froth. These must be sent safely and quickly: all except the bitumen froth are covered under Transportation of Dangerous Goods (TDG) requirements, and the bitumen froth and dilbit are known to experience aging effects, so should be in the warm for as short a time as possible.

Lab (University) Procedure:

- Send an email to Samson (ng.samson@syncrude.com) or Sujit (bhattacharya.sujit@syncrude.com) requesting material
- Bitumen Froth: 2 cans used per experiment (1 L cans)
- Diluted Bitumen: 1 4L can used for 2 experiments
- Once Samson or Sujit approve the request, another employee (such as Allan) will arrange for sampling
- Tell Kevin (Kevin.Heidebrecht@ualberta.ca) that he will be receiving a package soon and ask him to inform you as soon as he does.
- Once the material is prepared, order a pickup from Matt Express or a similar, same day service. You will need to tell them:
- Contact info (at University and Syncrude)
- Pickup point and instructions
- Drop-off point and instructions (ICE Building Dock, back up to door and wait until it opens, 1-2 minutes, call University contact)
- Unpack, store froth cans upside-down in fridge (dilbit cannot be stored upside-down; it will leak). Naphtha goes in flammable storage, demulsifier in fridge.
- Add the received to the chemical receiving form in the lab safety binder.

Syncrude Procedure:

- Note: Same-day shipment is critical as aging effects have been observed. Minimizing the time outside of refrigerated storage is important.
 - Store froth at 5°C until courier pickup.
 - Package and prepare for shipment per TDG requirements (TDG is not required for shipments of froth only, but is required for naphtha, demulsifier, and diluted bitumen).
- Request pickup from lab contact (Colin 306 280 0357, Anna, Marcio) to receive shipment. You will need to inform the student:
 - Your contact info
 - Address
 - Weight of shipment
 - Size of shipment
- Send email when shipment is picked up so student knows to expect it.

B.3 Karl Fischer Procedures

Karl Fischer titration is a technique for finding water content. Samples taken from the experiment are then diluted and titrated to find the water content in the vessel.

Unisol Preparation

Unisol is used to dilute bitumen samples for use with the Karl Fischer titration cell. It is simply a 3:1 mixture of high grade toluene and isopropanol.

- Fill desired container with silica beads.
- Mix high-purity toluene and isopropanol in a graduated cylinder or beaker in approximately 3:1 proportions. Approximately 90 mL fills a 200 mL vessel with glass beads.
- Pour into vessel until full.

Karl Fischer Titration

Karl Fischer titration tells you how many micrograms of water are in an injected sample. By carefully monitoring weighs, you can back calculate water content in the sample taken from the vessel. *Setting up an Excel sheet ahead of time with all the calculations is recommended.*

Determine Unisol water content

- Shake Unisol bottle while closed, tap the lid to remove beads
- Remove a sample with a small needle, clearing 3-5 times depending on the last sample taken in this needle.
- Wipe the tip and weigh the needle.
- Press Run on KF and inject sample, ensuring tip is below liquid level.
- Wipe needle again and record empty syringe weight and KF reading.
- Calculate water content (it helps to set up an Excel sheet ahead of time to calculate this).

Determine Sample Water Content

- Measure weights of empty sample bottles.
- Take samples.
- *After* removing sample for microscope slides, weigh sample bottle.
- Dilute the sample by injecting approximately 5x (for dilbit) or 25-30x (for froth) the weight of the sample in Unisol.
- Weigh the sample bottle again and calculate actual dilution ratio.
- Ensuring lid is tight, agitate at 3000 rpm on the vortex mixer for 10s (for dilbit) or 20s (for froth).
- Remove sample with small needle. Clear 3-5 times.
- Wipe and weigh full needle.
- Press Run and inject sample, ensuring tip is below the liquid level in the cell.
- Wipe and weigh empty needle and record KF reading.
- Calculate actual water content.

Change KF Liquids

- Remove liquid cells, silica gel, injection port, electrode, and clean all connections with wipe and acetone if necessary. Be careful not to apply lots of pressure to glass ports (i.e. where the wire enters).
- Pour liquids into organic waste container.

- Fill large liquid cell first and place back in titrator along with silica gel and injection port connections.
- Snap small Karl Fischer liquid with bottle, using plastic safety cover or lab towel to protect hands from glass cuts.
- Use pipette to transfer most liquid from small bottle.
- Cover glass connections (about a pea-sized amount) with Apiezon M grease and insert.
- Press run, and increase speed, ensuring magnetic stirrer is working. Allow titration to run until completion. This can take half an hour to several hours, depending on how much quickly the transfer was done.

B.4 Sending End-of-Run Samples to Syncrude

Syncrude performs a few tests at their facility to complement those done at the University. Dean Stark extraction gives the oil, water, and solids constant, and computerized particle analysis gives solid particle sizing.

Procedure

- Ensure samples are bottled correctly in 100 mL sample bottles with alternative cap (Qorpak Catalogue: CAP-00268).
- Fill out a sample tag for each sample ensuring separate series for CPA/OWS and EXM analysis. These are provided by Syncrude in the form of a booklet. Fill them out as follows:
 - Date and Time of sample taken
 - Submitter: U of A
 - Stream: Your identifier. Put a tag such as Run #-Sample A.
 - Work Order: Leave it empty. Syncrude will fill this part.
 - Wet/Dry/Pan: Leave it empty.
 - Check the desired tests: CPA and OWS
- Keep the left side of the sample tag for matching up with the data received later and for tracking. Affix the right sample tag to the sample with a rubber band and ensure it is secure. Copy the serial numbers and stream names into lab records.
- Put the samples into a box in numerical order, with consecutive tag numbers if possible, and write “start here” at the first sample.
- Tighten all the sample bottle lids to make sure that none of them leak.
- Pack small box into a larger box with absorbent material.
- Fulfill other TDG requirements (labelling, shipment documentation, etc). This should be done with a person trained in TDG or checked by one. Consult with the CME safety resource to clarify requirements.
- Store the sample box in the refrigerator until pick-up.
- Inform Allan (yeung.allan@syncrude.com) or other Syncrude resource in advance that he will be receiving samples.

- Fill out the shipping form located on the department website and get it signed by Marcio or Dr Kresta. The signed shipping form, the TDG ground form, your TDG training record if applicable, and the applicable MSDS should be sent to SMS (780-492-4121; shipping@ualberta.ca) for review 2-3 days prior to shipping day. Wait for SMS approval before sending the samples.
- It is extremely important that the samples be delivered on the same day as shipping day. Matt Express (780-944-1582) provides same day shipping. Matt Express can pick up the samples from you directly (not through SMS) if you are certified in TDG (Transportation of Dangerous Goods) and you have complete paper work (MSDS, shipping form, TDG ground form).

Syncrude delivery address:

Allan Yeung

Syncrude Canada Ltd

Research and Development Centre

9421-17 Avenue NW

Edmonton, AB T6N 1H4

E: yeung.allan@syncrude.com T: 780-970-6942